AN ABSTRACT OF THE DISSERTATION OF

James Elliott Fowler for the degree of Doctor of Philosophy in Chemical Engineering presented on June 1, 2018.

Title: Multi-Technique Characterizations of Natural and Biomimetic Adhesives

Abstract approved: _____

Joe E. Baio

There have been many attempts to characterize and mimic natural fluid-based adhesive systems. However, very few of these studies have examined surface or interfacial interactions between adhesive and substrate. Furthermore, until now no study has used a combination of surface analytical and kinematic techniques to determine the precise chemical mechanisms that govern the success or failure of a natural adhesive in different environments. The work presented here demonstrates how the composition, order and relative orientation of adhesive molecules at functional interfaces can be determined using complementary surface analytical techniques.

Initially, the chemical makeup and pressure-sensitive nature of frog mucus was examined with Near Edge X-Ray Absorption Fine Structure (NEXAFS) Spectroscopy and Sum Frequency Generation (SFG) Vibrational Spectroscopy to determine if mucus glycoprotein molecules located at the mucus-prey interface formed fibrils during prey capture. NEXAFS sampled photons associated with bond orbitals of molecular bonds within the top few nanometers of the interface while SFG measured order-sensitive intensity of vibrational modes at this same surface with sub-monolayer resolution. NEXAFS images at the N1s and C1s K-edges at two incident x-ray angles were collected by rastering the x-ray beam at across the surface of the mucus, showed that surface chemical bonds associated with glycoproteins were uniformly distributed. Angle-resolved NEXAFS experiments and SFG spectra indicated a glycoprotein tertiary structure

consistent with fibril formation and methyl and methylene groups on amino acid side chains oriented normal to fibrils on the surface.

Next, insect tarsal fluid adhesive was investigated, utilizing SFG spectroscopy to probe the presence of ordered molecular bonds at the functional interface between adhesive fluid and substrate. Fluid footprints of a model species, the seven-spotted ladybird beetle, were collected on three substrates with varying surface energies and hydrophobicities. Film thickness and roughness were determined with profilometry and atomic force microscopy respectively to ensure only smooth surfaces were tested. Resulting SFG spectra revealed that the chemical environment at the interface was not affected by substrate hydrophobicity. However, the ordering of observed hydrocarbon groups within the fluid increased with a corresponding increase in substrate hydrophobicity. The interfacial layer of beetle adhesive fluid was determined to promote lubrication of foot contact, rather than adhesion.

Building upon these results, a biomimetic adhesive fluid inspired by ladybird beetle foot adhesive was designed. A water-in-oil emulsion was formulated using 3 components - squalane, deuterated stearic acid and water. SFG spectra of the mimetic fluid on both hydrophilic and hydrophobic surfaces revealed that molecular vibrations in each case closely resembled those of the natural fluid, with squalane the only surface-active component. Preexisting molecular dynamics simulation of squalane at solid surfaces showed that it prefers to orient parallel to the surface with its methyl branches pointing in the surface normal direction. Spectra of pure squalane and a squalane/deuterated stearic acid mixture on the same substrates revealed the that the surface-inactive components (d-stearic acid and D_2O) have an observable effect on the ordering of these squalane layers at the interface. Pull-off force, traction force and viscometry measurements of each fluid showed an increase in viscosity and pull-off force and a decrease in traction force with increasing fluid complexity. Based upon this, it is concluded that the surface-inactive components of ladybird beetle adhesive created a more cohesive fluid which allowed it to accurately mimic the functional properties of natural ladybird beetle adhesive.

Multi-Technique Characterizations of Natural and Biomimetic Adhesives

By

James Elliott Fowler

A DISSERTATION

submitted to

Oregon State University

in partial fulfillment of
the requirements for the
degree of

Doctor of Philosophy

Presented June 1st, 2018

Commencement June 2018

Doctor of Philosophy dissertation of James Elliott Fowler presented on June 1, 2018

APPROVED:

_____

Major Professor, representing Chemical Engineering

_____

Head of the School of the Department of Chemical, Biological and Environmental Engineering

_____

Dean of the Graduate School

I understand that my thesis will become part of the permanent collection of Oregon State University libraries. My signature below authorizes release of my thesis to any reader upon request.

_____

James Elliott Fowler, Author

ACKNOWLEDGEMENTS

I would like to express sincere appreciation to the International Max Planck Research Schools, particularly the Max Planck Institute for Polymer Science in Mainz, Germany, for funding a Graduate Research Fellowship during which part of this research was conceived and conducted. Additionally, I would like to thank Dr. Stanislav Gorb, Dr. Thomas Kleinteich and the Zoological Institute of the University of Kiel for providing the animal samples used in this work. I wish to recognize the contributions of all of my colleagues at Oregon State and the Max Planck Institute for their assistance, advice and feedback throughout my time as a graduate student. Finally, thank you to my advisor, Dr. Joe Baio, and my fellowship advisor, Dr. Tobias Weidner, for all of their support, guidance and patience.

CONTRIBUTION OF AUTHORS

In Chapter 3, Thomas Kleinteich and Stanislav Gorb assisted with the collection of frog tongue mucus. Cherno Jaye and Daniel Fischer were involved with NEXAFS data collection and designed spectra interpretation software. Johannes Franz and Tobias Weidner assisted with data interpretation. In Chapter 4, Stanislav Gorb collected adhesive fluid samples and Johannes Franz, Thaddeus Golbek and Tobias Weidner assisted with data collection and interpretation. In Chapter 5, Tobias Weidner and Stanislav Gorb were involved with data interpretation.

TABLE OF CONTENTS

TABLE OF CONTENTS (Continued)

Page

TABLE OF CONTENTS (Continued)

Page

TABLE OF CONTENTS (Continued)

Page

LIST OF FIGURES

Figure Page

LIST OF FIGURES (Continued)

Figure Page

LIST OF FIGURES (Continued)

DEDICATION

To Briana and my parents Jim and Leslie, without whom this document would have never been possible.

Chapter 1 - Introduction

1.1 Overview

Despite centuries of innovation in design, man-made adhesives pale in comparison to those developed by animals in nature, particularly when it comes to adaptability, reusability and resilience [1, 2]. This has led to the characterization of animal adhesives and adhesive systems as biomimetic inspiration. Perhaps the most popular case involves dry adhesion of the feet of the Tokay gecko [3-6]. However, one can also find a broad range of research into both wet or dry adhesive systems utilized by snails, mussels, insects, reptiles and amphibians [7-12]. While a range of creatures possess unique adhesive abilities, there is no governing “model” system that accurately describes this global set of systems. Instead, individual animal systems have been studied based upon connections to comparable man-made adhesives.

For this reason, we have chosen to study two fluid-mediated adhesive systems: the sticky-tongue mechanism of the frog and tarsal (foot) adhesion of insects and bugs [12, 13]. The sticky-tongue mechanism is perhaps the most iconic trait of frogs – in which they rapidly project their tongue towards prey, latch onto it, and pull it back into their mouth. Frog tongues are highly flexible, powerful muscles and this mechanism was originally thought to be the result of a physical grabbing or confining of the prey with the tongue [14]. However, recent studies have determined that a mucus coating the tongue is what provides for both strong adhesive forces and easy detachment from the prey once inside the mouth – functioning similar to a pressure sensitive adhesive (PSA) [12, 15]. Thus, one can imagine a piece of duct tape (an example of a manmade PSA) with the ability to stick, un-stick and re-stick thousands of times in often extremely humid, warm and wet environments. This would represent a dramatic increase in utility, with uses ranging from lowered construction costs, to improved wound dressing, to inspiration of thousands of consumer products [16-18].

To accurately mimic this system, we must first identify the chemical mechanisms within frog tongue mucus that provide consistent adhesion over an entire lifespan. Recent work has visually observed that, in response to the high strain applied by a frog’s tongue

during adhesion and retraction, fibrils form within the mucus [12, 19]. However, the chemical structure of mucus at the interface before and after fibril formation is unknown [15, 19]. Therefore, it is necessary to determine what chemical groups are active at the mucus interface and if fibrils are formed. If fibril formation is the key mechanism in frog tongue adhesion, then it is also important to extract a precise structure of these fibrils. With this information, a more precise model of frog tongue adhesion can be distinguished.

As with frog tongues, insect foot adhesion is a phenomenon that has puzzled humans for centuries. Insects exhibit adhesive forces much larger than their body weight while traversing seamlessly across smooth, rough, vertical, inverted hydrophobic and hydrophilic surfaces [9, 20-23]. Like geckos, insects possess feet which are covered in hair-like microstructures known as setae [23]. This fact follows the concept that, by splitting contact with a surface from a single, flat foot (with radius R) to millions of tiny setae (with radius $R/\sqrt{n}$), Van der Waals adhesive forces are amplified by $\sqrt{n}$ [24]. However, unlike geckos, insects secrete a small amount of fluid from their foot pads, which mediates contact between setae and substrate and further enhances adhesive strength [25, 26]. Recently, biologists have carefully classified the hierarchal structure of insect feet and measured and compared the adhesive forces they generate on different types of surfaces [20, 21, 27, 28]. Insects generated significantly higher traction pull-off and traction forces when the fluid was present versus when it was removed [21]. However, the mechanism that allows this fluid to aid adhesion is still not understood.

For example, the adhesive system of the seven-spotted ladybird beetle (*Coccinella septempunctata*) has been thoroughly investigated [21, 29-31]. It is known that these beetles adhere better on hydrophilic surfaces than hydrophobic ones and have a fluid comprised of hydrocarbons, fatty acids, sugars and alcohols [21, 29]. Furthermore, the adhesive force generated by this system is sensitive to manipulation or loss of chemical components within the fluid [21]. However, these experiments have been limited to studying macro effects of fluid or substrate changes, while clearly suggesting that chemical mechanisms at the adhesive interface are responsible. Therefore, determination of interactions and dynamics of molecules at the adhesive fluid-substrate

interface is necessary to explain biologists' kinematic observations. From this, the function of the fluid in the overall success of insect foot adhesion can be determined.

Each of these adhesive systems is highly unique; however, they share the general characteristic of utilizing a chemically complex fluid to enhance and terminate adhesion at will over many cycles without diminishing ability. Furthermore, they are each the subject of ongoing debate regarding the precise physical and chemical mechanisms that allow them to enhance the adhesive abilities of the animal [12, 20, 32-34]. Fluid-mediated adhesive systems are poorly understood for obvious reasons; whereas dry systems rely primarily on promotion of Van der Waals adhesive forces and can be studied in-situ in a straightforward manner, wet systems provide additional factors - capillary effects, viscoelastic properties and chemical interactions - all of which must often be considered at multiple contact interfaces. Traditionally, these systems are studied using kinematic tools, such as friction force tests, traction force tests, and viscometry, or bulk chemical tools, such as gas chromatography/mass spectrometry [9, 12, 19-21, 32, 35-38]. These methods are useful for measuring the tenacity of wet adhesives on a variety of surfaces, as well as explaining the importance of a fluid layer in enhancing adhesive forces. However, these methods only investigate causal relationships between adhesive fluid and substrate – they alone cannot determine the chemical mechanisms that govern success or failure of adhesion.

1.2. Objectives

The following studies will utilize a suite of surface specific analytical tools to determine chemical structures, molecular order and overall chemical mechanisms that occur at the surface of both frog sticky-tongue and insect foot adhesion. For example, one technique is sum frequency generation vibration spectroscopy (SFG), an interface specific spectroscopic technique capable of providing molecular level information with sub-monolayer sensitivity. Using SFG - and other techniques - that provide information about molecular structure at the adhesive interface, we can compare these structures to known models from other systems. For instance, frog mucus fibrils have not been examined with surface analytical techniques, but fibrils have been in the context of biological protein aggregation [39, 40]. Likewise, oily, multicomponent fluids have been

studied with SFG and complementary techniques to determine the structure and function of lipid monolayers [41]. By comparing the experimentally determined chemical adhesive mechanisms to those of other systems and to the kinematic experiments previously performed by biologists, the goal of this research is to generate governing models of frog tongue and insect foot adhesion. With these insights, a simple, biomimetic insect adhesive is then formulated and tested with surface analytical and kinematic tools to gain a more complex understanding of how natural insect adhesives function.

Specific Aim 1 – Investigate the role of mucus fibril formation in the frog sticky-tongue mechanism using complimentary surface analytical tools.

Hypothesis - Complimentary surface analytical techniques will demonstrate that frog sticky-tongue mucus-air surface consists primarily of glycoproteins which fibrillate under the strain of tongue adhesion to act as a pressure sensitive adhesive.

Methodology – NEXAFS imaging and SFG spectroscopy are applied to the characterization of mucus molecules at the surface as well as order and relative orientation of molecular bonds. With this we can determine how the structure of surface mucus molecules respond to prey-capture and generate temporary but large magnitude adhesive forces. This work can be found in Chapter 3.

Specific Aim 2 – Identify the effect of varying substrate chemistry on interfacially active molecular groups in ladybird beetle tarsal adhesive fluid.

Hypothesis - Insect adhesive fluid is a chemically complex mixture of natural molecules with varying wetting properties; thus, the chemistry of the adhesive fluid-substrate interface will change dynamically with changes in substrate hydrophobicity.

Methodology – SFG spectroscopy is used to investigate the presence of ordered vibrational modes at the fluid-substrate interface for set of substrates with substantially different water contact angles. The ordering ratio of hydrocarbons at each interface is calculated and compared to the traction force generated by beetles on similar substrates. This work can be found in Chapter 4.

Specific Aim 3 – Formulate a simple, biomimetic insect adhesive to determine the mechanisms allowing natural insect adhesive to aid foot adhesion on most surfaces.

Hypothesis - Based upon our characterizations of natural ladybird beetle adhesive fluid, we predict that the interfacial chemistry of the biomimetic fluid is not affected by varying substrate chemistry. Furthermore, we hypothesize that organization of the consistent hydrocarbon layer at the interface is influenced by the surface-inactive components of the adhesive fluid such that these molecules form a bulk fluid structure which constrains surface hydrocarbons. This structure is responsible for maintaining a necessary amount of adhesive force in the pull-off direction, as well as enhancing traction forces and aiding lubrication of the foot to assist with climbing.

Methodology – A three component (squalane, stearic acid, water) adhesive fluid is formulated as a water-in-oil emulsion. The adhesive is characterized with several tools to determine particle size, viscosity and adhesive forces. SFG spectroscopy is also utilized to determine the presence of ordered molecular bonds at the surface of PS and PEO thin film substrates for comparison with natural beetle adhesive. Spectra of squalane and squalane/stearic acid solutions are also collected to reveal the effect of surface-inactive components of adhesive on the organization of interfacially-active molecules. This work can be found in Chapter 5.

1.3 References

[1] He, B., Wang, Z., Li, M., Wang, K., Shen, R. & Hu, S. 2014 Wet Adhesion Inspired Bionic Climbing Robot. *Ieee-Asme Transactions on Mechatronics* **19**, 312-320. (doi:10.1109/tmech.2012.2234473).

[2] Favi, P.M., Yi, S., Lenaghan, S.C., Xia, L. & Zhang, M. 2014 Inspiration from the natural world: from bio-adhesives to bio-inspired adhesives. *Journal of Adhesion Science and Technology* **28**, 290-319. (doi:10.1080/01694243.2012.691809).

[3] Autumn, K. & Gravish, N. 2008 Gecko adhesion: evolutionary nanotechnology. *Philosophical Transactions of the Royal Society of London A: Mathematical, Physical and Engineering Sciences* **366**, 1575-1590.

[4] Irschick, D.J., Crosby, A.J. & Federle, W. 2013 The evolution of Gecko adhesion: An integrative perspective. *Integrative and Comparative Biology* **53**, E100-E100.

[5] Autumn, K. 2006 How Gecko Toes Stick The powerful, fantastic adhesive used by geckos is made of nanoscale hairs that engage tiny forces, inspiring envy among human imitators. *American scientist* **94**, 124-132.

[6] Gao, H., Wang, X., Yao, H., Gorb, S. & Arzt, E. 2005 Mechanics of hierarchical adhesion structures of geckos. *Mechanics of Materials* **37**, 275-285.

[7] Smith, A.M. & Morin, M.C. 2002 Biochemical differences between trail mucus and adhesive mucus from marsh periwinkle snails. *The Biological Bulletin* **203**, 338-346.

[8] Dalsin, J.L. & Hu, B.H. 2003 Mussel adhesive protein mimetic polymers for the preparation of nonfouling surfaces. *Journal of the American …*, 4253-4258.

[9] Dirks, J.-H. & Federle, W. 2011 Fluid-based adhesion in insects - principles and challenges. *Soft Matter* **7**, 11047-11053. (doi:10.1039/c1sm06269g).

[10] Walker, G. 1993 Adhesion to smooth surfaces by insects—a review. *International Journal of Adhesion and Adhesives* **13**, 6-10.

[11] Autumn, K., Dittmore, A., Santos, D., Spenko, M. & Cutkosky, M. 2006 Frictional adhesion: a new angle on gecko attachment. *Journal of Experimental Biology* **209**, 3569-3579.

[12] Kleinteich, T. & Gorb, S.N. 2015 Frog tongue acts as muscle-powered adhesive tape. *Open Science* **2**, 150333.

[13] Vogel, M.J. & Steen, P.H. 2010 Capillarity-based switchable adhesion. *Proceedings of the National Academy of Sciences* **107**, 3377-3381.

[14] Nishikawa, K.C. & Cannatella, D. 1991 Kinematics of prey capture in the tailed frog Ascaphus truei (Anura: Ascaphidae). *Zoological journal of the Linnean Society* **103**, 289-307.

[15] Noel, A.C., Guo, H.-Y., Mandica, M. & Hu, D.L. 2017 Frogs use a viscoelastic tongue and non-Newtonian saliva to catch prey. *Journal of The Royal Society Interface* **14**, 20160764.

[16] Lal, N., Yadav, P., Rastogi, V., Verma, A. & Verma, N. 2017 Aspects of Pressure Sensitive Adhesives in Fabricating Drug-in-Adhesive Transdermal Therapeutic Systems. *Drug Delivery Letters* **7**, 3-15.

[17] Baek, S.-S. & Hwang, S.-H. 2017 Preparation of biomass-based transparent pressure sensitive adhesives for optically clear adhesive and their adhesion performance. *European Polymer Journal* **92**, 97-104.

[18] Fukuta, S., Ogawa, K., Nomura, M., Yamasaki, M. & Sasaki, Y. 2017 Shear properties of metal-free wooden load-bearing walls using plywood jointed with a combination of adhesive tape and wood dowels. *European Journal of Wood and Wood Products* **75**, 429-437.

[19] Kleinteich, T. & Gorb, S.N. 2014 Tongue adhesion in the horned frog Ceratophrys sp. *Scientific reports* **4**, 5225-5225. (doi:10.1038/srep05225).

[20] England, M.W., Sato, T., Yagihashi, M., Hozumi, A., Gorb, S.N. & Gorb, E.V. 2016 Surface roughness rather than surface chemistry essentially affects insect adhesion. *Beilstein Journal of Nanotechnology* **7**, 1471-1479.

[21] Gorb, E.V., Hosoda, N., Miksch, C. & Gorb, S.N. 2010 Slippery pores: anti-adhesive effect of nanoporous substrates on the beetle attachment system. *Journal of the Royal Society, Interface / the Royal Society* **7**, 1571-1579. (doi:10.1098/rsif.2010.0081).

[22] Federle, W., Riehle, M., Curtis, A.S.G. & Full, R.J. 2002 An integrative study of insect adhesion: mechanics and wet adhesion of pretarsal pads in ants. *Integrative and comparative biology* **42**, 1100-1106. (doi:10.1093/icb/42.6.1100).

[23] Arzt, E., Gorb, S. & Spolenak, R. 2003 From micro to nano contacts in biological attachment devices. *Proceedings of the National Academy of Sciences* **100**, 10603-10606.

[24] Spolenak, R., Gorb, S., Gao, H. & Arzt, E. 2005 Effects of contact shape on the scaling of biological attachments. *Proceedings of the Royal Society A: Mathematical, Physical and Engineering Sciences* **461**, 305-319. (doi:10.1098/rspa.2004.1326).

[25] Dirks, J.-H., Clemente, C.J. & Federle, W. 2010 Insect tricks: two-phasic foot pad secretion prevents slipping. *Journal of the Royal Society Interface* **7**, 587-593. (doi:10.1098/rsif.2009.0308).

[26] Gerhardt, H., Betz, O., Albert, K. & Lämmerhofer, M. 2016 Insect Adhesion Secretions: Similarities and Dissimilarities in Hydrocarbon Profiles of Tarsi and Corresponding Tibiae. *Journal of chemical ecology* **42**, 725-738.

[27] Gorb, E. & Gorb, S. 2002 Attachment ability of the beetle Chrysolina fastuosa on various plant surfaces. *Entomologia Experimentalis et Applicata* **105**, 13-28.

[28] Gorb, E., Voigt, D., Eigenbrode, S.D. & Gorb, S. 2008 Attachment force of the beetle Cryptolaemus montrouzieri (Coleoptera, Coccinellidae) on leaflet surfaces of mutants of the pea Pisum sativum (Fabaceae) with regular and reduced wax coverage. *Arthropod-Plant Interactions* **2**, 247-259.

[29] Geiselhardt, S.F., Geiselhardt, S. & Peschke, K. 2011 Congruence of epicuticular hydrocarbons and tarsal secretions as a principle in beetles. *Chemoecology* **21**, 181.

[30] Peisker, H. & Gorb, S.N. 2012 Evaporation dynamics of tarsal liquid footprints in flies (Calliphora vicina)and beetles (Coccinella septempunctata). *The Journal of experimental biology* **215**, 1266-1271. (doi:10.1242/jeb.065722).

[31] Hosoda, N. & Gorb, S.N. 2012 Underwater locomotion in a terrestrial beetle: combination of surface de-wetting and capillary forces. *Proceedings of the Royal Society of London B: Biological Sciences* **279**, 4236-4242.

[32] Noel, A.C., Guo, H.-Y., Mandica, M. & Hu, D.L. 2017 Frogs use a viscoelastic tongue and non-Newtonian saliva to catch prey. *Journal of The Royal Society Interface* **14**. (doi:10.1098/rsif.2016.0764).

[33] Betz, O., Frenzel, M., Steiner, M., Vogt, M., Kleemeier, M., Hartwig, A., Sampalla, B., Rupp, F., Boley, M. & Schmitt, C. 2017 Adhesion and friction of the smooth attachment system of the cockroach Gromphadorhina portentosa and the influence of the application of fluid adhesives. *Biology Open* **6**, 589-601. (doi:10.1242/bio.024620).

[34] Dirks, J.H. 2010 Insect tricks: two-phasic foot pad secretion prevents slipping. *Journal of The …*, 587-593.

[35] Zhou, Y., Robinson, A., Steiner, U. & Federle, W. 2014 Insect adhesion on rough surfaces: analysis of adhesive contact of smooth and hairy pads on transparent microstructured substrates. *Journal of the Royal Society Interface* **11**. (doi:10.1098/rsif.2014.0499).

[36] Geiselhardt, S.F., Federle, W., Prüm, B., Geiselhardt, S., Lamm, S. & Peschke, K. 2010 Impact of chemical manipulation of tarsal liquids on attachment in the Colorado potato beetle, Leptinotarsa decemlineata. *Journal of insect physiology* **56**, 398-404.

[37] Vötsch, W., Nicholson, G., Müller, R., Stierhof, Y.D., Gorb, S. & Schwarz, U. 2002 Chemical composition of the attachment pad secretion of the locust Locusta migratoria. *Insect biochemistry and molecular biology* **32**, 1605-1613.

[38] Peisker, H., Heepe, L., Kovalev, A.E. & Gorb, S.N. 2014 Comparative study of the fluid viscosity in tarsal hairy attachment systems of flies and beetles. *Journal of the Royal Society Interface* **11**. (doi:10.1098/rsif.2014.0752).

[39] Weidner, T. & Castner, D.G. 2013 SFG analysis of surface bound proteins: a route towards structure determination. *Physical chemistry chemical physics : PCCP* **15**, 12516-12524. (doi:10.1039/c3cp50880c).

[40] Baio, J.E., Weidner, T., Samuel, N.T., McCrea, K., Baugh, L., Stayton, P.S. & Castner, D.G. 2010 Multitechnique characterization of adsorbed peptide and protein orientation: LK3(10) and Protein G B1. *Journal of Vacuum Science & Technology B* **28**, C5D1-C5D8. (doi:10.1116/1.3456176).

[41] Roke, S., Schins, J., Müller, M. & Bonn, M. 2003 Vibrational spectroscopic investigation of the phase diagram of a biomimetic lipid monolayer. *Physical review letters* **90**, 128101.

Chapter 2 - Materials and Methods

2.1 Experimental Design

Contamination is one of the greatest challenges in surface science. Surface analytical techniques are often sensitive down to single molecular monolayers, which means that any undesired molecules on sample surface have the potential to affect the accuracy of measurements. To ensure that all surfaces prepared for analysis were free of contaminants such as previous sample fluid or advantageous carbon, a rigorous cleaning procedure was established which generally involved successive sonication of substrates in dicholoromethane, acetone and ethanol and storage under inert atmosphere.

In insect tarsal adhesive experiments, substrate wettability was modified by spin coating and annealing thin films of deuterated or non-deuterated polymers. These surfaces needed to be characterized for hydrophobicity, film thickness and film roughness to ensure repeatability of surface analytical measurements. Water contact angle was a quick, cheap and well-established metric to evaluate a sample surface's hydrophobicity.

The foundation behind water contact angle (Θ_c) is Young's equation [1], which relates the equilibrium surface tensions of a drop of liquid (L) on a solid surface (S) in an inert atmosphere (G) as follows:

$$\gamma_{SG} - \gamma_{SL} - \gamma_{LG}cos(\Theta c) = 0$$

When the liquid drop is water, it is straightforward to relate substrate hydrophobicity to measured contact angle, with values less than 90° indicating a hydrophilic surface and values above 90° indicating a hydrophobic surface [2]. For our natural and biomimetic insect adhesive experiments, the two polymers were chosen to spin thin films onto CaF_2 windows to create one hydrophilic and one hydrophobic surface based upon known properties of the polymers. Despite the well-characterized nature of these polymers in literature [3-5] it was important to determine the water contact angle of our sample films due to known effects of film thickness and film roughness on the measured angle [6].

Profilometry was a simple way to measure film thickness and was done by rastering a stylus across the film surface from a base (substrate) height while optically sensing the deflection of the stylus to determine the change in height from substrate to film [7]. It has been shown that polymer films which are greater than several hundred nanometers can affect the intensity of SFG signal, thus it was important to maintain thin films throughout SFG experiments [8].

To determine film roughness, Atomic force microscopy (AFM) operated in tapping mode, was used to generate of a topographical map of the polymer film surface over a small area. The root mean square (RMS) roughness of the surface was then determined. In the following studies, only smooth surfaces were desired because surface roughness has been shown to have a significant effect on insect tarsal adhesion [9, 10]. Study of insect adhesion on smooth and rough surfaces indicated that surfaces with RMS roughness above ~3 nm exhibited this effect and were considered “rough” [9]. This established a baseline for the following studies.

2.3 Fluid Characterization Techniques

Traditional characterization of natural adhesives has focused on bulk analysis techniques, such as rheometry, adhesive force measurement, and mass spectrometry [11-13]. In this work, the primary aim was to demonstrate that surface specific analysis techniques can determine precise chemical mechanisms at the contact interface and then apply this toolset to two natural adhesive mechanisms of interest. The two surface analytical techniques utilized herein were NEXAFS and SFG spectroscopy.

NEXAFS spectroscopy can provide detailed molecular bonding information for a surface layer of molecules [14]. In principal, NEXAFS works by exposing a sample to polarized x-rays from a synchrotron source which leads to energy absorption within the sample surface. Excited electrons in the sample surface are excited up to unoccupied molecular orbitals and these holes are filled by electrons from higher energy levels leading to an emission of auger electrons and photons. The inelastic scattering of electrons from deeper within the sample leads to an effective sampling depth of ~10 nm, although it is often closer to 3-5 nm. The tunability and high resolution of synchrotron x-rays allows for investigation of multiple absorption edges (I.E. C, N, O K-edge) and

determination of small changes in structure via tracking changes in the absorption energy [14-17].

Following absorption intensity as the angle of the sample with respect to the x-ray beam is varied allows for determination of bond orientation [18-20]. Several studies have shown that the higher order structure of molecules such as proteins, which have characteristic amide backbone bonds and amino acid side chains, can be determined by comparing the absorption intensity between high angle and low angle incident x-ray absorption [21, 22]. For instance, the π* orbital of amide N-C=O backbone bonds is oriented in a “dumbbell shape” pointed perpendicularly from the bond [22]. Thus, the orientation of a set of amide bonds can be determined by following the absorption intensity of this orbital with varying x-ray angle. Furthermore, secondary and tertiary protein structure leads to well-defined distributions of these π* orbitals, which can be similarly observed with NEXAFS.

Finally, modification of this technique to include imaging allows for the creation of a surface map of molecular bonds across a region of interest [16, 20, 23]. This is achieved by rastering the incident x-ray beam across the sample surface and recording absorption edge spectrum at each point. This generates an image wherein each pixel is a set of NEXAFS spectra. Thereby, observation of significant changes in bond distribution or orientation across the sample surface is enabled. For detailed information about the NEXAFS setup used in this work, please refer to Chapter 3.

SFG is a second-order, nonlinear vibrational spectroscopy capable of detecting the order of vibrational modes at sub-μM concentrations. SFG is sensitive to both infrared and Raman modes, therefore the principle physics of both FTIR and Raman spectroscopy are highly relevant. FTIR is a linear vibrational spectroscopy, where a tunable infrared photons excite vibrational modes in a sample and the resulting spectrum is a direct function of the type of vibrational modes excited and the number of these modes present [24]. Raman spectroscopy involves the scattering of a photon via collision with a surface, in which the energy of the scattered photon is correlated to individual vibrational modes in the sample [25].

On the other hand, SFG involves the use of three photons. A fixed visible source is overlapped in space and time with a tunable IR source at the interface of interest. When the sum of the frequencies of these two sources matches the vibrational energy of a mode at that interface a third photon is reflected, which is known as the SFG photon. This photon reflection is tied to a change in the second order nonlinear susceptibility $X^{(2)}$ which is related to the sample vibrational modes by the following equation

$$\chi_{\mathrm{eff}}^{(2)} = \chi_{\mathrm{nr}} + \sum_{\mathrm{q}} \frac{\mathrm{A_q}}{\omega_2 - \omega_{\mathrm{q}} + \mathrm{i}\Gamma_{\mathrm{q}}}$$

Defined by the non-resonant phase, non-resonant background (χ_{nr}), location (ω_q), individual peak full width half maximum (FWHM; Γ_q) and individual peak amplitude (A_q). The selection rules of SFG are such that no signal is generated when inversion symmetry exists, however this is always true at surfaces [26].

SFG signal is only generated when ordered vibrational modes exist at the interface. Furthermore, changing the polarization of the incident and SFG beams allows for the determination of the orientation of a layer of molecules at the interface. For example, in this work spectra of a layer of alkane chains will be compared between SSP and PPP polarization combinations. It has been shown that a well-organized layer of alkane chains with tilt angles perpendicular to the surface will produce spectra where the amplitude of some modes (CH_3 symmetric, CH_2 symmetric) are more intense in SSP, while other modes (CH_2 asymmetric, CH_3 asymmetric) are more intense in PPP polarization combination [20, 27-29]. For detailed information about the SFG setup used in this work, please refer to Chapters 3, 4 and 5.

2.3 References

[1] Adam, N. 1957 Use of the term ‘Young's Equation’for contact angles. *Nature* **180**, 809.

[2] Chaudhury, M.K. & Whitesides, G.M. 1992 Correlation between surface free energy and surface constitution. *Science* **255**, 1230-1232.

[3] Yang, C.S.C., Wilson, P.T. & Richter, L.J. 2004 Structure of Polystyrene at the Interface with Various Liquids. *Macromolecules* **37**, 7742-7746. (doi:10.1021/ma049692s).

[4] Li, Y., Pham, J.Q., Johnston, K.P. & Green, P.F. 2007 Contact angle of water on polystyrene thin films: Effects of CO2 environment and film thickness. *Langmuir* **23**, 9785-9793.

[5] Van Oss, C., Arnold, K., Good, R., Gawrisch, K. & Ohki, S. 1990 Interfacial tension and the osmotic pressure of solutions of polar polymers. *Journal of Macromolecular Science-Chemistry* **27**, 563-580.

[6] Morra, M., Occhiello, E. & Garbassi, F. 1990 Knowledge about polymer surfaces from contact angle measurements. *Advances in Colloid and Interface Science* **32**, 79-116.

[7] Gupta, S.A. & Gupta, R.K. 1998 A parametric study of spin coating over topography. *Industrial & engineering chemistry research* **37**, 2223-2227.

[8] Gracias, D., Chen, Z., Shen, Y. & Somorjai, G. 1999 Molecular characterization of polymer and polymer blend surfaces. Combined sum frequency generation surface vibrational spectroscopy and scanning force microscopy studies. *Accounts of chemical research* **32**, 930-940.

[9] England, M.W., Sato, T., Yagihashi, M., Hozumi, A., Gorb, S.N. & Gorb, E.V. 2016 Surface roughness rather than surface chemistry essentially affects insect adhesion. *Beilstein Journal of Nanotechnology* **7**, 1471-1479.

[10] Gorb, E.V., Hosoda, N., Miksch, C. & Gorb, S.N. 2010 Slippery pores: anti-adhesive effect of nanoporous substrates on the beetle attachment system. *Journal of the Royal Society, Interface / the Royal Society* **7**, 1571-1579. (doi:10.1098/rsif.2010.0081).

[11] Peisker, H. & Gorb, S.N. 2012 Evaporation dynamics of tarsal liquid footprints in flies (Calliphora vicina)and beetles (Coccinella septempunctata). *The Journal of experimental biology* **215**, 1266-1271. (doi:10.1242/jeb.065722).

[12] Scherge, M., Gorb, S. & Gorb, S.N. 2001 *Biological micro-and nanotribology*, Springer Science & Business Media.

[13] Peisker, H., Heepe, L., Kovalev, A.E. & Gorb, S.N. 2014 Comparative study of the fluid viscosity in tarsal hairy attachment systems of flies and beetles. *Journal of the Royal Society Interface* **11**. (doi:10.1098/rsif.2014.0752).

[14] Stöhr, J. 2013 *NEXAFS spectroscopy*, Springer Science & Business Media.

[15] Gainar, A., Stevens, J.S., Jaye, C., Fischer, D.A. & Schroeder, S.L. 2015 NEXAFS Sensitivity to Bond Lengths in Complex Molecular Materials: A Study of Crystalline Saccharides. *The Journal of Physical Chemistry B* **119**, 14373-14381.

[16] Baio, J.E., Jaye, C., Fischer, D.A. & Weidner, T. 2013 Multiplexed Orientation and Structure Analysis by Imaging Near-Edge X-ray Absorption Fine Structure (MOSAIX) for Combinatorial Surface Science. *Analytical chemistry* **85**, 4307-4310.

[17] Zubavichus, Y., Shaporenko, A., Grunze, M. & Zharnikov, M. 2007 NEXAFS spectroscopy of homopolypeptides at all relevant absorption edges: Polyisoleucine, polytyrosine, and polyhistidine. *The Journal of Physical Chemistry B* **111**, 9803-9807.

[18] Baio, J.E., Weidner, T., Baugh, L., Gamble, L.J., Stayton, P.S. & Castner, D.G. 2012 Probing the orientation of electrostatically immobilized Protein G B1 by time-of-flight secondary ion spectrometry, sum frequency generation, and near-edge X-ray adsorption fine structure spectroscopy. *Langmuir : the ACS journal of surfaces and colloids* **28**, 2107-2112. (doi:10.1021/la203907t).

[19] Weidner, T., Apte, J.S., Gamble, L.J. & Castner, D.G. 2010 Probing the Orientation and Conformation of alpha-Helix and beta-Strand Model Peptides on Self-Assembled Monolayers Using Sum Frequency Generation and NEXAFS Spectroscopy. *Langmuir* **26**, 3433-3440. (doi:10.1021/la903267x).

[20] Baio, J.E., Spinner, M., Jaye, C., Fischer, D.A., Gorb, S.N. & Weidner, T. 2015 Evidence of a molecular boundary lubricant at snakeskin surfaces. *Journal of The Royal Society Interface* **12**. (doi:10.1098/rsif.2015.0817).

[21] Baugh, L., Weidner, T., Baio, J.E., Nguyen, P.C.T., Gamble, L.J., Slayton, P.S. & Castner, D.G. 2010 Probing the Orientation of Surface-Immobilized Protein G B1 Using ToF-SIMS, Sum Frequency Generation, and NEXAFS Spectroscopy. *Langmuir* **26**, 16434-16441. (doi:10.1021/la1007389).

[22] Baio, J.E., Weidner, T., Samuel, N.T., McCrea, K., Baugh, L., Stayton, P.S. & Castner, D.G. 2010 Multitechnique characterization of adsorbed peptide and protein orientation: LK3(10) and Protein G B1. *Journal of Vacuum Science & Technology B* **28**, C5D1-C5D8. (doi:10.1116/1.3456176).

[23] Baio, J.E., Jaye, C., Fischer, D.A. & Weidner, T. 2014 High-throughput analysis of molecular orientation on surfaces by NEXAFS imaging of curved sample arrays. *ACS combinatorial science* **16**, 449-453.

[24] Lewis, S.P., Lewis, A.T. & Lewis, P.D. 2013 Prediction of glycoprotein secondary structure using ATR-FTIR. *Vibrational Spectroscopy* **69**, 21-29. (doi:http://dx.doi.org/10.1016/j.vibspec.2013.09.001).

[25] Davies, H.S., Singh, P., Deckert-Gaudig, T., Deckert, V., Rousseau, K., Ridley, C.E., Dowd, S.E., Doig, A.J., Pudney, P.D. & Thornton, D.J. 2016 Secondary Structure and Glycosylation of Mucus Glycoproteins by Raman Spectroscopies. *Analytical chemistry* **88**, 11609-11615.

[26] Shen, Y.-R. 1984 The principles of nonlinear optics. *New York, Wiley-Interscience, 1984, 575 p.*

[27] Chen, X., Wang, J., Kristalyn, C.B. & Chen, Z. 2007 Real-Time Structural Investigation of a Lipid Bilayer during Its Interaction with Melittin Using Sum Frequency Generation Vibrational Spectroscopy. *Biophysical Journal* **93**, 866-875. (doi:10.1529/biophysj.106.099739).

[28] Ma, G. & Allen, H.C. 2006 DPPC Langmuir monolayer at the air-water interface: Probing the tail and head groups by vibrational sum frequency generation spectroscopy. *Langmuir*, 5341-5349.

[29] Himmelhaus, M., Eisert, F., Buck, M. & Grunze, M. 2000 Self-assembly of n-alkanethiol monolayers. A study by IR-visible sum frequency spectroscopy (SFG). *The Journal of Physical Chemistry B* **104**, 576-584.

Chapter 3. Coming Together Under Pressure - Using Surface Analytical Tools to Dissect the Role of Fibril Formation in the Frog Sticky-Tongue Mechanism

J Elliott Fowler[1], Thomas Kleinteich[2], Johannes Franz[3], Cherno Jaye[4], Daniel A. Fischer[4], Tobias Weidner[3,5], Stanislav Gorb[2], Joe E. Baio[1]

[1]Oregon State University, Chemical, Biological and Environmental Engineering Department, Corvallis, OR;

[2]Zoological Institute of the University of Kiel, Department of Functional Morphology and Biomechanics, Kiel, Germany;

[3]Max Planck Institute for Polymer Research, Mainz, Germany;

[4]National Institute of Standards and Technology, Gaithersburg, MD, USA;

[5]Department of Chemistry, Aarhus University, Aarhus, Denmark

Key Words: Frog Tongue Mucus, Mucin, Adhesion, Fibril Formation, NEXAFS Spectroscopy, SFG Spectroscopy

Abstract

In the blink of an eye, frogs capture their prey with a highly-specialized tongue. Recent studies indicate this tongue is covered with a fibril-forming mucus that acts as a pressure sensitive adhesive. However, no chemical structure analysis of frog tongue mucus has been performed to validate this mechanism. Thus, the goal of this experiment is to examine the chemical structure of surface mucus layers, after a tongue strike, with complimentary surface analytical tools. Previous studies of mucus from other animals suggests that mucus from a frog's tongue consists of mucins - serine, threonine and proline rich glycoproteins. Therefore, we expect to observe chemical bonds associated with glycoproteins, as well as fibrils formed at the mucus-tongue interface. To test this hypothesis, we collected both near-edge x-ray absorption fine structure (NEXAFS) microscopy images and sum frequency generation (SFG) vibrational spectra from layers

of mucus left after frog tongue strikes on cleaned glass slides. NEXAFS imaging demonstrates a uniform distribution of amide, hydroxyl and carbon-carbon bonds across the mucus surface. Difference spectra of individual N1s and C1s K-edge spectra pulled from these images indicate structure consistent with fibril formation as well as disorder of oligosaccharide groups near the mucus surface. C-H region SFG spectra reveal surface active modes which likely stem from serine and threonine within the mucin protein. Combined, this work suggests that glycoproteins are well-ordered at the mucus-tongue interface.

3.1 Introduction

The rapid projection and retraction of a frog's tongue in the prey capture process is one of its most iconic traits. Frogs have a specialized tongue, outfitted with powerful muscles and a papilla coated surface, which is capable of capturing prey with a force that can exceed their own body weight [1-3]. This sticky-tongue mechanism has been described as a pressure sensitive adhesive due to its ability to generate large adhesive forces in response to the high strain of retraction [2]. Furthermore, mucus coating the tongue has been identified as a vital component of the adhesive mechanism [1-3].

Many animals utilize mucus for biological functions; however, mucus is not inherently an adhesive in its natural state. For instance, analysis of the marsh periwinkle snail indicated use of two chemically distinct types of mucus – one adhesive and one non-adhesive [4-6]. Additionally, some animals utilize mucus for multiple adhesive tasks which have no mechanistic connection. This is true for frogs, whose feet are coated in a mucus that allows for maximization of toe contact with a substrate [7, 8]. However, this adhesion is reversed through use of a peeling motion - which is entirely dissimilar from their sticky-tongue mechanism. These examples make it clear that mucus-mediated adhesion is a complex process and, in each case, physical and chemical factors may be important.

While physical analysis of the sticky-tongue mechanism has been explored recently, there has been no chemical analysis of this mechanism. What is known is that mucus of other, well-studied animals consists primarily of mucins regardless of adhesiveness [4, 9, 10]. Mucins are a class of glycoproteins comprised of cysteine rich ends and a serine, threonine and proline rich core, conjugated with O- and N-linked

saccharide chains in a bottle-brush formation [9, 10]. Additionally, they can form large, mesh-like tertiary structures through cysteine disulfide bonding of nearby linear, polymeric chains [10, 11]. However, they are primarily shown to be random coil clusters in solution [12]. Furthermore, recent study of bovine submaxillary mucin secondary structure with attenuated total reflectance - Fourier transform infrared spectroscopy reveals that mucins adopt a random coil, beta sheet, beta turn pattern in dried films; although, random coil is the predominant structure of the three [13]. The assignment of unordered or random coil secondary structure for mucins in solution and dried films is widely agreed upon in literature [13-15].

A recent study aimed at visualizing the adhesion and detachment process found that frogs pull their tongues perpendicularly from surface (or prey) during retraction [1]. This led to a visual observation of fibril formation within the mucus between the tongue and surface [Figure 3.1a]. Since mucins are found naturally to form linear polymeric chains with disordered or random coil secondary and tertiary structures, fibril formation indicates an induced change in mucus chemical structure during tongue retraction. Fibril formation may allow for tongue mucus to generate strain-responsive adhesive forces by acting as a shock absorber for the tongue. This phenomenon of storing energy within a fluid in response to a large applied force is commonly known as viscous dissipation.

Protein fibrils have a well-defined chemical structure; however, the chemical structure of frog tongue mucus has yet to be studied for comparison [16-18]. Additionally, fibril formation is occurring only at the interface between mucus and tongue. This makes bulk techniques poorly suited for interfacial mucus chemical structure analysis important in this mechanism. Therefore, we used surface analytical techniques, which are capable of probing both chemical structure and molecular order specifically within surface or interfacial layers. Utilizing these techniques, we expected to observe chemical structure associated with glycoproteins, as well as evidence of fibrils formed at the mucus-tongue interface – thus verifying the pressure sensitive adhesive hypothesis [Figure 3.1b]. To test this hypothesis, we collected Near-Edge X-Ray Absorption Fine Structure (NEXAFS) microscopy images and Sum Frequency Generation Spectroscopy (SFG) spectra from layers of mucus left after frog tongue strikes on cleaned glass slides. NEXAFS

microscopy imaging interrogated chemical bond orbital orientation and molecular structure across the region of interest but within only the top 10 nm of the mucus surface. SFG spectroscopy examined ordered, infrared active vibrational modes at the surface with the capability of sub-monolayer sensitivity. This combination of techniques has recently been used to classify the outermost skin layer of snakes [19]. Therefore, we can identify the primary, secondary and tertiary chemical structure of the surface mucus layers from NEXAFS and SFG spectra.

3.2 Methods

3.2.1 Tongue Mucus Collection

Tongue mucus collection was performed for three adult horned frogs (Anura: Ceratophryidae: Ceratophrys sp.) which were captive bred and housed separately in 26-29° C temperatures during the day and 24-26°C at night. Terrariums were kept a relative humidity of 70-80% and substrate-filled to a depth of roughly 5 cm, such that the frogs could bury themselves - a characteristic trait of this genus [1]. Tongue strikes were induced during the normal feeding period of the frogs, with only one strike per individual. This was done by placing glass microscopy slides, which were cleaned by sonication in successive solutions of dichloromethane, acetone and ethanol, approximately 5 cm in front of the semi-buried frogs and holding a cricket directly behind the slide. Strikes were collected on the slides as the frogs attempted to capture the cricket. The struck slides were placed in a petri-dish and sealed under inert atmosphere until data collection.

3.2.2 NEXAFS Microscopy Imaging

NEXAFS microscopy images were collected at the C_{1s} and N_{1s} K-edges on the parallel processing imaging system at the NIST U7A beamline at the National Synchrotron Light Source (NSLS – Brookhaven National Laboratory). A soft x-ray beam (flux ~ 5 x 1010 photons-s^{-1} (0.1% BW)) was rastered across the region of interest and a large area rapid imaging analytical tool (LARIAT, Synchrotron Research Inc.) measured partial electron yield. C1s K-edge scans were collected from 270-340 eV, with a ~0.1 eV resolution, 0.1 eV step size and 2-s dwell time. N1s K-edge scans were collected from 390-430 eV, with a ~0.2 eV resolution, 0.2 eV step size and 3-s dwell time. A full field imaging parallel magnetic field was used to guide any emitted photoelectrons to an

electron yield detector to produce two-dimensional NEXAFS images with 50 μm spatial resolution. The signal and the reference intensities were each divided by the NEXAFS signal of a gold-coated mesh, placed upstream, to adjust for variations in beamline intensity. An electron retardation voltage of 50 eV is used in this experiment, leading to an expected sampling depth of ~4 nm. Samples were mounted to allow rotation with respect to the vertical axis and variation of the angle between the surface of the sample and the synchrotron x-rays [Figure 3.2a]. The NEXAFS angle is the angle between the sample plane and incident electric field. All images and spectra presented here have been pre- and post-edge normalized. Previous experiments on this NEXAFS imaging endstation have demonstrated that it can handle either conducting or insulating samples without charging effects [19-24]. It can be shown that a molecule, or ensemble of atoms, when ordered in a singular plane, contain σ* and/or π* bond orbitals which are likewise oriented in well-defined directions relative to the corresponding atoms. Therefore, if bond orbital order exists in the interrogated region, NEXAFS spectra exhibit peak intensities that vary significantly by x-ray incident angle - commonly referred to as a dichroism - with greater intensity indicative of the orbital of interest oriented towards the incident plane.

3.2.3 SFG Spectroscopy

A Ti:sapphire femtosecond laser oscillator, paired with a regenerative amplifier pumped by a Nd:YLF laser, (Spitfire Ace, Spectra Physics) was used to generate a 4.65 mJ visible beam (pulse duration of 35 fs) centered at 791.8 nm. This amplified visible beam was split into two parts; the first of which was passed through a Fabry-Perot etalon to narrow the pulse spectrally (~15 cm^{-1}) and used as the visible pulse for sum-frequency generation. The second part of the beam was used to pump an optical parametric amplifier (OPA) system (TOPAS, Light Conversion). This generated a tunable IR pulse (3.1 – 6.1 μm) which was passed through a half-wave plate polarizer prior to use as the IR pulse in sum-frequency generation. The IR and visible pulses were overlapped temporally and spatially at the fluid-polymer interface to generate an SFG signal (Figure 3.3a). Correct height is achieved by aligning the visible and IR beams to a gold-coated reference slide and binning the measured signal to include only the SFG generated by the air-print fluid interface. In this study, SFG spectra were collected for three different polarization combinations: SSP (s-polarized SFG, s-polarized visible, p-polarized IR;

respectively), PPP and SPS in the C-H stretching region (2700-3100 cm^{-1}). SFG signal from the sample interface was focused into a spectrograph (Acton, Princeton Instruments) and then dispersed by a grating before being re-focused on an electron multiplying charge coupled device (CCD) camera (Newton, Andor). All spectra were normalized by the IR profile. Fitting was performed following a procedure described previously [19, 25, 26]. Briefly, spectra are iteratively fit to Equation 1 below assuming Lorentzian line-shapes, to determine non-resonant phase, non-resonant background (χ_{nr}), peak location (ω_q), peak full width half maximum (Γ_q) and individual peak amplitude (A_q).

Equation 1 - $$\chi_{eff}^{(2)} = \chi_{nr} + \sum_q \frac{A_q}{\omega - \omega_q + i\Gamma_q}$$

3.3 Results

3.3.1 NEXAFS Microscopy Images and Spectra

NEXAFS microscopy images of the entire tongue mucus print revealed how chemical composition varied spatially at the mucus surface (Supporting Info.). Specifically, we observed changes in emitted electron intensity across the mucus layer at energies corresponding to bond orbitals that can be associated with glycoprotein molecules. While we hypothesized that this layer would consist mostly of glycoprotein mucin, neither technique has ever been used to study whole glycoprotein molecules. Therefore, bond orbital assignments herein were based upon previous classifications of mucin's two primary components: oligosaccharide chains and proteins [Figure 3.2b]. To examine distribution of individual bond orbitals, we created images at energies near 285 eV, 289 eV, 298 eV, 402 eV and 407 eV, corresponding to C=C π*, C-OH σ*, C-C σ*, N-C=O π* and N-CH_2 σ* orbitals respectively [19, 20, 27-30]. While each of these orbitals was present across the entirety of the surface, there was no apparent variation in partial electron yield (PEY) within any sub-region.

Next, we examined a C1s K-edge spectrum extracted from the NEXAFS image [Figure 3.2c]. We observed a large feature near 289 eV. This feature was attributed to the many C-OH σ* bond orbitals from hydroxyl groups that comprise saccharide ring side chains [30]. There was a small positive dichroism for the feature near 289 eV, which was centered at an energy slightly below the primary peak energy (~0.3 eV). One explanation

for this mismatch was the existence of two different but overlapping resonances. The C=O π* orbital of COOH groups, as well as the C=O π* orbital from amino sugars and amide bonds, may influence this feature due to very similar characteristic energies [29, 30]. While a C=O π* feature near 288 eV was not clearly apparent in the C_{1s} K-edge spectra, it is often identified as a slight shoulder when it is expected to be present [31]. Discerning whether the C=O π* orbital or experimental error is responsible for the slight energy decrease of this dichroism would require further study of glycoproteins with varying lengths of oligosaccharide chains. Other C_{1s} K-edge features near 285.3 eV, 293 eV and 298 eV, are associated with C=C π*, OC-OH σ* and C-C σ* orbitals respectively [31, 32]. These orbitals do not produce dichroisms, although the latter two are indicative of common bonds within sugar groups (OC-OH σ*) and most organic species (C-C σ*) [30, 32]. The C=C π* peak likely results from slight beam damage of the surface or the presence of advantageous carbon; this conclusion is commonly accepted in cases such as this when it is not expected in the interrogated structure [31].

Finally, we examined an extracted N_{1s} K-edge spectrum [Figure 3.2d]. The most prominent feature observed is near 402 eV, associated with the N-C=O π* bond orbital of amide groups which comprise the backbone of peptides and proteins [21, 27, 33, 34]. A large positive dichroism is observed for this feature. Furthermore, there was a small feature near 404 eV, attributed to alternative conformations of protein/peptide backbones [35]. Secondary peaks near 407 eV and 414 eV were associated with N-CH_2 σ* and N-C=O σ* orbitals respectively, the former of which was related to either N-glycoside linkages or amino acid side chains expected within a representative mucin molecule [21, 31].

3.3.2 SFG Spectroscopy

SFG spectroscopy interrogated molecular vibrations which were specifically ordered at the mucus surface. In this study, we analyzed spectra in the C-H stretching region for ssp and ppp polarization combinations [Figure 3.3b]. Three modes appear in the spectrum with ssp polarization combination: 2858 cm^{-1}, 2878 cm^{-1} and 2931 cm^{-1}, which correspond to CH_2 symmetric, CH_3 symmetric and CH_3 fermi stretches respectively [19, 25, 36]. These stretches are diminished in the PPP spectrum, although

there is an additional peak at 2950 cm^{-1} corresponding to out-of-plane CH_3 stretching [36]. The signal strength in ssp mode (and corresponding lack of signal in ppp mode) suggests that molecular order of C-H stretch containing molecules at the interface is confined to a single plane, since each polarization mode probes different incident planes [36]. There is no evidence of ordered C-H ring stretches from the oligosaccharide chains of mucin. This could be due to the broadness of the measured SFG peaks - several C-H ring resonances are expected to appear at wavenumbers contained within the broad CH_2 and CH_3 resonances [37]. However, absence of saccharide ring stretches in SFG spectra may also have been due to extensive crosslinking, which would prevent these chains from exhibiting the net orientation order required for signal by SFG spectroscopy selection rules. Finally, the C=O stretching region was investigated in this study. However, no signal was observed at any spot across the mucus surface.

3.4 Discussion

We used complimentary surface analysis techniques to classify the chemical structure of the surface layer of mucus left after frog tongue strikes. However, it was first necessary to identify whether molecular bonds at the surface were consistent with the primary structure of mucin glycoproteins. Then, we used detailed information within NEXAFS and SFG spectra to determine higher order chemical structure. As previously established, no example of whole glycoprotein analysis exists using either NEXAFS or SFG spectroscopies. Therefore, comparisons are made to the two primary subunits which are well studied with these techniques – saccharide chains and proteins.

First, NEXAFS images and C_{1s} and N_{1s} K-edge spectra extracted from them were examined, as they provided most comprehensive view of molecular structures at the mucus surface layer. There were four features in the C_{1s} and N_{1s} K-edge spectra which were strongly indicative of each of these chemical units. Features near 289 eV (C-OH σ*; C1s K-edge) and 402 eV (-N-C=O π*; N1s K-edge) as well as minor features near 293 eV (OC-OH σ*; C1s K-edge) and 407 eV (N-CH2 σ*; N1s K-edge) could be mapped to these characteristic units of mucins [20, 30, 36]. There was also little variation in PEY intensity for these bonds in NEXAFS microscopy images, indicating consistent bond distribution across the surface mucus layer. Together, the combination of features from

both sugar chains and proteins and uniform layer distribution supports the hypothesis that mucin molecules primarily make up the mucus surface.

However, while we hypothesized that this layer would consist primarily of mucin molecules, we also expected to see evidence of fibril formation in NEXAFS microscopy images. Previous experiments using this technique have shown clear patterns in intensity corresponding to known topographical changes in chemistry or chemical structure of the surface [19, 22]. However, it is important to point out that the imaging tool mapped the chemical topography of the top ~10 nm of the mucus surface, which likely contains several layers of mucus. Therefore, the lack of observable chemical structures in the variation of PEY intensity for all bond orbitals of interest was likely due to contributions from the subsequent layers of mucus below the surface but within the top ~10 nm. Since, fibril formation was only expected to take place on the uppermost layer, any potential topographical clues were likely hidden by these under layers.

Next, structural and orientational information is provided by the NEXAFS spectroscopy experimental setup, which allowed for the sample stage to be rotated such that spectra were collected for incident x-ray angles that were at both head-on (70°) and glancing (30°) angles. In this case, the orientation and order of a specific bond orbital was determined by following its change in intensity as the x-ray angle was varied. Difference spectra for the C_{1s} and N_{1s} K-edge spectra are displayed at the bottom of their respective plot [Figures 3.2c and 3.2d]. The dichroism for the C-OH σ* orbital was both positive and small. These orbitals are donut shaped around the C-OH bond, thus, a positive dichroism indicates that the orbitals, as well as the hydroxyl groups, were more closely aligned with the 70° incident x-ray angle [29]. However, the intensity of this dichroism was small relative to the intensity at either incident angle. This was likely due to the distribution of hydroxyl groups all around the saccharide rings - off-axis rotations of these planar ring structures force some hydroxyl groups to point away from the surface normal axis and some to point towards it.

Furthermore, the dichroism for the -N-C=O π* orbital was also positive and was relatively small compared to the examples of secondary and tertiary structures previously examined in literature. Unlike σ*, π* orbitals are dumbbell shaped, pointing perpendicularly from the

axis of the -N-C=O bond. Therefore, a positive dichroism indicates that orbitals were oriented towards surface normal, while the amide bond sits along the surface parallel plane. Previous studies of protein structure with NEXAFS correlate relative magnitude of the -N-C=O π* orbital dichroism to secondary and tertiary structure. Small amide π* dichroisms are often associated with helical structures. In this case, the dichroism is small due to the amide bonds having uniform distribution along the radial axis (i.e. no dichroism) but a small net orientation along the cylindrical axis. Helical structures are consistent with the formation of fibrils, which are multiple protein chains that are twisted, like fibers, around a central axis. Fibril formation also corresponds with a prerequisite formation of mucin chain secondary structures, which is well supported in literature via the formation of disulfide bonds between neighboring molecules. However, as previously established, the tertiary structure of these mucin chains has been found to exist either as random coil clusters, mesh-like networks or in some cases as fibrils. Each of the former two tertiary structures can be eliminated by considering amide bond geometry. For instance, if the mucin chains were in a random coil state, we would have observed no dichroism. Likewise, if they were in a mesh-like, beta sheet conformation, the dichroism would have been much larger. Thus, our results were most consistent with fibril formation.

Finally, SFG spectroscopy allowed us to obtain vibrational spectra of the mucus surface with sub-monolayer sensitivity. As a second-order nonlinear optical technique, SFG's selection rules were such that signal can only be obtained from ordered and anisotropic materials. Thus, the bulk mucus, which was shown with NEXAFS imaging to contain a sufficiently arbitrary distribution of mucin molecules, did not produce SFG signal in this experiment. We collected spectra at the C-H stretching region (2800-3100 cm^{-1}) from two separate spots and two polarization combinations (ssp and ppp) on a mucus surface created after a Cera. sp. tongue strike on a cleaned microscope slide. Three distinct modes were observed in the resulting averaged ssp spectrum from CH_2 symmetric (2858 cm-1), CH_3 symmetric (2878 cm^{-1}) and CH_3 fermi (2931 cm^{-1}) stretches. This indicated order of methyl and methylene groups at the mucus surface. Within a representative mucin molecule, these groups were most highly concentrated on the amino acid side chains – including the many threonine amino acids found in the protein core. Interestingly, these modes were extremely diminished in the ppp spectrum. This corresponded with the

appearance of the CH_3 asymmetric stretch (near 2950 cm^{-1}) in ppp mode to suggest that the methyl and methylene groups were ordered together on a singular plane at the surface. Due to the already established tertiary protein order using NEXAFS, we infer that the most likely source of methyl and methylene symmetric stretches is within amino acid side chains sticking out from the fibril backbone.

Additionally, we observed no C-H ring stretches in either spectrum, suggesting that saccharide rings were not well oriented at the surface. This lends further support to the orientational disorder concluded from the small C-OH σ* dichroism in NEXAFS spectra. The presence of stretches from hydrophobic groups (methyl and methylene) with SFG and lack of stretches from hydrophilic sugar rings, suggests that hydrophilic hydroxyl groups were oriented downward (away from surface) and hydrophobic residues/side chains within protein backbone were oriented upward (towards surface). The directionally opposite nature of these two molecular groups may contribute to the adhesive ability of mucus fibrils by increasing the Van der Waals attraction of closely neighboring fibrils during tongue retraction, helping prevent breakage.

3.5 Conclusions

This study presents an overall picture of frog tongue mucus surface structure during adhesion and tongue detachment. Mucin glycoproteins form long chains which are twisted into a fibril structure, with amino acid side chains oriented towards the surface and hydroxyl groups oriented into the mucus layer [Figure 3.4]. This strongly supports previous classifications of the frog sticky-tongue mechanism as a pressure sensitive adhesive. Per this classification, fibrils form as the tongue is retracted, increasing the ability of mucus to withstand the large strain applied by the tongue muscles. Without fibril formation, mucus would be highly susceptible to delamination from the tongue, leading to loss of more massive prey or perhaps even tongue damage.

While our study indicates that a change in chemical structure of surface mucins is responsible for the amplification of adhesive forces in the frog sticky tongue mechanism, analysis of the other animal systems, such as the Marsh Periwinkle snail, shows that chemical composition of mucus is most important for that species. Thus, the mechanisms behind mucus adhesive systems cannot be generalized for all species – they are each

specialized to fit the evolutionary needs of an individual animal and must be studied as such. This study reinforces the concept that analysis of chemical structure at adhesive interfaces is critically important for better understanding of underlying mechanisms, which will ultimately lead to more effective biomimetic design. High throughput, surface sensitive techniques, such as those utilized herein, greatly increase our ability to examine chemical structure; however, they will also be vitally important for evaluating the quality of novel bioadhesives in the future.

3.6 Figures

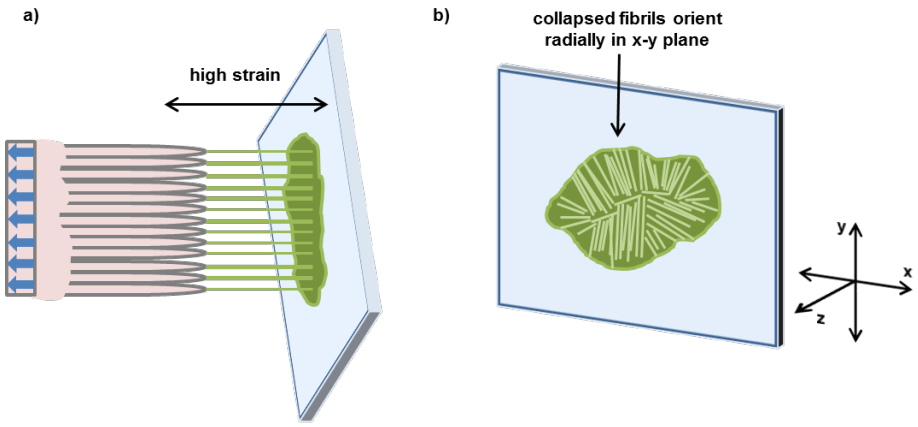

Figure 3.1 – Literature proposed mechanism of *Cera. ornata* tongue detachment (a). Mucus fibrillation occurs between tongue papillae and bulk mucus as tongue is pulled perpendicular to surface under high strain of tongue muscles. Hypothesized structure at mucus surface after tongue detachment (b).

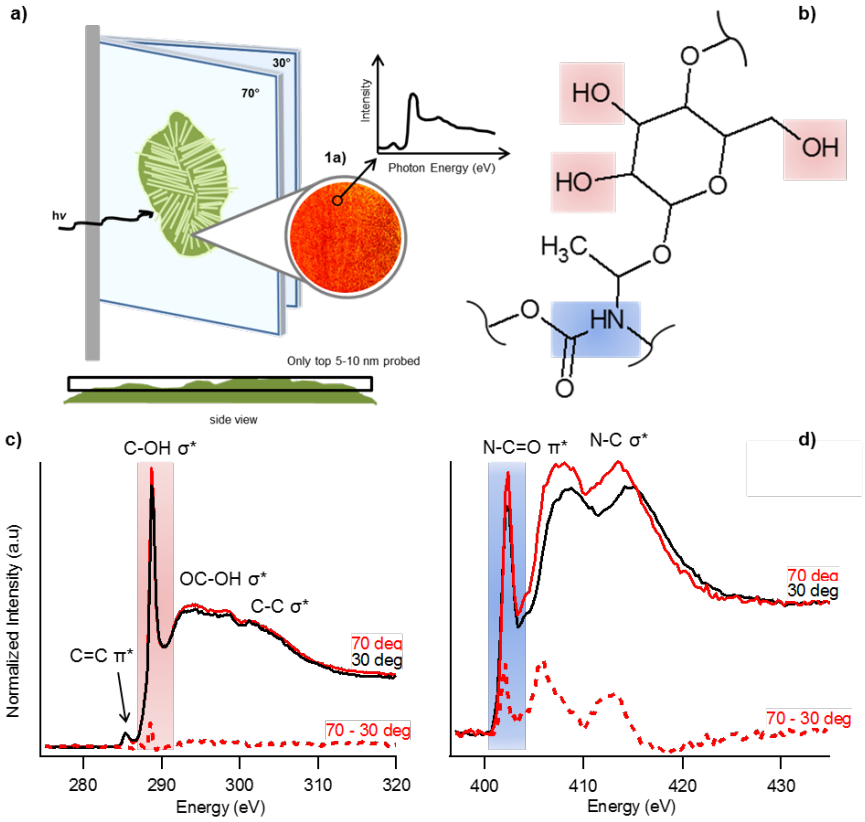

Figure 3.2– Experimental setup for NEXAFS microscopy imaging (a) Representative glycosylated threonine amino acid within mucin protein (b) Pre- and post- C1s K-edge spectra at incident angles of 70° and 30° as well as the difference spectrum (70° - 30°) (c) Pre- and post- N1s K-edge spectra for the same image location as b (d).

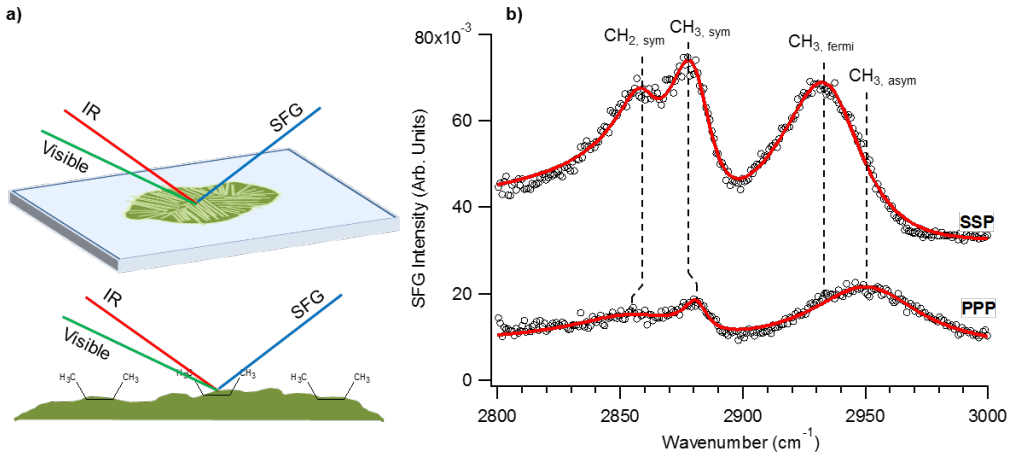

Figure 3.3 – Experimental setup for SFG spectroscopy. SFG spectra in the C-H stretching region (2800-3000 cm^{-1}) for the mucus interface after tongue detachment (a). CH_3 and CH_2 symmetric and CH_3 fermi stretches observed in SSP polarization mode near 2860 cm^{-1}, 2880 cm^{-1} and 2936 cm^{-1} respectively (b). CH_3 fermi stretch is replaced by CH_3 asymmetric stretch near 2951 cm^{-1} in PPP polarization mode.

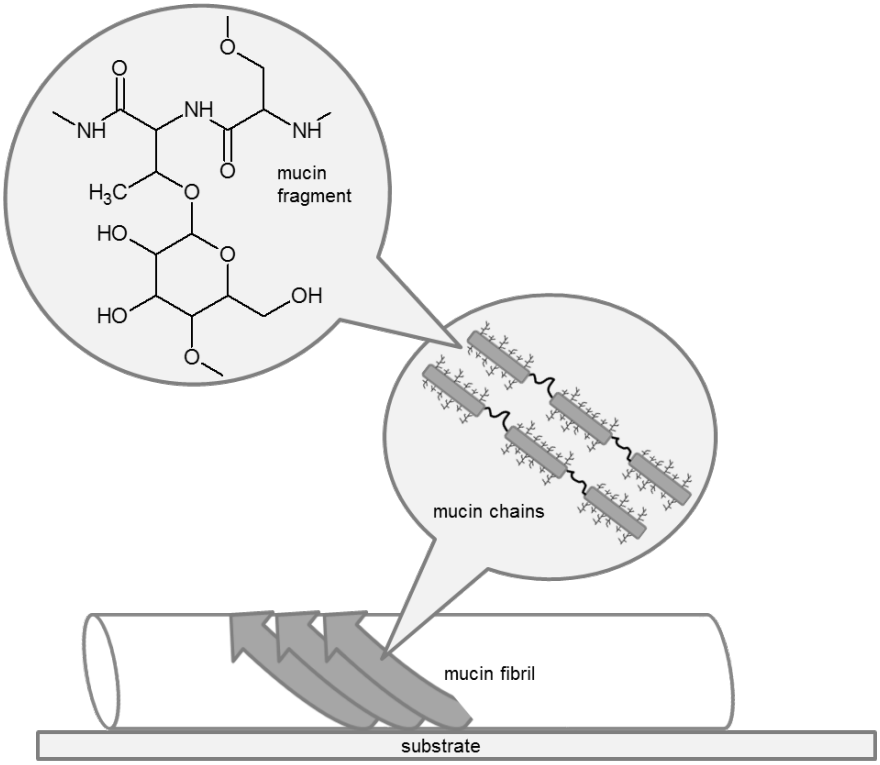

Figure 3.4 – Proposed mucin tertiary, secondary and primary structure at mucus surface after tongue detachment, based upon NEXAFS and SFG spectroscopic analysis

3.7 Supporting Information

3.7.1 NEXAFS Microscopy Images

NEXAFS data was collected via photoemitted electrons upon incident x-ray contact with the region of interest (ROI) outlined in S.I. Figure 1a, which encompasses nearly the entire frog tongue mucus print. Photoelectrons were for collected at energies across the C_{1s} and N_{1s} K-edges and this data was stored in each pixel of the resulting image. This allowed for the partial electron yield (PEY) intensity at an energy corresponding to a specific bond orbital of interest to be compared spatially across the ROI. S.I. Figures 1b, 1c and 1d, 1e and 1f were created by highlighting PEY intensity for C-OH σ*, C=C π*, C-C σ*, N-C=O π* and N-CH_2 σ* photons respectively. An increase in white-scale indicated an increase in intensity and vice-versa for black-scale. However, absolute values of intensities are arbitrary as all contained spectra are pre- and post-edge normalized prior to analysis. There were obvious edge effects in some of the images (i.e. 1b & 1d) which were likely due to the curved nature of the analyzer used in this novel setup. Besides these edge effects, there was little to no observable variation in PEY intensity for any bond orbital in any part of the ROI. This is further reinforced when compared to previous uses of the NEXAFS microscopy imaging tool in literature, which show clear topographical patterns when chemistry or chemical structure of the surface is varied [19, 22].

3.7.2 SFG Spectroscopy Fitting Table

SFG spectra in the C-H stretching region for ssp and ppp polarization combinations were collected and analyzed in this study. Spectral fitting was performed using a well-known procedure described elsewhere, using Lorentzian line shapes and iteratively calculating the non-resonant background and phase (A_{NR} and φ_{NR}), and the peak location (ω_n), full width half maximum (Γ_n) and amplitude (A_n) for all identified features. Assignments are based upon literature and the glycoprotein model. Fits are represented by solid red lines in main article.

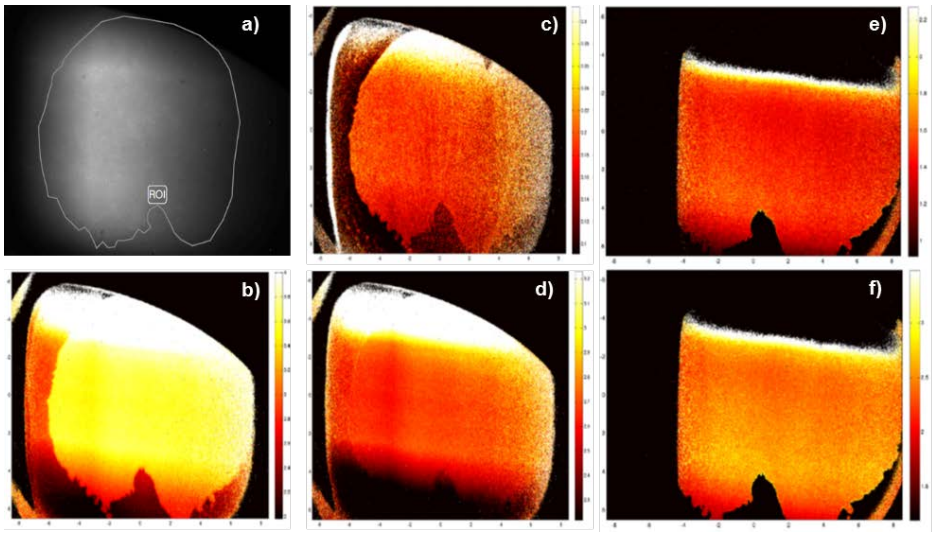

Figure 3.S1 - Region of Interest selected for imaging software (a). Pre- and post-edge normalized NEXAFS images (30°) for C-OH σ*, C=C π*, C-C σ* photons, respectively (b, c, d). An increase in white-scale indicates higher measured photon intensities. Pre- and post-edge normalized NEXAFS images for N-C=O π* (top) and N-C σ* (bottom) photons. Uniform distribution of bonds observed in each (e, f).

SFG Mode	A_{NR}	φ_{NR}	ω_n	Γ_n	A_n	Mode
SSP	0.081	3.57	2860	18.94	0.406	CH_2 sym
			2882	22.46	1.247	CH_3 sym
			2936	41.71	3.126	CH_3 fermi
PPP	0.054	4.29	2853	19.34	0.269	CH_2 sym
			2880	22.01	0.471	CH_3 sym
			2951	55.13	2.144	CH_3 asym

Table 3.S1 – Fitting parameters for SSP and PPP spectra of front tongue mucus at mucus-air interface

3.8 References

[1] Kleinteich, T. & Gorb, S.N. 2014 Tongue adhesion in the horned frog Ceratophrys sp. *Scientific reports* **4**, 5225-5225. (doi:10.1038/srep05225).

[2] Kleinteich, T. & Gorb, S.N. 2015 Frog tongue acts as muscle-powered adhesive tape. *Open Science* **2**, 150333.

[3] Noel, A.C., Guo, H.-Y., Mandica, M. & Hu, D.L. 2017 Frogs use a viscoelastic tongue and non-Newtonian saliva to catch prey. *Journal of The Royal Society Interface* **14**, 20160764.

[4] Smith, A.M. & Morin, M.C. 2002 Biochemical differences between trail mucus and adhesive mucus from marsh periwinkle snails. *The Biological Bulletin* **203**, 338-346.

[5] Smith, A.M. 2016 The biochemistry and mechanics of gastropod adhesive gels. In *Biological adhesives* (pp. 177-192, Springer.

[6] Smith, A.M. 2002 The structure and function of adhesive gels from invertebrates. *Integrative and Comparative Biology* **42**, 1164-1171.

[7] Endlein, T., Ji, A., Samuel, D., Yao, N., Wang, Z., Barnes, W.J.P., Federle, W., Kappl, M. & Dai, Z. 2013 Sticking like sticky tape: tree frogs use friction forces to enhance attachment on overhanging surfaces. *Journal of the Royal Society Interface* **10**, 1-11.

[8] Gu, Z., Li, S., Zhang, F. & Wang, S. 2016 Understanding surface adhesion in nature: a peeling model. *Advanced Science* **3**.

[9] Perez-Vilar, J. & Hill, R.L. 1999 The structure and assembly of secreted mucins. *Journal of Biological Chemistry* **274**, 31751-31754.

[10] Bansil, R. & Turner, B.S. 2006 Mucin structure, aggregation, physiological functions and biomedical applications. *Current Opinion in Colloid & Interface Science* **11**, 164-170.

[11] Celli, J., Gregor, B., Turner, B., Afdhal, N.H., Bansil, R. & Erramilli, S. 2005 Viscoelastic properties and dynamics of porcine gastric mucin. *Biomacromolecules* **6**, 1329-1333.

[12] Harding, S., Rowe, A. & Creeth, J. 1983 Further evidence for a flexible and highly expanded spheroidal model for mucus glycoproteins in solution. *Biochemical Journal* **209**, 893-896.

[13] Lewis, S.P., Lewis, A.T. & Lewis, P.D. 2013 Prediction of glycoprotein secondary structure using ATR-FTIR. *Vibrational Spectroscopy* **69**, 21-29. (doi:http://dx.doi.org/10.1016/j.vibspec.2013.09.001).

[14] Davies, H.S., Singh, P., Deckert-Gaudig, T., Deckert, V., Rousseau, K., Ridley, C.E., Dowd, S.E., Doig, A.J., Pudney, P.D. & Thornton, D.J. 2016 Secondary Structure and Glycosylation of Mucus Glycoproteins by Raman Spectroscopies. *Analytical chemistry* **88**, 11609-11615.

[15] Zappone, B., Patil, N.J., Madsen, J.B., Pakkanen, K.I. & Lee, S. 2015 Molecular structure and equilibrium forces of bovine submaxillary mucin adsorbed at a solid–liquid interface. *Langmuir* **31**, 4524-4533.

[16] Engel, M.F.M., vandenAkker, C.C., Schleeger, M., Velikov, K.P., Koenderink, G.H. & Bonn, M. 2012 The polyphenol EGCG inhibits amyloid formation less efficiently at phospholipid interfaces than in bulk solution. *Journal of the American Chemical Society* **134**, 14781-14788. (doi:10.1021/ja3031664).

[17] Kurouski, D., Deckert-Gaudig, T., Deckert, V. & Lednev, I.K. 2014 Surface characterization of insulin protofilaments and fibril polymorphs using tip-enhanced Raman spectroscopy (TERS). *Biophysical journal* **106**, 263-271.

[18] Amenabar, I., Poly, S., Nuansing, W., Hubrich, E.H., Govyadinov, A.A., Huth, F., Krutokhvostov, R., Zhang, L., Knez, M. & Heberle, J. 2013 Structural analysis and mapping of individual protein complexes by infrared nanospectroscopy. *Nature communications* **4**.

[19] Baio, J.E., Spinner, M., Jaye, C., Fischer, D.A., Gorb, S.N. & Weidner, T. 2015 Evidence of a molecular boundary lubricant at snakeskin surfaces. *Journal of The Royal Society Interface* **12**. (doi:10.1098/rsif.2015.0817).

[20] Baugh, L., Weidner, T., Baio, J.E., Nguyen, P.C.T., Gamble, L.J., Slayton, P.S. & Castner, D.G. 2010 Probing the Orientation of Surface-Immobilized Protein G B1 Using ToF-SIMS, Sum Frequency Generation, and NEXAFS Spectroscopy. *Langmuir* **26**, 16434-16441. (doi:10.1021/la1007389).

[21] Baio, J.E., Weidner, T., Baugh, L., Gamble, L.J., Stayton, P.S. & Castner, D.G. 2012 Probing the orientation of electrostatically immobilized Protein G B1 by time-of-flight secondary ion spectrometry, sum frequency generation, and near-edge X-ray adsorption fine structure spectroscopy. *Langmuir : the ACS journal of surfaces and colloids* **28**, 2107-2112. (doi:10.1021/la203907t).

[22] Baio, J.E., Jaye, C., Fischer, D.A. & Weidner, T. 2013 Multiplexed Orientation and Structure Analysis by Imaging Near-Edge X-ray Absorption Fine Structure (MOSAIX) for Combinatorial Surface Science. *Analytical chemistry* **85**, 4307-4310.

[23] Baio, J.E., Jaye, C., Fischer, D.A. & Weidner, T. 2014 High-throughput analysis of molecular orientation on surfaces by NEXAFS imaging of curved sample arrays. *ACS combinatorial science* **16**, 449-453.

[24] Pujari, S.P., Scheres, L., Weidner, T., Baio, J.E., Stuart, M.a.C., van Rijn, C.J.M. & Zuilhof, H. 2013 Covalently attached organic monolayers onto silicon carbide from 1-alkynes: molecular structure and tribological properties. *Langmuir : the ACS journal of surfaces and colloids* **29**, 4019-4031. (doi:10.1021/la400040e).

[25] Baio, J.E., Weidner, T., Samuel, N.T., McCrea, K., Baugh, L., Stayton, P.S. & Castner, D.G. 2010 Multitechnique characterization of adsorbed peptide and protein orientation: LK3(10) and Protein G B1. *Journal of Vacuum Science & Technology B* **28**, C5D1-C5D8. (doi:10.1116/1.3456176).

[26] Golbek, T.W., Franz, J., Elliott Fowler, J., Schilke, K.F., Weidner, T. & Baio, J.E. 2017 Identifying the selectivity of antimicrobial peptides to cell membranes by sum frequency generation spectroscopy. *Biointerphases* **12**, 02D406.

[27] Zubavichus, Y., Shaporenko, A., Grunze, M. & Zharnikov, M. 2009 NEXAFS spectroscopy of biological molecules: From amino acids to functional proteins. *Nuclear Instruments and Methods in Physics Research, Section A: Accelerators, Spectrometers, Detectors and Associated Equipment* **603**, 111-114. (doi:10.1016/j.nima.2008.12.171).

[28] Cheng, F., Gamble, L.J. & Castner, D.G. 2008 XPS, TOF-SIMS, NEXAFS, and SPR characterization of nitrilotriacetic acid-terminated self-assembled monolayers for controllable immobilization of proteins. *Analytical chemistry* **80**, 2564-2573.
[29] Stöhr, J. 2013 *NEXAFS spectroscopy*, Springer Science & Business Media.

[30] Gainar, A., Stevens, J.S., Jaye, C., Fischer, D.A. & Schroeder, S.L. 2015 NEXAFS Sensitivity to Bond Lengths in Complex Molecular Materials: A Study of Crystalline Saccharides. *The Journal of Physical Chemistry B* **119**, 14373-14381.

[31] Dietrich, P.M., Horlacher, T., Girard-Lauriault, P.-L., Gross, T., Lippitz, A., Min, H., Wirth, T., Castelli, R., Seeberger, P. & Unger, W.E. 2011 Multimethod chemical characterization of carbohydrate-functionalized surfaces. *Journal of Carbohydrate Chemistry* **30**, 361-372.

[32] Solomon, D., Lehmann, J., Kinyangi, J., Liang, B., Heymann, K., Dathe, L., Hanley, K., Wirick, S. & Jacobsen, C. 2009 Carbon (1s) NEXAFS Spectroscopy of Biogeochemically Relevant Reference Organic Compounds. *Soil Science Society of America Journal* **73**, 1817-1817. (doi:10.2136/sssaj2008.0228).

[33] Weidner, T. & Castner, D.G. 2013 SFG analysis of surface bound proteins: a route towards structure determination. *Physical chemistry chemical physics : PCCP* **15**, 12516-12524. (doi:10.1039/c3cp50880c).

[34] Zubavichus, Y., Shaporenko, A., Grunze, M. & Zharnikov, M. 2007 NEXAFS spectroscopy of homopolypeptides at all relevant absorption edges: Polyisoleucine, polytyrosine, and polyhistidine. *The Journal of Physical Chemistry B* **111**, 9803-9807.

[35] Stewart-Ornstein, J., Hitchcock, A.P., Cruz, D.H., Henklein, P., Overhage, J., Hilpert, K., Hale, J.D. & Hancock, R.E.W. 2007 Using intrinsic X-ray absorption spectral differences to identify and map peptides and proteins. *Journal of Physical Chemistry B* **111**, 7691-7699. (doi:10.1021/jp0720993).

[36] Weidner, T., Apte, J.S., Gamble, L.J. & Castner, D.G. 2010 Probing the Orientation and Conformation of alpha-Helix and beta-Strand Model Peptides on Self-Assembled Monolayers Using Sum Frequency Generation and NEXAFS Spectroscopy. *Langmuir* **26**, 3433-3440. (doi:10.1021/la903267x).

[37] Yatawara, A.K., Tiruchinapally, G., Bordenyuk, A.N., Andreana, P.R. & Benderskii, A.V. 2009 Carbohydrate surface attachment characterized by sum frequency generation spectroscopy. *Langmuir* **25**, 1901-1904.

Chapter 4. Investigation of the Chemical Interface Between Ladybird Beetle Adhesive Foot Fluid and Varying Surface Chemistry Using Sum Frequency Generation Spectroscopy

James Elliott Fowler[1], Johannes Franz[2], Thaddeus Golbek[1], Tobias Weidner[2,3], Stanislav Gorb[4], Joe E. Baio[1]

[1]Oregon State University, CBEE Department, Corvallis, OR;

[2]Max Planck Institute for Polymer Research, Mainz, Germany

[3]Department of Chemistry, Aarhus University, Aarhus, Denmark

[4]Zoological Institute of the University of Kiel, Department of Functional Morphology and Biomechanics, Kiel, Germany;

Email Correspondence – joe.baio@oregonstate.edu

Key Words – Insect Adhesion, Adhesive Fluid, Seven-Spotted Ladybird Beetle, Surface Analysis, Sum Frequency Generation (SFG) Spectroscopy

Abstract

Nature has coevolved highly adaptive and reliable bioadhesives across a multitude of animal species. Much attention has been paid in recent years to selectively mimicking these adhesives for improvement of a variety of technologies. However, very few of the chemical mechanisms that drive these natural adhesives are well understood. Many animals, such as geckos, use hairy foot pads to enhance adhesion. Many insects combine hairy feet with a secreted adhesive fluid, allowing for adhesion to surfaces that thwart dry-foot animals, such as considerably rough, slippery and inverted surfaces. One such insect, the seven-spotted ladybird beetle, is thought to have an adhesive fluid made up of a complex molecular mixture containing both hydrophobic and hydrophilic parts. We hypothesize this causes the adhesive interface to be dynamic, with molecules in the fluid selectively organizing and ordering at surfaces with complimentary hydrophobicity to maximize adhesion. In this study, we examine adhesive fluid of the ladybird beetle with a surface sensitive analytical technique, sum frequency generation spectroscopy, as the fluid interacts with three substrates of varied wettability. Resulting spectra present no

evidence of unique molecular environments between hydrophilic and hydrophobic surfaces, but exhibit significant differences in ordering of hydrocarbons. We conclude that insect adhesion is not dependent upon a dynamic molecular-interfacial response to an environmental surface. Instead, insect adhesive fluids have evolved highly specific compositions, which are consistent across most surfaces and optimize both foot adhesion and release in natural environments.

4.1 Introduction

To effectively move, hunt and evade predators, many animals have evolved the ability to climb at extreme angles and across challenging surfaces. Perhaps the most popular climbing animal is the gecko, which uses hairy, scoop-like microstructures on its feet to stick and climb across most surfaces effortlessly [1-3]. These foot microstructures, known as setae, allow animals to produce orders of magnitude higher Van der Waals adhesive forces compared to a smooth, flat foot pad [3, 4]. However, these dry adhesive foot systems do have considerable limits, such as rough, slippery and inverted surfaces. Interestingly, many insects do not have these same limitations. This is thought to be due to the presence of an additional adhesive element on their feet - a secreted fluid which mediates contact between setae and substrate [5]. So-called “wet adhesion” enhances adhesion via addition of capillary forces and promotion of static and dynamic frictional adhesive forces [6-8].

One insect’s wet adhesion system, the seven-spotted ladybird beetle (*Coccinella septempunctata*), has been well studied due to its availability in the field and comparatively large body size (6 – 8 mm) [9-12]. These insects must traverse a range of terrain, from the smooth and waxy coating of leaves, to the rough and wettable ground of fields and forests. Recent experiments have shown that both surface chemistry and surface roughness have effects on the adhesive force generated by these beetles [10, 13]. For instance, when made to walk on smooth substrates of varied surface chemistry, they generate significantly higher traction forces on hydrophilic substrates [10]. Further investigations varying both surface wettability and roughness on silicon substrates found that both increasing hydrophobicity and increasing roughness have anti-adhesive effects on these insects [13].

Therefore, an insect's ability to properly stick to a surface must depend not only on surface chemistry and geometry, but also on the composition of the adhesive fluid. Bulk chemical characterization methods, such as mass spectrometric analysis, indicate that insect adhesive fluids may consist of natural lipids as well as sugars, alcohols and proteins [14]. For beetle species, adhesive fluid is commonly described as a water-in-oil emulsion, implying the existence of a continuous oily phase with watery sub-phases [9, 12]. Characterization of the hydrophilic phase or the entirety of *Cocc. sept.* (or similar species') adhesive fluid has not yet been performed. However, it has been routinely suggested that the emulsion nature of beetle adhesive fluid enables it to adapt to and enhance adhesive forces on both hydrophobic and hydrophilic surfaces [7, 15].

Mass spectrometric analysis of a variety of beetle's hydrocarbon fluid portion, obtained via solid phase microextraction, showed that it was made up of a mixture of straight chain and methyl-branched hydrocarbons and concluded that the relative abundance of unbranched vs. branched hydrocarbons influenced a beetle's adhesive tenacity [16-18]. A more thorough inspection of *Coccinella septempunctata* results revealed that a majority of hydrocarbon species in its adhesive fluid were branched [Figure 4.1] [18]. This is significant when considering a follow up experiment, which manipulated the composition of a similar beetle species' fluid by contamination with different types of alkanes and alkenes and found that this had a significant impact on adhesive force generated [17]. Clearly, chemical composition at the adhesive interface is an important factor in the overall beetle adhesive mechanism.

Until now, study of seven-spotted ladybird beetle adhesion has been limited to the determination of the causal relationship between substrate manipulation and magnitude of the adhesive force in response. However, these experiments inadvertently reveal that intra-fluid, as well as interfacial adhesive fluid – substrate molecular interactions play an important role in the success of the mechanism. Due to the high expense and expertise often needed to examine interfacial or surface-specific chemistry, this area has yet to be explored. Thus, in this study we utilized a surface sensitive laser technique, sum frequency generation spectroscopy (SFG) to determine the relationship between varied surface wettability and order of adhesive molecules in the foot fluid of a seven-spotted

ladybird beetle. We hypothesize that this fluid, which has a complex composition consisting of both oil and water phases, will reorganize at the molecular level when the wettability of the contacting surface is substantially changed, to maximize chemical, dispersive and capillary adhesive forces [Figure 4.2].

To do this, we introduced the adhesive fluid of *Cocc. sept.* to three smooth surfaces – hydrophilic, deuterated polyethylene oxide (PEO), slightly hydrophobic CaF_2 optical windows, and hydrophobic, deuterated polystyrene (PS). We then collected vibrational spectra in the C-H, C-D and C=O stretching regions which were sensitive to order of molecules at the targeted interface. Fitting these spectra allowed for the comparison or order between substrates. Finally, we considered whether trends in our results match with the established relationships between seven-spotted ladybird beetle adhesive force and surface chemistry.

4.2 Methods

4.2.1 Polymer Film Preparation

All substrates were prepared on calcium fluoride optical windows (15 mm diameter; International Crystal Laboratories, Garfield, NJ) cleaned via consecutive sonication in dichloromethane, acetone and ethanol. Two polymers: deuterated poly-ethylene oxide [PEO, MW = 8960 Da] and deuterated polystyrene [PS, MW = 7420 Da; Polymer Source Inc., Montreal, CA] were each dissolved into a 3 wt% polymer/toluene solution. Thin polymer films were formed via spin coating at 2000 RPM for 60s. Excess solvent was removed by annealing the films in a vacuum oven at 80° C and 10^{-3} torr for 20 hours. This resulted in optically transparent thin films of PEO and PS of approximately 100 nm in height, as measured with a profilometer. Prepared windows were stored in sealed Petri dishes under N_2 atmosphere until footprint samples were collected.

4.2.2 Contact Angle Goniometry

An FTA 135 instrument was used to measure the contact angle of water on replicates of each substrate, prepared as previously described. 10 µL droplets were pipetted onto each surface and a high-resolution image was collected. The droplet shape, relative to the horizon line, was traced and a contact angle was generated by the

instrument software. This procedure was repeated ten times for each of the three substrates in this experiment.

4.2.3 Insects

Ladybird beetles were collected in their natural environment near Stohl, Schleswig-Holstein, Germany, stored in a wine fridge at 10°C, fed with hard honey and sprayed with water once a week. Beetles were stored for 24 h prior to footprint collection on clean paper towels to prevent foot contamination.

4.2.4 Ladybird Beetle Footprint Collection

Two pairs of forceps were rinsed thoroughly with acetone and ethanol immediately before collection of adhesion fluid samples. Legs were removed with fine forceps and contacted directly in the center of the substrates while applying a small shear stress to simulate natural tarsal movement. This process was repeated several times with additional beetle legs to ensure adequate coverage of the sampling areas.

4.2.5 Sum Frequency Generation (SFG) Vibrational Spectroscopy

An EKSPLA Nd:YAG laser, operating at 50 Hz, was used to generate both a fixed visible (532 nm^{-1}) and tunable IR beam (1000-4000 cm^{-1}) via sequential pumping through an EKSPLA optical parametric generation/amplification and difference frequency unit, which utilized barium borate and $AgGaS_2$ crystals respectively. The visible and IR beams (~150 μJ/pulse) were overlapped spatially and temporally at the desired interface to generate SFG photons, which were spectrally filtered, dispersed by a monochromator and detected with a gated photomultiplier tube. Both beams were focused to a ~ 1 mm diameter at the interface. Spectra were collected in 4 cm^{-1} steps with 400 acquisitions per step. Four consecutive spectra with 1 cm^{-1} offsets were collected at two distinct spots on both the footprint-substrate and footprint-free surface.

SFG spectra were generated at two different polarization combinations – *ssp* (*s*-polarized SFG, *s*-polarized visible, *p*-polarized IR) and *ppp* (*p*-polarized SFG, *p*-polarized visible, *p*-polarized IR) in 3 different vibrational regions (C-H – 2800-3100 cm^{-1}; C=O – 1600-1800 cm^{-1}; C-D – 2000-2300 cm^{-1}) through the backside of a CaF_2 window which rests on a Teflon o-ring (ID – 7.9 mm) attached to a flat, cylindrical Teflon chuck (Figure 4.S1).

SFG signal is optimized in each wavenumber region using an Au-coated CaF_2 window in the same set-up. The fitting routine for SFG spectra is previously detailed elsewhere. Briefly, spectra were iteratively fit to the equation below (Eq. 1) to determine non-resonant phase, non-resonant background (χ_{nr}), location (ω_q), individual peak full width half maximum (FWHM; Γ_q) and individual peak amplitude (A_q). Four C-H spectra, offset by one wavenumber, at each of two fluid-substrate and bare substrate spots were collected for each surface in this experiment.

$$\chi_{eff}^{(2)} = \chi_{nr} + \sum_{q} \frac{A_q}{\omega_2 - \omega_q + i\Gamma_q} \quad (Eq.\ 1)$$

4.3 Results

4.3.1 Substrate Characterization

Before vibrational spectra were collected, each substrate was characterized to determine polymer film thickness, wettability and surface roughness. Static contact angle goniometry, with 10 µL ultrapure water as the test fluid, was used to measure the angle between droplet and substrate, with low angles correlating to hydrophilicity and vice versa. Contact angles of 49.0° ± 3.3°, 63.6 ± 2.3° and 90.0 ± 1.5° were measured for the PEO, CaF_2 and PS surfaces respectively [Inset on Figure 4.3]. A separate but simultaneously prepared set of surfaces was scanned using tapping mode atomic force microscopy with 1 x 1 µm scan size [Figure 4.S2]. Root mean squared roughnesses of 1.33 nm and 0.24 nm were calculated for PEO and PS thin films, respectively. According to a recent study comparing adhesion on both smooth and rough surfaces, these RMS roughnesses fall within the “smooth” classification (< 2 nm) [13].

4.3.2 SFG Spectroscopy

Surface-sensitive vibrational spectra were collected in three separate stretching regions – C-D (1900-2300 cm^{-1}), C=O (1600 – 1800 cm^{-1}) and C-H (2800 – 3000 cm^{-1}). Selectively deuterating the polymer surfaces (PEO and PS) allowed for confinement of SFG signal from the substrate side of the interface to the C-D stretching region. Thus, all signal measured in the C-H and C=O stretching regions must only come from molecular order within the interfacial layer of adhesive fluid.

First we collected the C-D stretching region spectra for two reasons: to verify that polymer thin films matched standards and to interrogate any possible effect of the adhesive fluid on the organization of polymer side chains. PEO spectra contained a single feature near 2080 cm^{-1} corresponding to the CD_2 stretching mode [Figure 4.S3] [19]. PS spectra also contained a single feature with a shoulder, this time near 2270 cm^{-1} (shoulder) and 2290 cm^{-1} (peak) corresponding to CD stretching modes of the pendant phenyl rings. The intensity of each mode was not significantly changed after addition of adhesive fluid to the substrate, which indicated that the fluid had no impact on the polymer film ordering.

Next, spectra were collected at the C=O stretching region for fluid on each substrate to determine the order of any water, lipids, amino acids, proteins or other carboxyl group containing molecules at the interface. Although these types of molecules have not been explicitly observed in chemical analysis of ladybird beetle foot fluid to date, analysis of locusts and other similar species have indicated the presence of lipids or amino acids. Interestingly, spectra of adhesive fluid on all three substrates produced no discernable signal, indicating that these molecules are either absent from *Cocc. sept.* adhesive fluid or not surface active [Figure 4.S3].

Finally, the C-H stretching region was interrogated. Saturated and unsaturated hydrocarbons were the only types of molecules confirmed to be present within the bulk of *Cocc. sept*. adhesive fluid by existing chemical analysis. Methyl and methylene groups from the backbone of these molecules have been well studied with SFG and have several vibrations in this region. Resulting SFG spectra in SSP polarization combination (s-polarized SFG, s-polarized visible, p-polarized IR) contained three distinct modes near 2858 cm^{-1}, 2880 cm^{-1} and 2930 cm^{-1} corresponding to CH_2 symmetric, CH_3 symmetric and CH_3 fermi stretches respectively [Figure 4.3] [20-22]. The previously assigned three vibrations, as well as two additional features were observed after switching to PPP polarization combination. These additional modes were located near 2900 cm^{-1} and 2950 cm^{-1} corresponding to CH_2 fermi and CH_3 asymmetric stretches respectively [20, 22]. The three SSP modes and five PPP modes (three overlapping modes) consistently appeared in all fluid-substrate C-H spectra as substrate chemistry was varied. However, the amplitude of each mode varied substantially between substrate chemistries.

To quantitatively compare the ordering of molecules within the adhesive fluid interfacial layer, it was first necessary to fit each spectrum to determine the location, full width half maximum and amplitude of each mode as well as non-resonant background and phase. From these values, the square root of the ratio of CH_3 to CH_2 symmetric stretch amplitudes was determined. This ratio is a well-known metric for evaluating order of a layer of hydrocarbon chains, where large ratios correspond to a high degree of hydrocarbon ordering [23]. This is because hydrocarbon chains or molecules contain methyl groups at their ends followed by a backbone of methylene groups which are aligned centrosymmetric when these chains are well packed with similar tilt angles. SFG selection rules, as well as literature, make clear that the methylene symmetric mode should have very low amplitude in the case of well-packed, uniform layers. Thus, low CH_2 symmetric amplitude produces a high value of CH_3/CH_2 symmetric ratio. Fits of resulting spectra generated ratios of 1.03 ± 0.07, 2.66 ± 0.16 and 3.46 ± 0.40 for fluid-dPEO, -CaF_2 and -dPS substrates respectively. Lastly, significant difference in variation between these ratios was tested by performing a single-factor ANOVA against the null hypothesis that all amplitude ratios were equal. This produced a p-value of 0.002, which led to a rejection of the null hypothesis. A post-hoc Tukey's test was then utilized to evaluate pairwise significant differences between the three ratios. This analysis indicated that the largest ratio, found in spectra of the fluid-dPS interface, differed significantly from the ratios of both the fluid-PEO and -CaF_2 interfaces. Contrarily, the PEO and CaF_2 ratios were not found to differ significantly.

4.4 Discussion

The goal of this study was to use a surface-specific analytical technique to gain insight into the chemical mechanisms of seven-spotted ladybird beetle wet adhesion that have otherwise been impossible to learn with traditional kinematic biological experiments. More specifically, the adhesive fluid of these beetles was introduced to substrates that were designed to exhibit a range of wettabilities and SFG spectroscopy was utilized to measure the order of vibrational modes from chemical groups either known or expected to exist within the fluid. Due to the selection rules of SFG spectroscopy, only vibrational modes which were active and ordered at the interface between fluid and substrate were measured. We hypothesized that the complex composition of adhesive foot fluid

contributed to the insect's ability to adhere to nearly all types of smooth surface, via a molecular reorganization of the fluid at the interface to create favorable interaction energies and amplify adhesive tenacity.

Therefore, it is particularly interesting that the same five vibrational modes appear in spectra of fluid in contact with all three substrates, with no modes unique to any one spectrum. With SFG alone it is not possible to rule out the presence of carbonyl-containing molecules or water in the bulk fluid of *Cocc. sept*.; although, the results present no additional evidence that they are contributing to the chemical adhesive mechanism in a substantial way. One possible explanation is that there are too few of the lesser groups at the interface to detect. However, this is unlikely as SFG is sensitive enough to the detect order at sub-μM concentration [19]. Rather, the interface appears to be dominated by hydrocarbons or hydrocarbon containing molecules. This result fits in well with established descriptions of beetle adhesive fluids as "oily" [9, 10, 17]. Additionally, it merits a larger focus on previous chemical analysis of the "oily fraction" of Cocc. sept. fluid, which may in fact be a characterization of all or most of this species' adhesive fluid [18].

As previously described, inspection of the mass spectroscopic results collected by Geiselhardt et al. shows that *Cocc. sept.* tarsal fluid contains a mixture of saturated and unsaturated, as well as branched and unbranched hydrocarbons [18]. While seemingly innocuous, the presence of a hydrocarbon mixture may help explain an unusual pattern observed in the change in amplitude of the CH_2 and CH_3 symmetric stretches as surface hydrophobicity is increased. Specifically, we observed an increase in CH_3/CH_2 ordering ratio with increased surface hydrophobicity, while also observing a decrease in absolute magnitude of both CH_3 and CH_2 symmetric stretch amplitudes. A pure, unbranched, layer of hydrocarbon chains, when brought into contact with a hydrophobic surface, will readily order and closely pack such that the chains of methylene groups exhibit local centrosymmetry. This then leads to a decrease in fitted peak amplitude. However, the end-chain methyl groups do not share this centrosymmetry the interface, which leads to a substantial increase in peak amplitude under the same circumstances. Our results appear to show that order, and thus amplitude, is reducing for both methyl and methylene

symmetric moieties; however, the methylene symmetric mode experiences a much larger amplitude loss allowing the ordering ratio to increase as expected as the substrate is varied from PEO, to CaF_2 to PS. In contrast, a hydrocarbon layer, with branched hydrocarbons mixed into it, adds additional methyl groups to the interface, which increases CH_3 symmetric centrosymmetry, decreases order and thusly decreases peak amplitude [Figure 4.4]. In summation, the results of this study provide corroborating evidence that the layer of adhesive fluid interacting with environmental surfaces primarily or entirely consists of a mixture of linear and branched hydrocarbons.

Within the broader context of the mechanisms which dictate success or failure of adhesion of *Cocc. sept*., the positive, linear relationship between substrate hydrophobicity and hydrocarbon ordering ratio matches inversely with adhesive force tests of similar species on comparable surfaces [Figure 4.5] [24]. In multiple instances, these beetles exhibited significantly larger traction forces on smooth, hydrophilic substrates than on smooth, hydrophobic ones [10, 12]. Considering the beetle's adhesive fluid has consistently been classified as oily, the kinematic results appeared counterintuitive, as an oily fluid should have more readily wet a hydrophobic surface, amplifying interaction forces and by result adhesive forces.

However, by utilizing the information gained from our SFG experiments, the kinematic observations can be clearly correlated to a reduction of friction forces between insect foot and surface via the greatly enhanced ordering of hydrocarbon chains within the adhesive fluid interfacial layer. This is extremely important, because traditional logic has centered on the adhesive fluid evolving such that it maximizes adhesive force absolutely in all cases. Instead, our results, combined with existing literature, support a more nuanced purpose for insect foot fluid - one in which it optimizes contact for both efficient foot adhesion and retraction by enhancing some contact forces (capillary, Van der Waals) and reducing others (static and dynamic friction). After all, seven-spotted ladybird beetles spend much of their lives on the waxy surfaces of leaves, both hunting aphids and avoiding predation by larger animals. Thus, rapid locomotion is equally as important to their survival as successful adhesion.

4.5 Conclusions

This study emphasizes the importance of understanding the interface when determining the mechanisms which control naturally evolved wet adhesives. Ultimately, the goal of studying insect wet adhesion the ability to thoroughly define the kinematic and chemical mechanics, such that they can be translated into design of a biomimetic product which makes adhesion more reliable, tenacious and adaptable. To this end, the kinematic properties of insect wet adhesion have been thoroughly studied for a large number of species, and many specific observations have been agreed upon. Some examples include the advantage of hairy foot pads to smooth foot pads on rough surfaces, the importance of maintaining natural fluid composition to the ability to stick and the adaptation of fluid composition to maximally benefit an insect species in its natural habitat. However, exploration of chemical mechanisms has been hindered by the lack of accessibility to tools with the necessary sensitivity to analyze nano- to picoliter sized droplets of fluid at the interface of interaction with a substrate.

In doing this for the adhesive foot fluid of the seven-spotted ladybird beetle, we have shown that several of the kinematic observations have a greater significance to the overall success of adhesion than previously thought. Specifically, we found spectral evidence that the beetle's fluid has a consistent composition organized at the fluid-substrate interface regardless of substrate hydrophobicity. Furthermore, fits of these spectra indicate that the ordered molecules contributing to the observed amplitudes for CH_3 and CH_2 symmetric modes are most likely a mixture of linear and branched hydrocarbons. This agrees well with recent mass spectrometric analysis of *Cocc. sept.* fluid. Lastly, the hydrocarbon ordering ratios on each substrate were compared to kinematic measurements of these beetles' traction force, which led to the conclusion that reduction of force on hydrophobic substrates is most likely due decreasing static friction as the hydrocarbon surface layer becomes well aligned. Most importantly, we believe that the original question, "what makes the insect stick so well?" is too limited in scope. Rather, the question must be "what makes the insect *optimized* for all forms of locomotion?"

To mimic beetle adhesive fluid for design of novel bioadhesives, it is still necessary to determine the sensitivity of interfacial hydrocarbon ordering to changes in the

branched/unbranched hydrocarbon composition. For instance, we must know that if our biomimetic adhesive is exposed to surfaces which are “dirty” (i.e. covered in hydrocarbons), what effect this will have on adhesive performance. For seven-spotted ladybird beetles, interfacial composition is key – fluid viscosity, foot static and dynamic friction, substrate compatibility and many more variables are largely influenced by this factor. However, this beetles’ adhesive fluid composition appears to be less diverse than previously thought. Ultimately, to determine if interfacial composition is a determining factor for all insect wet adhesion, the fluid of insects known to have more diverse, complex fluids must also be studied.

4.6 Figures

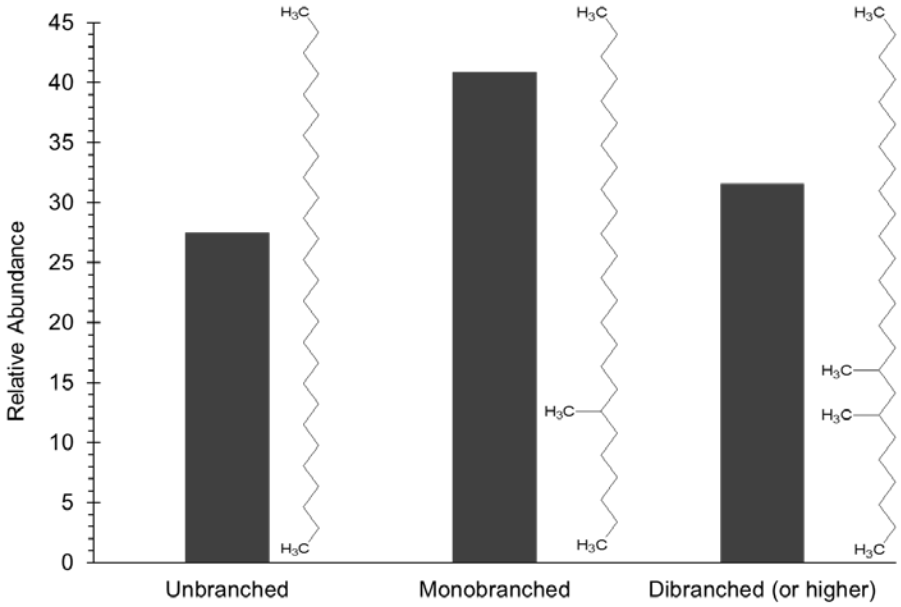

Figure 4.1 – Relative abundance of unbranched, monobranched and multibranched hydrocarbons (as a proportion of all unsaturated hydrocarbons) in the tarsal fluid of *Coccinella sept.* as reported in Geiselhardt et al. 2011.

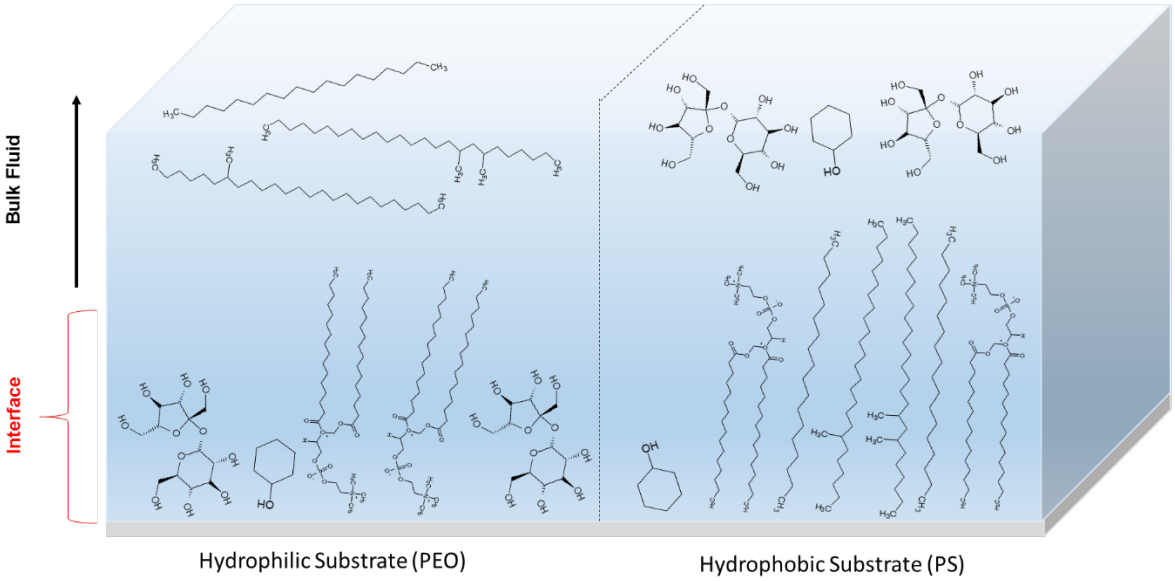

Figure 4.2 – Hypothesized view of the surface ordering of ladybird beetle adhesive fluid when contacted with hydrophilic and hydrophobic substrates. Hydrophilic sugars and carbohydrates and polar domains of alcohols and lipids predicted to interact and order on the PEO substrate, while hydrocarbons and apolar domains of lipids and alcohols predicted to interact and order on the PS substrate.

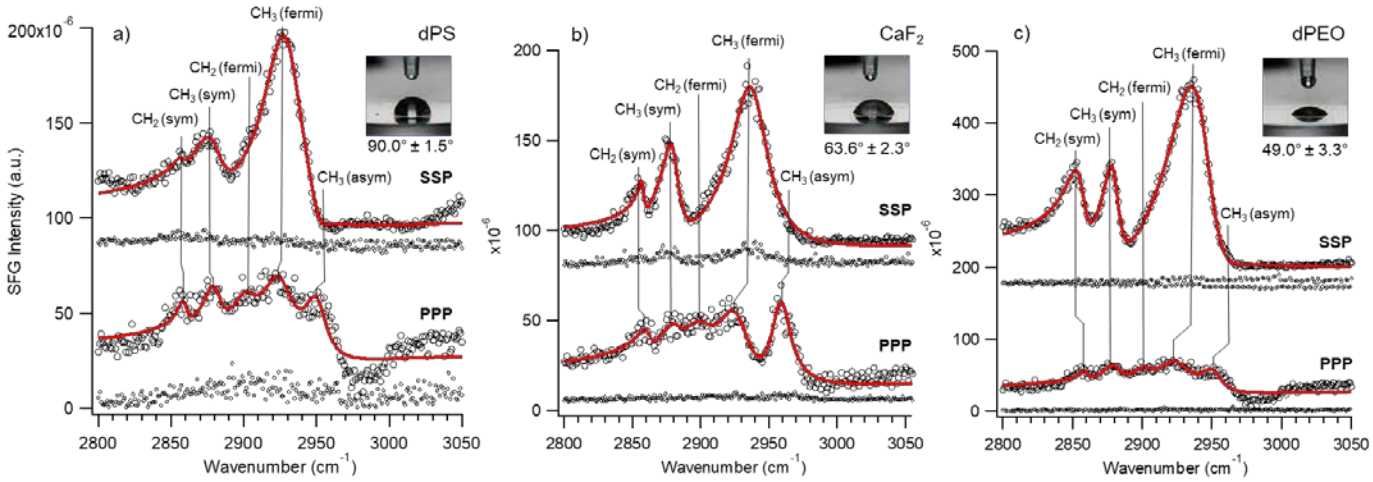

Figure 4.3 – CH region spectra in SSP and PPP polarization combinations of dPS substrates with beetle footprints (black circles), spectral fit (red line), and without footprints (black dots) a). Same spectra on CaF_2 substrate b). Same spectra on dPEO substrate c). The primary modes observed in each of the SSP spectra are the CH_2 symmetric stretch (near 2858 cm^{-1}), the CH_3 symmetric stretch (near 2880 cm^{-1}) and the CH_3 fermi resonance (near 2932 cm^{-1}). PPP spectra include two additional modes, the CH_2 fermi stretch (near 2900 cm^{-1}) and the CH_2 antisymmetric stretch (near 2955 cm^{-1}).

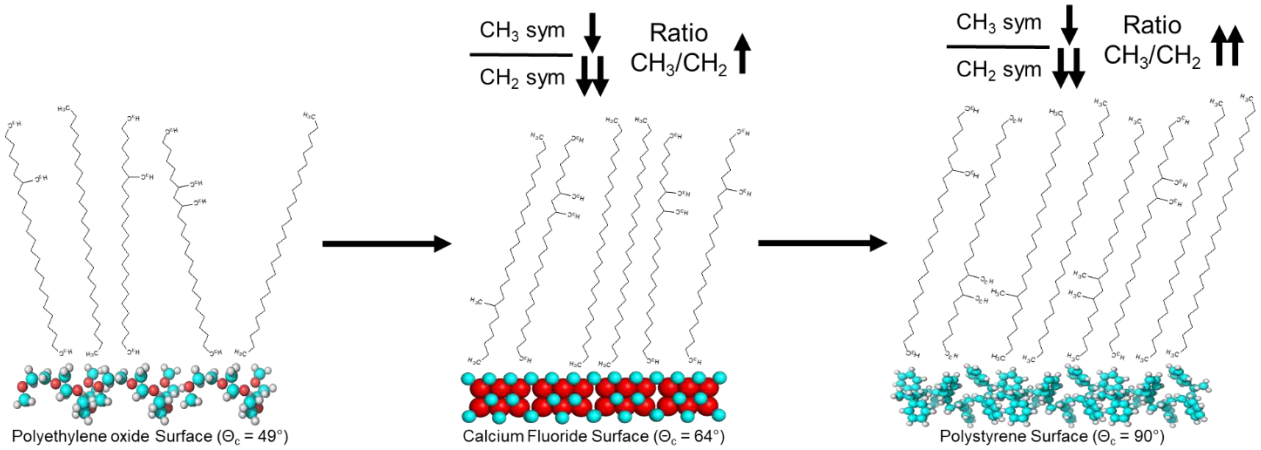

Figure 4.4 – Experimentally determined ordering at adhesive fluid – substrate interface for each of the three substrates. Differences in measured hydrocarbon ordering ratio explained by change in substrate water contact angle and presence of branched and unbranched hydrocarbons at the interface.

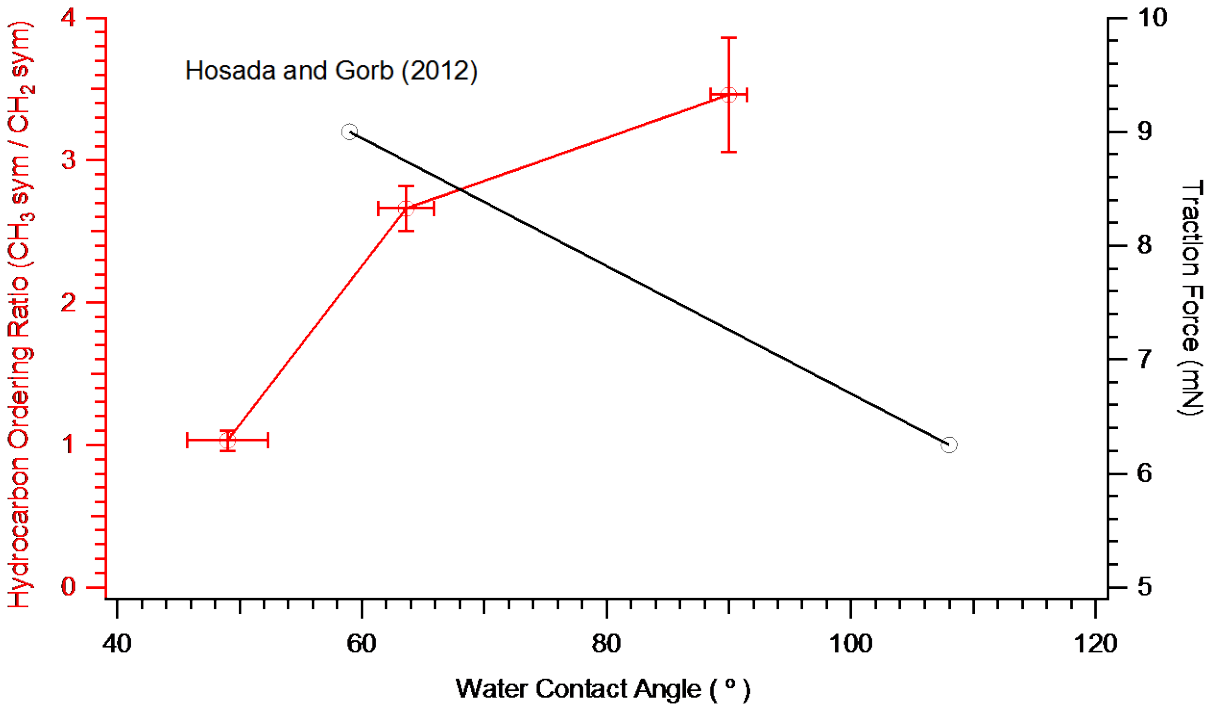

Figure 4.5 - Plot of characteristic hydrocarbon ordering ratio vs. water contact angle (red) and traction force vs. water contact angle adapted from Hosada and Gorb 2012 (black).

4.7 Supporting Information

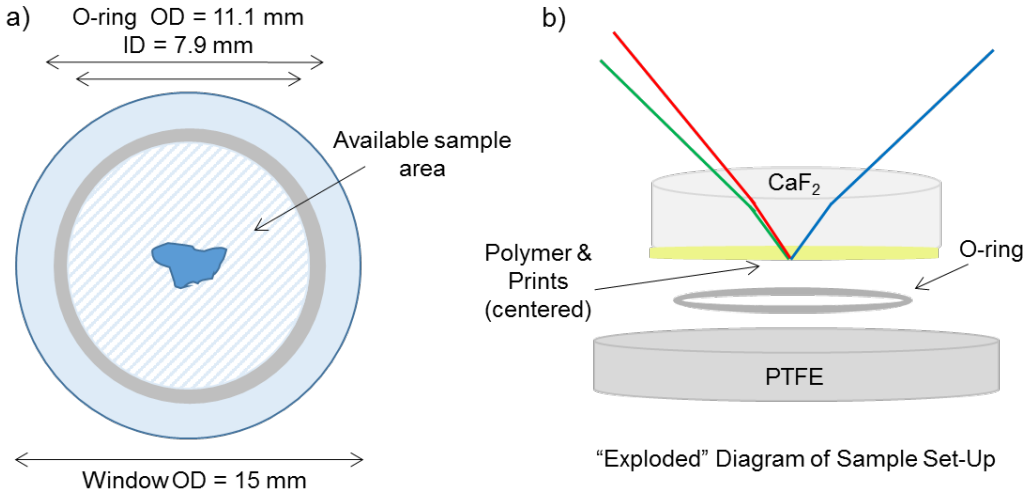

Figure 4.S1 - Schematic of sample placement - beetle footprints are placed in the center of the CaF2 window – SFG interrogation takes place only within the shaded region a). Exploded diagram of experimental set-up – visible and IR beams are overlapped in backside reflection to ensure SFG signal is generated only from the polymer-footprint interface b).

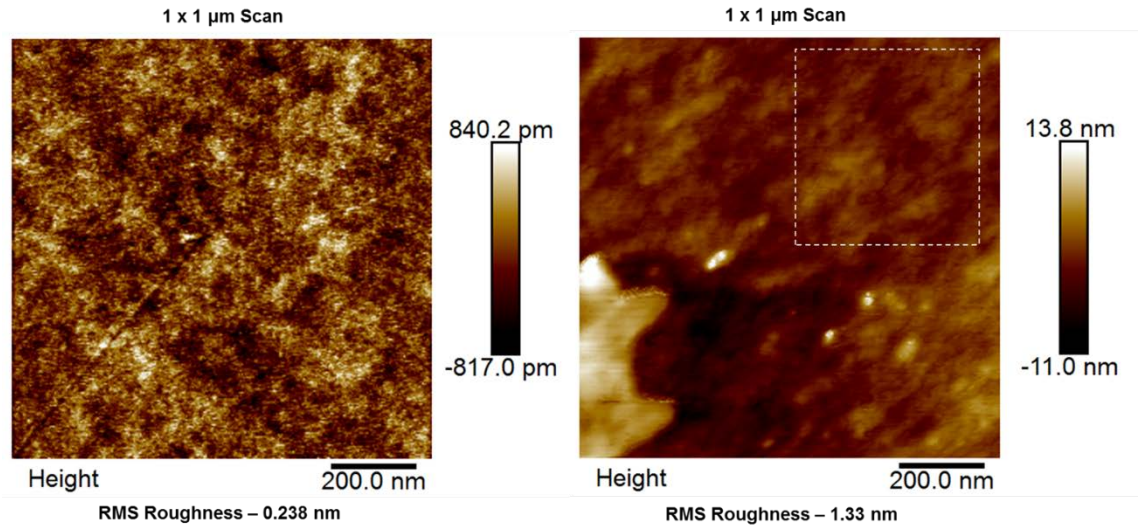

Figure 4.S2 – 1 x 1 µm scan of deuterated PEO thin film on CaF_2 substrate and calculated RMS roughness (below figure) a). 1 x 1 µm scan of deuterated PS thin film on CaF_2 substrate and calculated RMS roughness b).

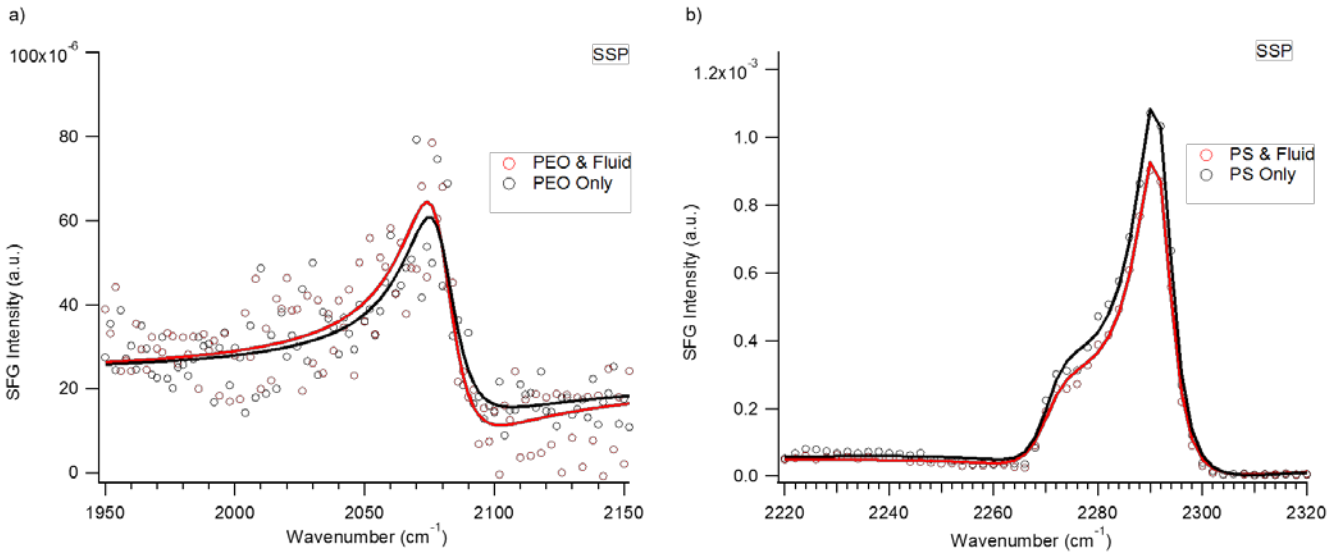

Figure 4.S3 – C-D stretching region spectra for deuterated PEO thin film before and after addition of adhesive fluid a). Raw data is represented by open dots, fits are represented by solid lines. C-D stretching region spectra for deuterated PS thin film before and after addition of adhesive fluid b).

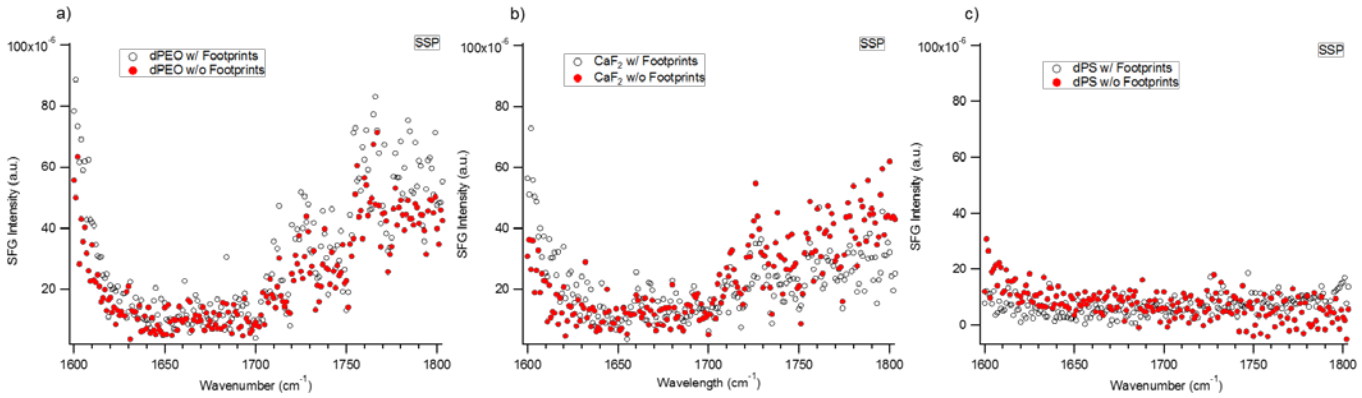

Figure 4.S4 – C=O stretching region spectra for deuterated PEO thin film a) CaF_2 substrate b) deuterated PS thin film c) before and after addition of adhesive fluid.

4.8 References

[1] Autumn, K. & Gravish, N. 2008 Gecko adhesion: evolutionary nanotechnology. *Philosophical Transactions of the Royal Society of London A: Mathematical, Physical and Engineering Sciences* **366**, 1575-1590.

[2] Irschick, D.J., Crosby, A.J. & Federle, W. 2013 The evolution of Gecko adhesion: An integrative perspective. *Integrative and Comparative Biology* **53**, E100-E100.

[3] Gao, H., Wang, X., Yao, H., Gorb, S. & Arzt, E. 2005 Mechanics of hierarchical adhesion structures of geckos. *Mechanics of Materials* **37**, 275-285.

[4] Autumn, K., Dittmore, A., Santos, D., Spenko, M. & Cutkosky, M. 2006 Frictional adhesion: a new angle on gecko attachment. *Journal of Experimental Biology* **209**, 3569-3579.

[5] Gorb, S.N. 2001 *Attachment Devices of Insect Cuticle*. Dordrecht, The Netherlands, Kluwer Academic Publishers.

[6] Walker, G. 1993 Adhesion to smooth surfaces by insects—a review. *International Journal of Adhesion and Adhesives* **13**, 6-10.

[7] Dirks, J.-H., Clemente, C.J. & Federle, W. 2010 Insect tricks: two-phasic foot pad secretion prevents slipping. *Journal of the Royal Society Interface* **7**, 587-593. (doi:10.1098/rsif.2009.0308).

[8] Drechsler, P. & Federle, W. 2006 Biomechanics of smooth adhesive pads in insects: influence of tarsal secretion on attachment performance. *Journal of Comparative Physiology A* **192**, 1213-1222.

[9] Peisker, H. & Gorb, S.N. 2012 Evaporation dynamics of tarsal liquid footprints in flies (Calliphora vicina)and beetles (Coccinella septempunctata). *The Journal of experimental biology* **215**, 1266-1271. (doi:10.1242/jeb.065722).

[10] Gorb, E.V., Hosoda, N., Miksch, C. & Gorb, S.N. 2010 Slippery pores: anti-adhesive effect of nanoporous substrates on the beetle attachment system. *Journal of the Royal Society, Interface / the Royal Society* **7**, 1571-1579. (doi:10.1098/rsif.2010.0081).

[11] Peisker, H., Heepe, L., Kovalev, A.E. & Gorb, S.N. 2014 Comparative study of the fluid viscosity in tarsal hairy attachment systems of flies and beetles. *Journal of the Royal Society Interface* **11**. (doi:10.1098/rsif.2014.0752).

[12] Heepe, L., Wolff, J.O. & Gorb, S.N. 2016 Influence of ambient humidity on the attachment ability of ladybird beetles (Coccinella septempunctata). *Beilstein Journal of Nanotechnology* **7**, 1322-1329.

[13] England, M.W., Sato, T., Yagihashi, M., Hozumi, A., Gorb, S.N. & Gorb, E.V. 2016 Surface roughness rather than surface chemistry essentially affects insect adhesion. *Beilstein Journal of Nanotechnology* **7**, 1471-1479.

[14] Vötsch, W., Nicholson, G., Müller, R., Stierhof, Y.D., Gorb, S. & Schwarz, U. 2002 Chemical composition of the attachment pad secretion of the locust Locusta migratoria. *Insect biochemistry and molecular biology* **32**, 1605-1613.

[15] Dirks, J.-H. & Federle, W. 2011 Fluid-based adhesion in insects - principles and challenges. *Soft Matter* **7**, 11047-11053. (doi:10.1039/c1sm06269g).

[16] Geiselhardt, S.F., Geiselhardt, S. & Peschke, K. 2009 Comparison of tarsal and cuticular chemistry in the leaf beetle Gastrophysa viridula (Coleoptera: Chrysomelidae) and an evaluation of solid-phase microextraction and solvent extraction techniques. *Chemoecology* **19**, 185.

[17] Geiselhardt, S.F., Federle, W., Prüm, B., Geiselhardt, S., Lamm, S. & Peschke, K. 2010 Impact of chemical manipulation of tarsal liquids on attachment in the Colorado potato beetle, Leptinotarsa decemlineata. *Journal of insect physiology* **56**, 398-404.

[18] Geiselhardt, S.F., Geiselhardt, S. & Peschke, K. 2011 Congruence of epicuticular hydrocarbons and tarsal secretions as a principle in beetles. *Chemoecology* **21**, 181.

[19] Golbek, T.W., Franz, J., Elliott Fowler, J., Schilke, K.F., Weidner, T. & Baio, J.E. 2017 Identifying the selectivity of antimicrobial peptides to cell membranes by sum frequency generation spectroscopy. *Biointerphases* **12**, 02D406.

[20] Baio, J.E., Spinner, M., Jaye, C., Fischer, D.A., Gorb, S.N. & Weidner, T. 2015 Evidence of a molecular boundary lubricant at snakeskin surfaces. *Journal of The Royal Society Interface* **12**. (doi:10.1098/rsif.2015.0817).

[21] Ma, G. & Allen, H.C. 2006 DPPC Langmuir monolayer at the air-water interface: Probing the tail and head groups by vibrational sum frequency generation spectroscopy. *Langmuir*, 5341-5349.

[22] Casford, M.T.L., Ge, A., Kett, P.J.N., Ye, S. & Davies, P.B. 2014 The Structure of Lipid Bilayers Adsorbed on Activated Carboxy-Terminated Monolayers Investigated by Sum Frequency Generation Spectroscopy. *The journal of physical chemistry. B*. (doi:10.1021/jp410401z).

[23] Watry, M.R., Tarbuck, T.L. & Richmond, G.L. 2003 Vibrational sum-frequency studies of a series of phospholipid monolayers and the associated water structure at the vapor/water interface. *The Journal of Physical Chemistry B* **107**, 512-518.

[24] Hosoda, N. & Gorb, S.N. 2012 Underwater locomotion in a terrestrial beetle: combination of surface de-wetting and capillary forces. *Proceedings of the Royal Society of London B: Biological Sciences* **279**, 4236-4242.

Chapter 5. Multi-Technique, Mechanistic Investigation of a Biomimetic Beetle Tarsal Adhesive Fluid

James Elliott Fowler[1], Tobias Weidner[2,3], Stanislav Gorb[4], Joe E. Baio[1]

[1]Oregon State University, CBEE Department, Corvallis, OR;

[2]Max Planck Institute for Polymer Research, Mainz, Germany

[3]Department of Chemistry, Aarhus University, Aarhus, Denmark

[4]Zoological Institute of the University of Kiel, Department of Functional Morphology and Biomechanics, Kiel, Germany;

Email Correspondence – joe.baio@oregonstate.edu

Key Words – Insect Adhesion, Biomimetic, Fluid-Mediated Adhesion, Surface Analysis, Sum Frequency Generation (SFG) Spectroscopy

Abstract

There is substantial motivation to develop novel adhesives which take advantage of the superior tenacity and adaptability of many natural animal adhesives; however, the tools typically used to study these mechanisms are incapable of determining the precise interactions of molecules at an adhesive interface. In this study, a surface specific, order sensitive vibrational spectroscopy called sum frequency generation (SFG) is, for the first time, combined with multiple bulk characterization techniques to examine a novel, simple biomimetic beetle tarsal adhesive fluid. Insects have complex adhesive demands, including sticking, climbing vertically and hanging upside-down with little difficulty. Thus, we hypothesize that both bulk and surface specific properties of the fluid contribute to the success of this adhesive mechanism. SFG spectra of biomimetic emulsion exhibited similar hydrocarbon organization on hydrophobic and hydrophilic substrates to natural beetle fluid. Bulk characterization techniques indicated that the emulsion had a shear-thinning profile conducive to enhanced traction force during climbing and low surface tension ideal for surface wetting on all surfaces. Multi-technique comparisons between emulsion and pure squalane revealed that a hydrocarbon only fluid could not replicate the

traction promoting properties of the emulsion. We conclude that the beetle tarsal fluid adhesive mechanism relies upon contributions from both surface-specific properties optimizing traction force and lubrication and bulk properties promoting rapid surface wetting and moderating pull-off force for fast escape.

5.1 Introduction

Nature has been designing novel adhesive systems for millions of years and the study of one such system, insect tarsal adhesion, has led to improvements in materials design such as non-stick surfaces and climbing robots [1, 2]. However, these improvements have focused on mimicry of the physical structure of insect feet, only one-half of the hypothesized adhesive system. The other half is a fluid secreted from insect pads which mediates contact between foot and surface [3, 4]. Many studies have shown that this fluid was vital to the ability of insects to walk and climb without slipping and sliding on various environmental surfaces [5-13]. However, a consensus explanation for precisely how this fluid aids adhesion does not currently exist.

The composition of various insect species has been analyzed directly, using techniques such as mass spectrometry, and indirectly, by assessing its interaction with various chemicals and surfaces [10, 14-18]. Mass spectrometry results have concluded that insect adhesive fluid consists of branched and unbranched, long and short chain hydrocarbons, fatty acids, sugars, and alcohols [16, 19]. Overall, beetle adhesive has been suggested to be an oil-in-water emulsion, as this would be an ideal contacting fluid for its ability to spread easily on a wide range of substrates [20]. Manipulations of the tarsal fluid of the Colorado Potato Beetle (*Leptinotarsa decemlineata)*, as well as traction force experiments of Seven-Spotted Ladybird Beetles (*Coccinella septempunctata*) on nanoporous substrates, showed that removal of just part of the fluid significantly diminished their adhesive force [10, 14]. Additionally, study of the traction force of Cocc. sept. on smooth substrates revealed that these beetles generated more force on hydrophilic substrates [10]. Thus, studies have consistently demonstrated that there was a complex relationship between the chemistry of insect adhesive fluid and the chemistry of the contacting surface [3, 6, 21].

Recently, natural *Cocc. sept.* fluid was studied with sum frequency generation (SFG) spectroscopy, a surface specific, order sensitive vibrational spectroscopy, on surfaces with a range of wettabilities to determine what molecular groups were surface active and ordered at the interface. It was hypothesized that interfacial chemistry and molecular order were dynamic; however, it was instead found that interfacial fluid consisted of ordered hydrocarbons regardless of substrate hydrophilicity. It was concluded that the hydrocarbons were a mixture of branched and unbranched alkanes which were more highly ordered at hydrophobic interfaces, decreasing traction force of the bugs, thusly enhancing lubrication. Nevertheless, this study did not reveal a mechanism that explained beetle tarsal fluid adhesion.

Therefore, in this study we designed a biomimetic beetle adhesive with the distinct aim of deducing the mechanism that enabled natural beetle tarsal fluid to generate necessary adhesive forces. We hypothesized that the fluid must take advantage of both surface and bulk properties to maximize traction force while generating appropriate pull-off force. Thus, we believed that both the surface active and surface-inactive components of the emulsion played an important role in the insect tarsal adhesive mechanism.

A simple, three-component biomimetic adhesive emulsion was formulated from squalane, deuterated stearic acid and D_2O, chosen such that each component contained distinct chemical bonds which could be probed at the fluid-substrate interface. This emulsion was initially characterized with dynamic light scattering, surface tensiometry and rheology. SFG spectroscopy was then used to probe C-H, O-D, C-D and C=O vibrations at the interface between the biomimetic fluid and two surfaces - hydrophobic polystyrene and hydrophilic polyethylene oxide – to determine the effect of substrate chemistry on organization of surface active fluid molecules. The fluid was then iteratively deconstructed to determine the influence of the surface-inactive components on the organization of the surface-active layers of fluid.

5.2 Materials and Methods

5.2.1 Emulsion Formulation

Ten mL of squalane (96% purity, Sigma Aldrich, St. Louis, MO) was added to a scintillation vial cleaned by rinsing with ethanol and heated to 70° C. A 1 mM deuterated stearic acid in squalane solution was made by adding 3.2 mg of stearic-d_{35} acid (98 atom% d, Sigma Aldrich) and mixing with a magnetic stir-bar at 1000 rpm. Finally, 0.5 mL of D_2O was added dropwise and allowed to mix for three minutes. Emulsions were formed by ultrasonication at 60°C for two minutes. All experiments were performed with freshly made emulsion.

5.2.2 Rheological and Tribological Characterization of Fluids

The rheological behavior of the formulated emulsion, as well as pure squalane, was determined using a DHR3 Rheometer (TA Instruments, New Castle, DE) in cone-and-plate geometry with a 60 mm, 1.01°, titanium Peltier plate. Flow sweeps were performed at 25°C by measuring the viscosity and shear stress of the fluids while varying the shear rate from 1 x 10^{-3} to 1000 s^{-1}. Pull-off force measurements were performed in plate-plate geometry with a 20 mm, titanium plate and an initial gap size of 300 µm. The gap was filled with either emulsion or squalane and the axial force was zeroed. The top plate was lifted at a rate of 300 µm/s and the minimum axial force measured was reported as the pull-off force.

5.2.3 Surface Tensiometry

The surface tension of the emulsion and precursor fluids was measured with an FTA-T10 tensiometer (First Ten Angstroms, Portsmouth, VA) using a Du Nouy Ring. The reported surface tension was the average of ten consecutive dipping cycles. Measurements began only after a consistent force per wetted length peak was achieved.

5.2.4 Substrate Preparation

15 mm diameter CaF_2 optics (International Crystal Laboratories, Garfield, NJ) were cleaned via successive sonication in dichloromethane, acetone and ethanol and spun-coat (Laurell Technologies, North Wales, PA) at 2000 rpm for 60 s with 3 wt% solutions of one of the following: polyethylene oxide [PEO, MW = 100,000 Da] (Sigma Aldrich), polystyrene [PS, MW = 35,000 Da] (Sigma Aldrich), deuterated poly-ethylene oxide [dPEO, MW = 8960 Da] (Polymer Source Inc., Montreal, CA) or deuterated polystyrene [dPS, MW = 7420 Da] (Polymer Source Inc.) in toluene. Films were then

baked at 80°C for 20 hours at 500 mtorr to remove excess solvent. We have previously shown that this produced optically transparent polymer films of ~100 nm in thickness. Substrates were stored under N_2 atmosphere in sealed petri dishes until use to prevent contamination.

5.2.5 Sum Frequency Generation Spectroscopy

An EKSPLA Nd:YAG laser, operating at 50 Hz, was used to generate both a fixed visible (532 nm-1) and tunable IR beam (1000-4000 cm-1) via sequential pumping through an EKSPLA optical parametric generation/amplification and difference frequency unit, which utilized barium borate and AgGaS2 crystals respectively. The visible and IR beams (~150 μJ/pulse) were overlapped spatially and temporally at the desired interface to generate SFG photons, which were spectrally filtered, dispersed by a monochromator and detected with a gated photomultiplier tube. Both beams were focused to a ~ 1 mm diameter at the interface. Spectra were collected in 4 cm^{-1} steps with 400 acquisitions per step.

SFG spectra were generated at two different polarization combinations – ssp (s-polarized SFG, s-polarized visible, p-polarized IR) and ppp (p-polarized SFG, p-polarized visible, p-polarized IR) in 4 different vibrational regions (C-H – 2800-3100 cm-1; D-O – 2450 – 2650 cm^{-1}; C=O – 1600-1800 cm-1; C-D – 2000-2300 cm-1) through the backside of a CaF2 window which rests on a Teflon o-ring (ID – 7.9 mm) attached to a flat, cylindrical Teflon platform. The void volume of the o-ring was filled with the sample fluid such that the fluid was in full contact with the top window surface at all times during the experiment. SFG signal is optimized in each wavenumber region using an Au-coated CaF2 window in the same set-up. The fitting routine for SFG spectra is previously detailed elsewhere [22-25]. Briefly, spectra were iteratively fit to the equation below (Eq. 1) to determine non-resonant phase, non-resonant background (χ_{nr}), frequency (ω_q), individual peak full width half maximum (FWHM; Γ_q) and individual peak amplitude (A_q).

$$\text{(Eq. 1)} \quad \chi^{(2)}_{\text{eff}} = \chi_{\text{nr}} + \sum_{\text{q}} \frac{\text{A}_\text{q}}{\omega_2 - \omega_\text{q} + \text{i}\Gamma_\text{q}}$$

5.3 Results

5.3.1 Emulsion Characterization

From visual observation, the emulsion was stable over short periods of time (hours) but was susceptible to aggregation of the particle phase overnight. Particle aggregation was supported by dynamic light scattering measurements, which determined the mean particle size of the emulsion to be 8.0 µm with a polydispersity index of 0.4. This indicated a suspension on the borderline between a medium and broad distribution of particle sizes [26]. Additionally, particles of various sizes were clearly visible in light microscope images of fresh emulsion (Figure 1).

Next, the surface tensions of emulsion as well as two control fluids: pure squalane and a 1 mM d-stearic acid in squalane solution, were determined (Table 5.S1). The surface tension of pure squalane was measured at 28.4 ± 0.1 mN/m, which was consistent with the reported literature value of 28 mN/m [27]. The surface tension of the 1 mM d-stearic acid in squalane solution was lower at 27.1 ± 0.1 mM/m, which was expected due to the amphiphilic nature of stearic acid [28]. Finally, the emulsion had a surface tension of 27.5 ± 0.1 mN/m. Overall, the surface tensions of all three fluids were consistent with the estimated surface tension of a hydrophobic secretion (~30 mN/m) [29].

Rheometry experiments of both the emulsion and pure squalane revealed distinctly different viscosity profiles. Unsurprisingly the viscosity of a film of pure squalane was constant (29 mPa*s) across a wide range of shear rates, which was consistent with the many previous analyses of the hydrocarbon as a low viscosity Newtonian fluid [30]. However, viscosity measurements taken from a film of emulsion provided a shear-thinning profile, with a very small yield stress of ~0.01 Pa. Additionally, a plate-plate geometry was used to determine the pull-off adhesive strength of the two fluids. There was no difference in the tackiness of the emulsion compared to the hydrocarbon, with forces of 0.533 ± 0.009 and 0.527 ± 0.007 respectively (Table 5.S2).

5.3.2 SFG Spectroscopy

As previously mentioned, the composition of the emulsion was carefully selected to allow for isolation of representative molecular bonds from each component in separate vibrational regions, which were measured with SFG spectroscopy. This allowed for the determination of which components in the fluid were surface active. For example, the C-H stretching region (2800 - 3000 cm^{-1}) was used to measure ordered modes at the

interface corresponding to squalane as the only source of methyl and methylene modes was that component of the emulsion. Likewise, the O-D stretching region (2450 - 2650 cm^{-1}) was used to observe D_2O at the interface, while the C-D (2000 - 2350 cm^{-1}) and C=O (1650 - 1800 cm^{-1}) regions were for observing d-stearic acid vibrational modes.

SFG spectra of emulsion at dPEO and dPS surfaces in SSP polarization combination at the C-H stretching region are shown in Figure 2b. Four vibrational modes were observed in both spectra: near 2855 cm^{-1}, 2880 cm^{-1}, 2914 cm^{-1} and 2935 cm^{-1}, corresponding to CH_2 symmetric, CH_3 symmetric, CH_2 asymmetric and CH_3 fermi modes respectively [22, 31-34]. All of these modes were also observed in SSP, C-H region spectra of the natural *Cocc. sept.* fluid on the same substrates, except for the CH_2 asymmetric mode (Figure 2a). Spectra of the emulsion at the same surfaces in PPP polarization combination produced substantially different spectral profiles. Five total modes were observed in PPP spectra: near 2864 cm^{-1}, 2884 cm^{-1}, 2900 cm^{-1}, 2925 cm^{-1} and 2962 cm^{-1} corresponding to CH_2 symmetric, CH_3 symmetric, CH (tertiary), CH_2 asymmetric and CH_3 asymmetric vibrational modes respectively (Figure 5.S1). However, unlike in SSP combination, the same set of modes were not present across spectra of fluid on both surfaces, with the CH_2 and CH_3 symmetric and CH_2 asymmetric modes absent in the emulsion – dPS spectrum.

The relative ratio of CH_3 symmetric to CH_2 symmetric stretch amplitudes has been shown to be indicative of the relative organization of a layer of hydrocarbons, with larger values indicating a more uniform angle in relation to the surface [31, 35]. These values, and the trend between substrates, were similar for the same substrates in the natural and biomimetic fluid spectra, with values of 3.46 ± 0.40 and 1.03 ± 0.07 for the dPS and dPEO spectra of the natural fluid and 4.47 ± and 1.70 ± for spectra of the same surfaces with biomimetic fluid. However, there was one major difference between the C-H SSP spectra of the natural and biomimetic fluids – the presence of a peak corresponding to CH_2 asymmetric stretching near 2914 cm^{-1} in the latter (Figure 2b). Previous SFG studies of alkane chains oriented towards the surface normal at solid/air and liquid/air interfaces have shown that the CH_2 asymmetric stretch has a substantially lower intensity in SSP compared to PPP or SPS polarization combinations. In this study, this trend was

reversed, with stronger peak amplitude in SSP than PPP spectra. The mode amplitude was particularly strong at the hydrophobic surface – at which squalane would interact with more favorably. One explanation for this result is that squalane has been shown, via molecular dynamics (MD) simulations for squalane on hydrophilic silicon, to prefer a chain orientation parallel to solid surfaces with its methyl side chains arranged perpendicular from the chain (Figure 3) [36, 37]. As mode amplitudes are sensitive to beam polarization as well as molecular bond orientation and order, it follows that a substantial rotation in chain angle could have led to the observed shifting in preference for the CH_2 asymmetric stretch from PPP to SSP polarization combination [38]. Thus, although organization of squalane chains at the emulsion interface was consistent with organization of hydrocarbons in natural adhesive fluid, the squalane layers were rotated perpendicularly from the natural fluid hydrocarbons. Lastly, spectra of the emulsion at non-deuterated substrates collected in the other three (O-D, C-D, C=O) stretching regions did not produce any SFG signal originating from either the D_2O or d-stearic acid molecules at either substrate (Figures 5.S2 and 5.S3). This was consistent with characterizations of natural *Cocc. sept.* fluid, in which hydrocarbons were shown to be the only surface-active component.

Next, spectra of pure squalane and a 1 mM d-stearic acid in squalane solution at PEO and PS surfaces were compared to emulsion spectra to determine the whether surface-inactive components of the emulsion (d-stearic acid, D_2O) influenced the organization of the interfacially-active squalane molecules. While spectra were collected in all four regions (C-H, O-D, C-D, C=O) again, we only observed signal in C-H region spectra for each of the control fluids. The four modes previously identified in C-H SSP spectra were present in both control fluids spectra; however, an additional mode was observed near 2868 cm^{-1} (Figure 4). Due to the wavenumber proximity of this mode to the CH_3 symmetric mode near 2880 cm^{-1}, we attributed this mode to the resonance created by the dimethyl branching at either end of squalane molecules. Interestingly, it was only clearly observed in pure squalane spectra for both surfaces [39]. There were distinctly different trends in amplitude for the CH_2 symmetric, CH_3 symmetric and CH_2 asymmetric modes observed between the hydrophobic and hydrophilic surfaces and across the set of fluids. For example, the CH_2 asymmetric stretch amplitude decreased from emulsion

to squalane/d-stearic acid to squalane only spectra at the PS surface (Figure 4b); however, at the PEO surface, the amplitude was initially negligible, increased for the squalane/d-stearic acid solution and was then negligible again for squalane (Figure 4a). Similarly, on the PS surface the CH_2 symmetric stretch was greater for the control fluids compared to the emulsion, but on the PEO surface the amplitude initially decreased for the squalane/d-stearic acid solution and then increased substantially for squalane only. Overall, the mode amplitude trends in this experiment showed that the removal of an amphiphilic molecule and D_2O led to apparent changes in the organization of interfacial squalane, although the specific changes were unique to the wettability of the contacting surface. However, on both surfaces the emulsion spectra exhibited greater organization of interfacial squalane layers than pure squalane.

5.4 Discussion

One of the strongest instincts many beetles have is negative geotaxis – climbing upwards in response to environmental stressors [40, 41]. To evaluate the role of secreted tarsal fluid in the adhesion of these insects, promotion of climbing ability must be considered as a vital function. However, several other factors must also be taken into account. For instance, a beetle standing upright and still on a flat substrate must generate enough contact with the surface to prevent sliding but must not generate too much adhesive force that it cannot detach from the surface to escape danger. A successful adhesive fluid must also be able to handle transitioning from wet to dry, smooth to rough, hydrophobic to hydrophilic or upright to inclined or inverted without failure. Thus, an ideal beetle tarsal adhesive fluid would utilize a mechanism which was inherently complex – no single characteristic of the fluid responsible for mitigating all of the aforementioned challenges singularly.

While there have been many attempts to ascertain this mechanism using kinematic experiments, surface analytical approaches have been underutilized. Thus, this study used SFG, a surface-specific, order sensitive nonlinear vibrational spectroscopy, to investigate the organization of molecules within the biomimetic emulsion at the surface of hydrophobic and hydrophilic substrates. As previously introduced, this technique was recently used to probe natural *Cocc. sept.* tarsal adhesive and it was found that a layer

of branched and unbranched hydrocarbons organized at all substrate surfaces with organization dependent upon substrate wettability. It has been shown that beetles exhibited significantly different traction forces depending upon the wettability of the contacting surface [8, 9]. An inverse relationship existed between the ordering of a layer of hydrocarbons at the interface and the magnitude of traction force measured on similar surfaces. Thus, it was concluded that the fluid enhanced traction force on hydrophilic substrates, where an oily fluid would interact less strongly, and increased lubrication of hydrophobic substrates, where interactions would naturally be stronger.

Yet, limiting factors such as the very small volume (pL) of fluid droplets and the suspected volatility of some components of the fluid limited the ability to definitively conclude whether chemical surface analytical results were representative of the complete mechanism [17]. In this study, a biomimetic emulsion was created in quantities with which fluid volume and chemistry could be carefully controlled during SFG experiments. Resultant SFG spectra provided clear evidence that the hydrocarbon component, squalane, was the only substrate-active chemical in the emulsion. Additionally, the emulsion displayed very similar hydrocarbon chain organization (CH_3/CH_2 stretching ratios) to the natural *Cocc. sept.* fluid (Figure 2). Both results supported the previous conclusion that a surface-active hydrocarbon component in beetle tarsal fluid was responsible for moderating traction and lubrication in response to changing environmental surface chemistry.

However, rheological testing of the biomimetic fluid revealed the additional benefit of an emulsion to generation of traction force. The resistance of the hydrophilic particle phase against the hydrophobic bulk phase when shear was applied, led to a shear-thinning non-Newtonian fluid with a small yield stress (Figure 5.S4) [42]. The higher viscosity exhibited by a fluid with this profile during events with very low or no shear rate, such as clinging on inclined surfaces, would be ideal for slip prevention [3, 42, 43]. However, the shear rate applied by this system at average beetle walking speed (~5 mm/s) and with a biomimetic fluid layer 100 nm thick (a conservative estimate of natural fluid thickness) would be well above the rate necessary for the fluid to exhibit a constant, low viscosity like that of pure squalane (Figure 5.S4) [3, 44]. Thus, this fluid would provide

a beetle resistance to sliding on inclined surfaces at rest without increasing the effort required to resume movement. Combined, a slip-resistant bulk structure and a lubricating surface layer sensitive to substrate chemistry indicated that the tarsal adhesive fluid mechanism was well-designed to support the climbing instinct of beetles.

Despite this conclusion, it has been hypothesized that some beetle fluids may consist only of hydrocarbons [11, 14, 16]. Thus, it was necessary to determine whether a fluid consisting of only hydrocarbon molecules reasonably replicated the adhesive properties of the biomimetic emulsion. Squalane, a low viscosity, low surface tension fluid has been shown to have low cohesive forces, which can be correlated to both easier filling of small asperities and faster de-wetting from a surface [20, 45, 46]. These properties would be desired for maximizing contact area and pull-off adhesive force. In fact, if the only consideration for adhesion was pull-off force and surface wetting, pure squalane may be considered an ideal mimic for beetle adhesive fluid. It generated the same pull-off force as the emulsion in this study while having a comparable surface tension (Figure 5.S5 and Tables 5.S1 and 5.S2).

However, we have established traction force to be at least as important as these factors, if not more so [47, 48]. Consequently, comparing the SFG spectra of emulsion versus pure squalane on hydrophobic and hydrophilic substrates revealed clear differences in the organization of squalane layers between the two fluids on each substrate (Figure 3). Most importantly, the contrast in ordering ratio observed in both the emulsion and natural *Cocc. sept.* fluid spectra were not present between the squalane spectra on each substrate. This corresponded to no difference in traction force between the hydrophobic and hydrophilic substrate, which was inconsistent with beetle kinematic experiments. Thus, the emulsion was the only fluid which combined the low surface tension spreading advantages to control pull off force and the dynamic organizational response to substrate hydrophobicity to optimize traction force. Furthermore, we have demonstrated that the surface inactive components of the biomimetic tarsal adhesive fluid – the water and stearic acid which form the particle phase of the emulsion – clearly influence the organization of the surface active squalane layers and by extension the adhesive properties of the fluid.

5.5 Conclusions

Our experiments on natural and biomimetic beetle adhesives have shown that the interfacial interactions between fluid and substrate are an important component of the foot adhesive mechanism, ensuring lubrication of the foot during movement across different surface as well as maintaining sufficient surface contact via low surface tension. However, chemistry of the bulk, surface-inactive fluid played an equally important role by bestowing a shear-thinning profile to the fluid and regulating the magnitude of traction forces generated by influencing order of the interfacial components (Figure 4).

An immediate application of biomimetic beetle tarsal adhesive is in the development of climbing robots, as the fluid resists shear well while generating relatively small pull-off forces. This would minimize the necessary energy input for successive climbs. However, work is still needed to improve the stability the oil-in-water emulsion. In this study, composition was limited to naturally occurring chemicals with very specific molecular bonds so that each chemical could be tracked. Future formulations may explore surfactants which have stronger affinities for water to prevent aggregation of particles above micron sizes. Regardless, herein we have shown that a combination of surface specific and bulk analytical techniques can be used to carefully determine a complex adhesive mechanism developed by nature.

5.6 Figures

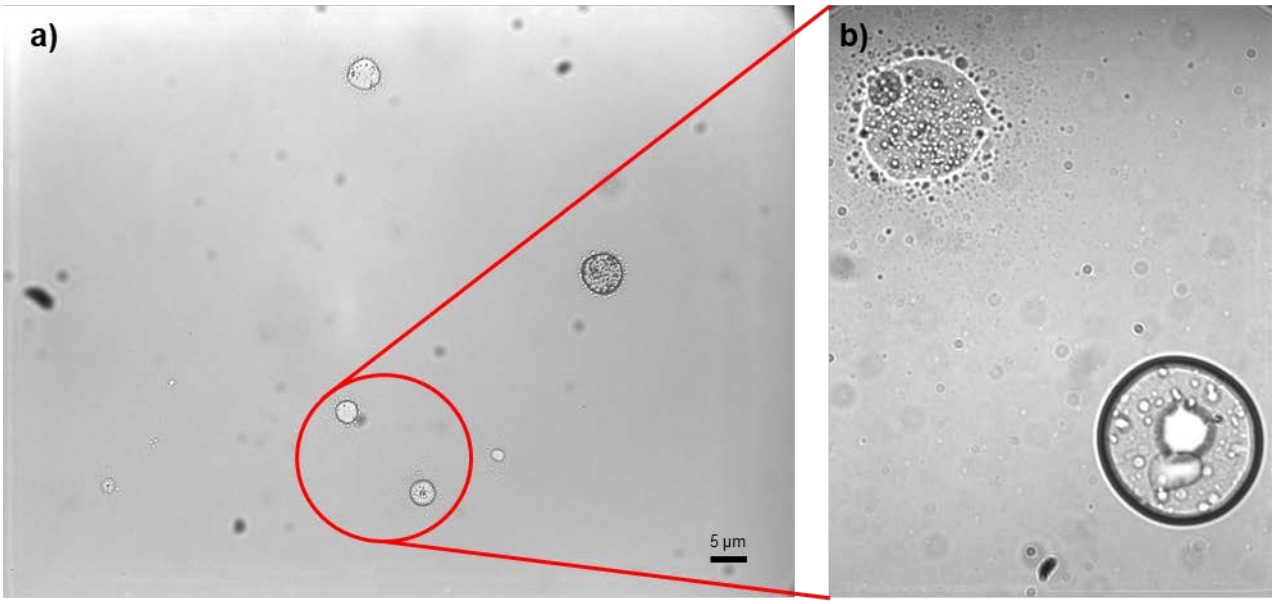

Figure 1 – Microscope image of biomimetic emulsion in 10x (a) and 50x (b) magnification.

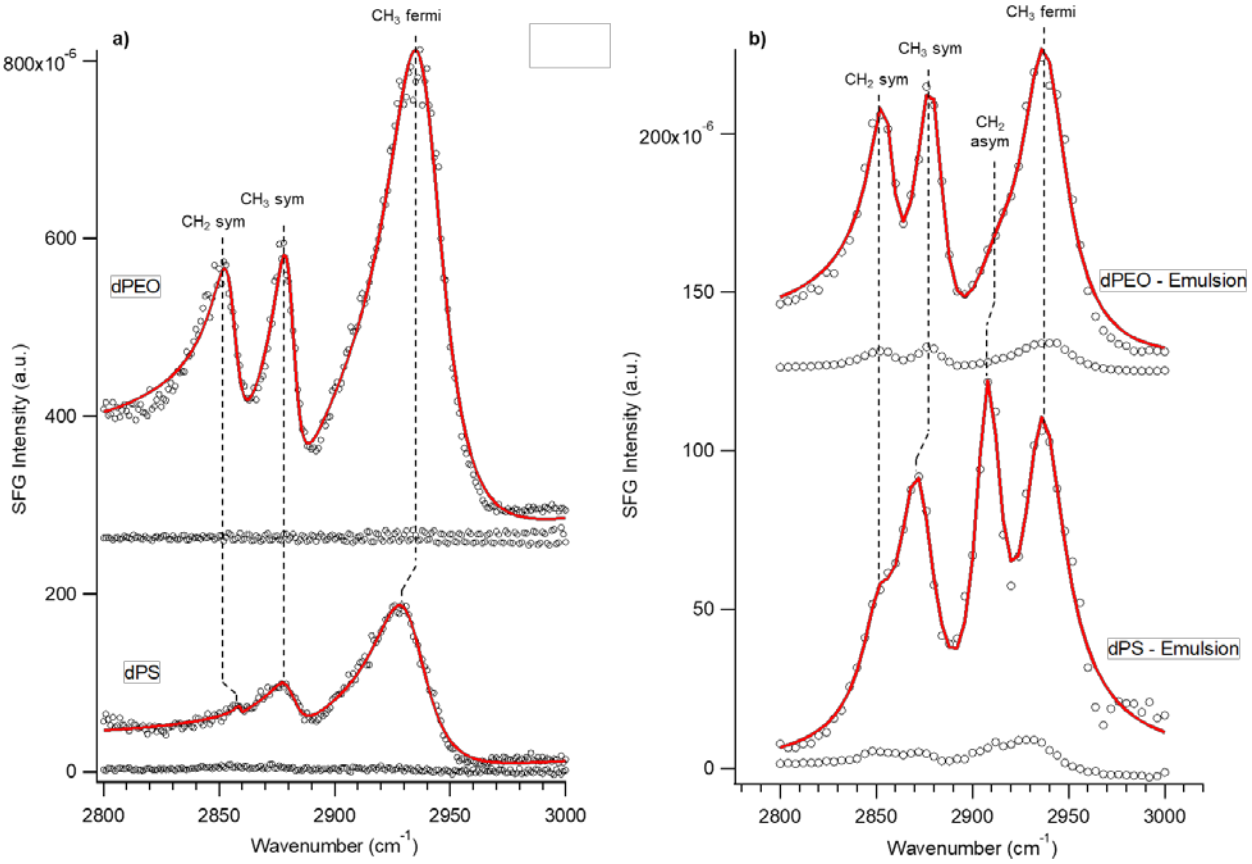

Figure 5.2 – SFG spectra in the C-H stretching region and SSP polarization combination of a) natural *Cocc. sept.* tarsal fluid on PEO and PS substrates and b) biomimetic emulsion on PEO and PS substrates. Three vibrational modes were observed in all four spectra: near 2855 cm^{-1}, 2880 cm^{-1} and 2935 cm^{-1} corresponding to CH_2 symmetric, CH_3 symmetric and CH_3 fermi vibrational modes respectively. One mode is unique to the biomimetic emulsion/substrate interfaces, the CH_2 asymmetric stretch near 2914 cm^{-1}, likely due to different orientation of surface hydrocarbons between natural and biomimetic fluids. Relative SFG intensity of CH_3 and CH_2 symmetric modes and the change in this intensity as hydrophobicity is increased is similar between natural and biomimetic fluid interfaces.

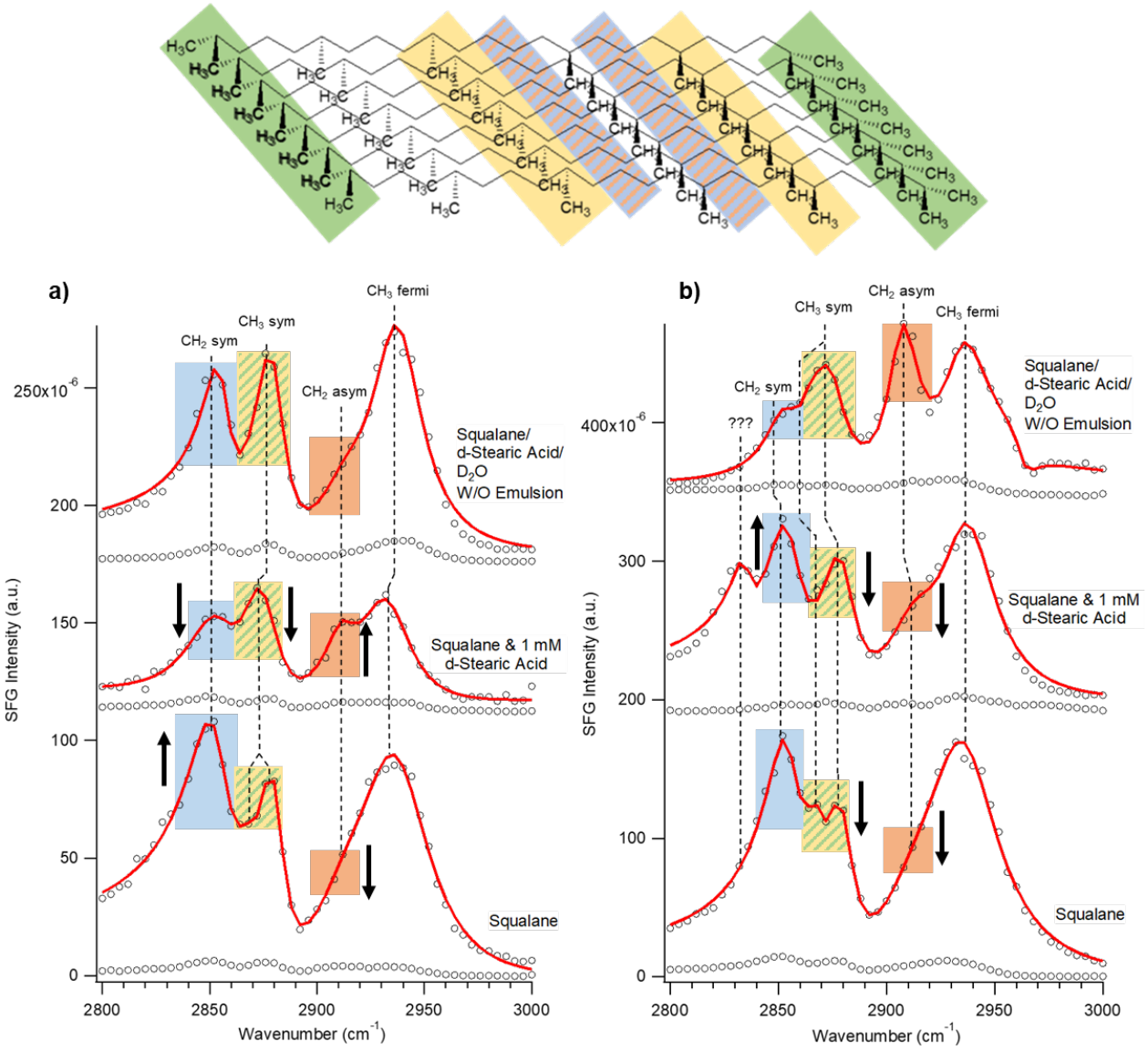

Figure 5.3 – SFG Spectra of biomimetic emulsion and control fluids at PEO (a) and PS (b) surfaces in the C-H vibrational region and SSP polarization combination. Spectra and fits are represented by black circles and red dots, respectively. Five vibrational modes were observed in all of the spectra: near 2855 cm^{-1}, 2868 cm^{-1}, 2880 cm^{-1}, 2914 cm^{-1} and 2935 cm^{-1} corresponding to CH_2 symmetric, CH_3 symmetric, CH_2 asymmetric and CH_3 fermi vibrations, respectively. Colored bars indicate vibrational mode locations on a layer of squalane molecules present at the interface. Black arrows indicate relative change in mode amplitude from the same mode in the spectrum above it.

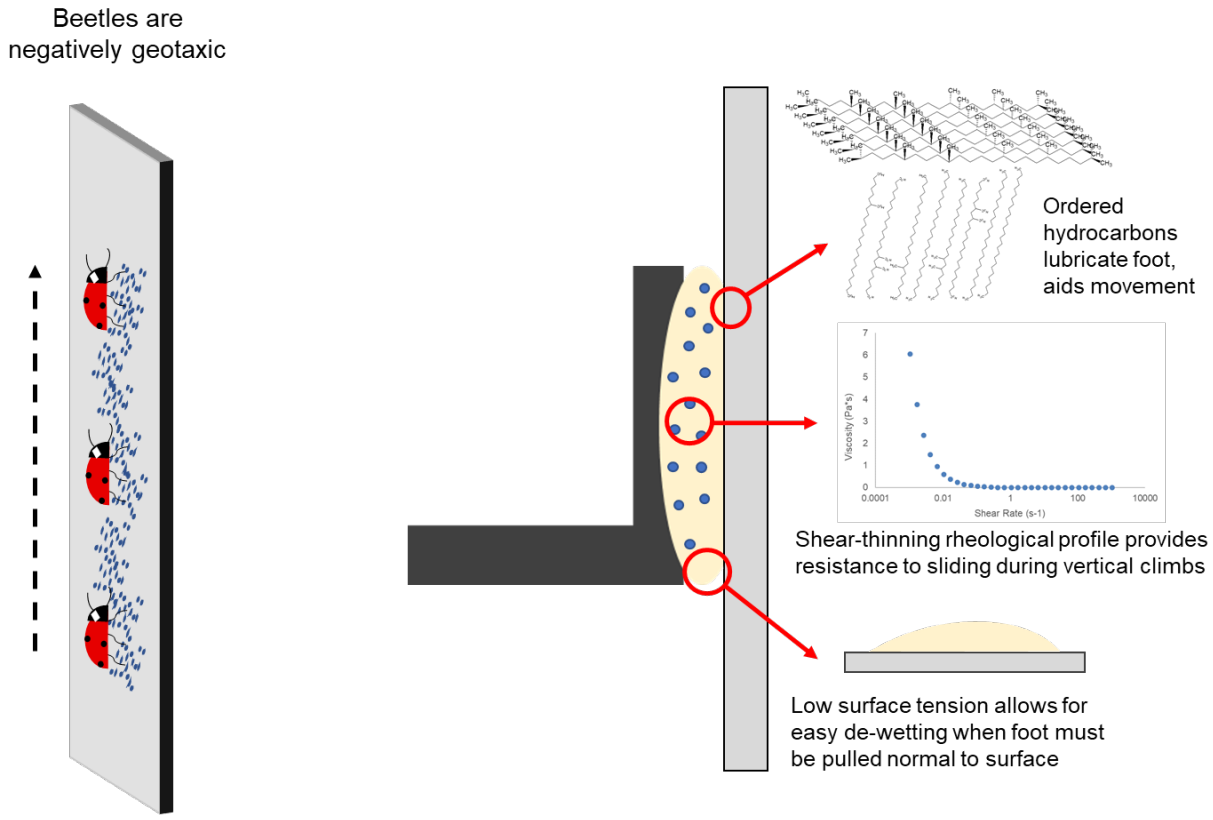

Figure 5.4 – Diagram illustrating the purpose of beetle tarsal adhesion (left) and the corresponding properties of natural and biomimetic beetle tarsal adhesive fluid which allow it to perform its necessary functions (right).

5.7 Supporting Information

The primary aim of this study was to formulate a simple, biomimetic beetle tarsal adhesive in large quantities and with a known composition such that the chemical mechanisms governing this type of fluid-mediated adhesion could be better understood. Before surface chemical analysis could be performed, it was necessary to characterize our biomimetic adhesive to ensure that the bulk properties of the fluid matched well with previous classifications of bulk natural beetle adhesive. Therefore, we initially determined the droplet size, surface tension, rheological profile and pull-off force of the emulsion for comparison.

Previous microscopy characterization of the tarsal fluid of the Asian weaver ant (Oecophylla smaragdina) and stick insect (*Carausius morosus*) have shown two distinct chemical phases, with internal phase diameters of approximately 5 µm and 0.5 µm respectively. As previously mentioned, no direct measurement currently exists of an internal “volatile” phase within *Cocc. sept.* tarsal fluid, although AFM experiments estimated a volume loss of a single droplet at ~25% over the course of an hour at ambient temperature and pressure. Thus, parameters were set in this study for an emulsion with micron-sized particles and an internal phase of </=25%. Initial attempts at emulsion formulation attempted to integrate up to 2.5 mL (25% v/v) of D_2O into the internal phase. However, we found that increasing the volume of D_2O above 5% v/v led to immediate phase separation between D_2O and squalane without particle formation. Conversely, 5% v/v D_2O led to stable water-in-oil emulsions with mean particle sizes of 8.0 µm. To maximize similarity to both desired length and volume parameters, this formulation was used in further experiments.

Rheological characterization of natural insect adhesive fluids has been recently explored to explain the difference in attachment abilities between various insects. Determination of not only the viscosity, but also whether the fluid behaves Newtonian or non-Newtonian has been considered a major factor in understanding foot adhesion tenacity in the shear direction (also known as traction force). For example, a non-Newtonian fluid will provide greater traction force and thus greater resistance to sliding when insects climb vertical or severely inclined surfaces. In this study, the biomimetic

emulsion displayed a non-Newtonian, shear-thinning profile with a very small yield stress of ~0.01 Pa (Figure 5.S4). At higher shear rates, the emulsion maintained a viscosity that closely resembled the viscosity of pure squalane (~30 mPa*s) which had a Newtonian profile. The shear-thinning profile of our biomimetic emulsion was consistent with studies of the Asian weaver ant, which had internal phases of roughly the same size. However, tarsal fluid of the Colorado potato beetle (*Leptinotarsa decemlineata*) as well as *Cocc. sept.* was found to be Newtonian in nature with 100 mPa*s and 22 mPa*s viscosities respectively. While our biomimetic emulsion more closely resembled the *Oeco. smar.* fluid in terms of profile, its viscosity of 30 mPa*s at higher shear rate is very close to the value of 22 mPa*s measured for *Cocc. sept.* However, resistance to flow in the shear direction is only half of the story when it comes to beetle adhesion – a beetle's ability to generate the proper amount of adhesive force in the tensile direction (also known as pull-off force) is vital for both hanging and enabling so called "fast escape" from a surface in the face of danger. In this study, we observed no change in pull-off force between a liquid film of biomimetic emulsion and pure squalane (Figure 5.S5). While this may seem counterintuitive, a recent study, which manipulated the chemical composition of *Lept. decem.* fluid found that replacement of the natural adhesive fluid with n-alkanes had an insignificant effect on attachment force. This is likely because a water-in-oil emulsion with a low v/v% internal phase has highly similar surface tension to pure alkane. This was demonstrated in our study, wherein the surface tensions of the biomimetic emulsion and pure squalane differed by slightly more than 3%. Overall, the similarities to natural beetle adhesive that our emulsion exhibited across a spectrum of physical properties allowed for the determination that it was an acceptable mimic.

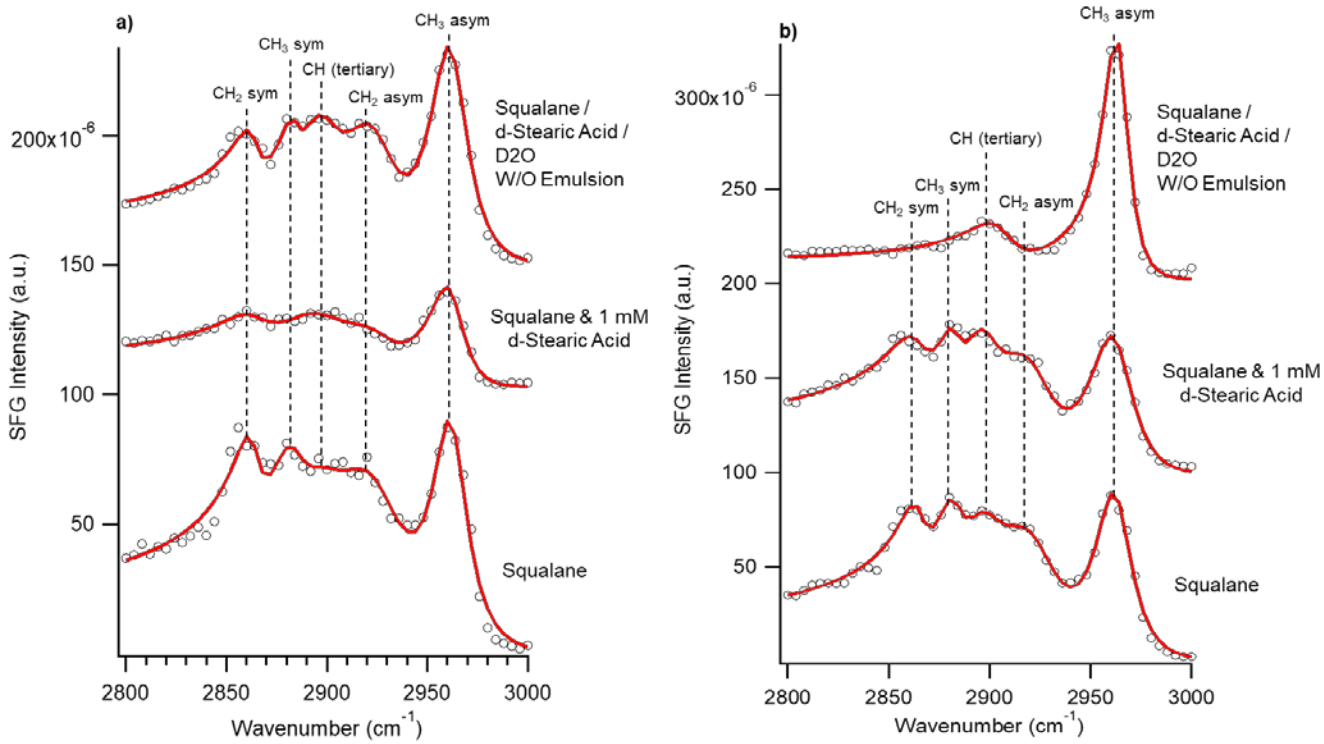

Figure 5.S1 – PPP polarization combination, C-H region (2800 – 3000 cm^{-1}) spectra (black circles) and fits (red lines) for biomimetic emulsion and control fluids on dPEO a) and dPS b) surfaces.

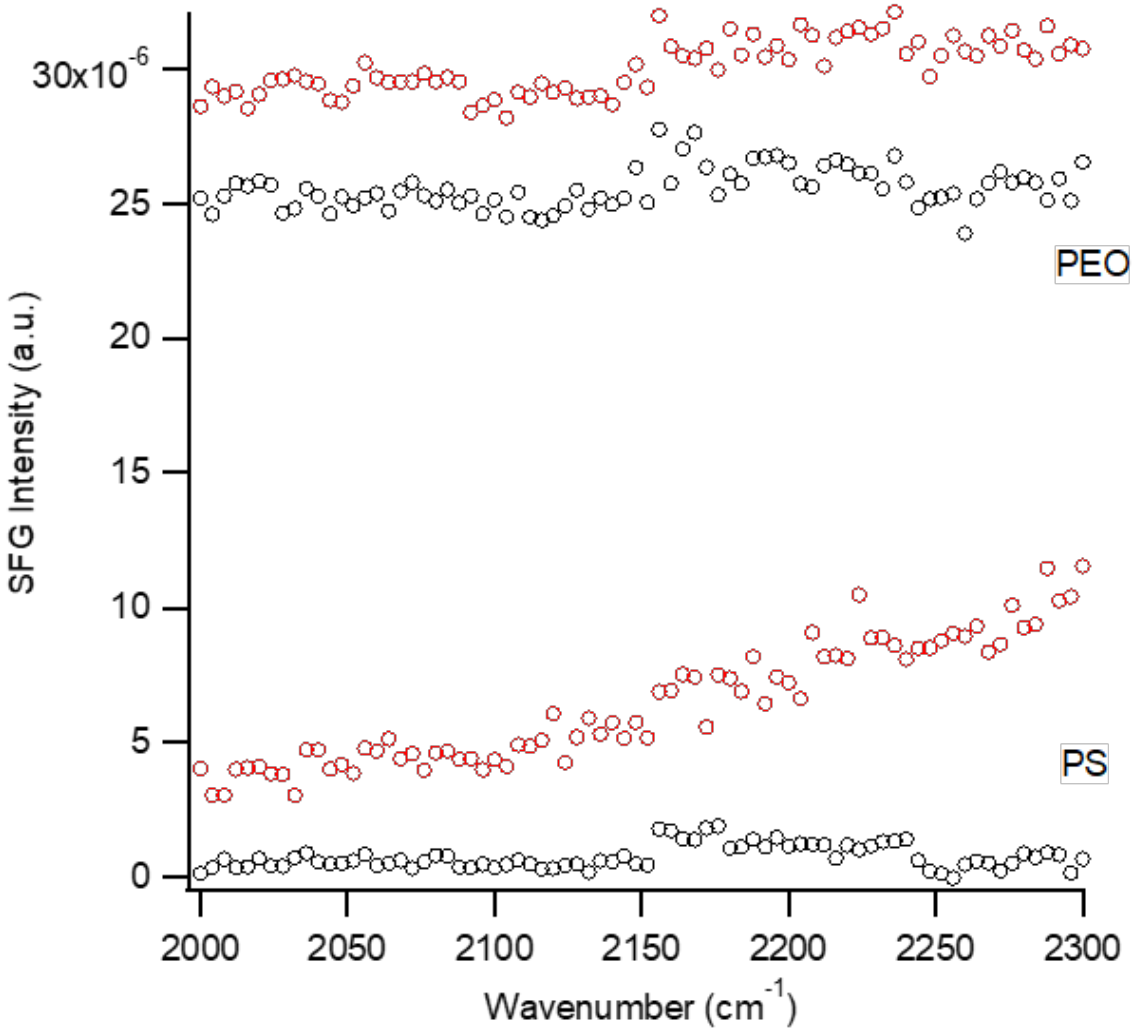

Figure 5.S2 – SFG spectra of biomimetic emulsion at PEO and PS substrates in the C-D stretching region (2000 – 2300 cm^{-1}). Red circles represent spectra where emulsion is present, black circles represent spectra of bare substrate.

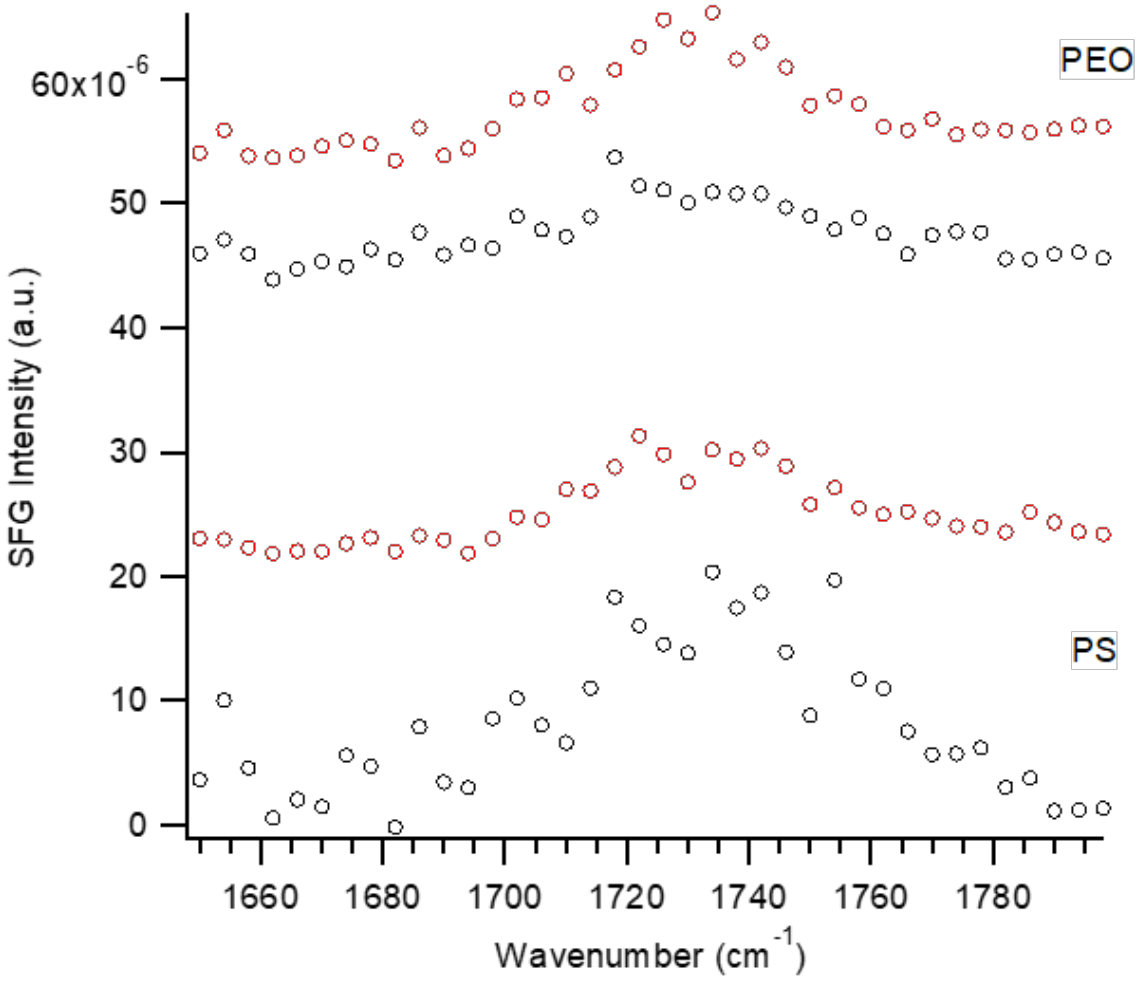

Figure 5.S3 – SFG spectra of biomimetic emulsion at PEO and PS substrates in the C=O stretching region (1650 – 1800 cm^{-1}). Red circles represent spectra where emulsion is present, black circles represent spectra of bare substrate.

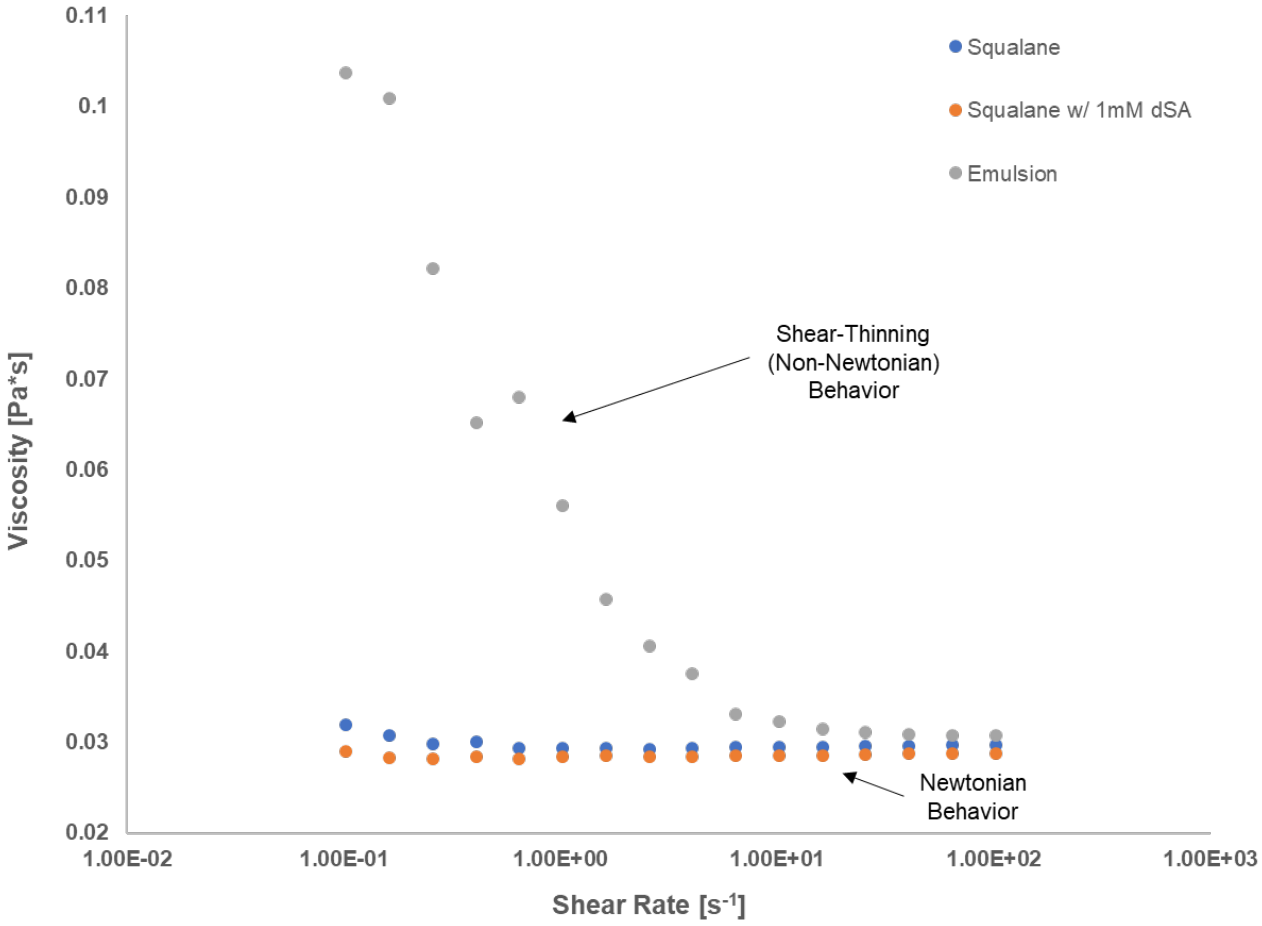

Figure 5.S4 – Viscosity profiles of squalane, squalane with 1 mM d-stearic acid and pure squalane.

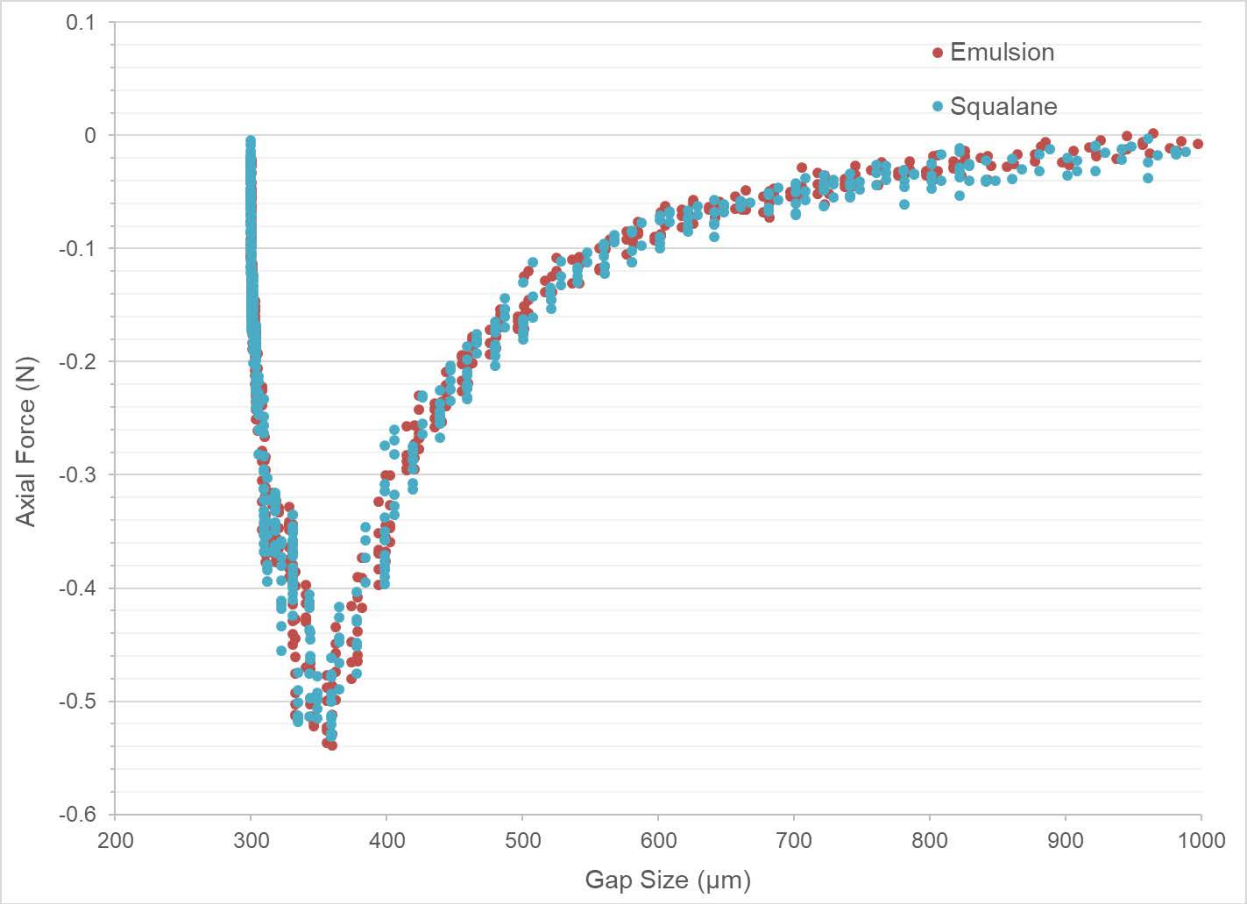

Figure 5.S5 – Pull-off force measurements of squalane and biomimetic emulsion fluids performed on a rheometer in parallel plate geometry.

Fluid	Surface Tension (mN/m)
Squalane	28.4 ± 0.1
Squalane/d-Stearic Acid (1 mM)	27.1 ± 0.1
Emulsion	27.5 ± 0.1

Table 5.S1 – Surface tension results for all three experimental fluids

Fluid	Trial	Pull-Off Force (N)	Average Force (N)	Std. Dev.
Emulsion	*1*	0.522	0.533	0.009
	2	0.537		
	3	0.539		
Squalane	*1*	0.531	0.527	0.007
	2	0.518		
	3	0.530		

Tables 5.S2. – Pull-off force results for biomimetic emulsion and squalane

5.8 References

[1] Gorb, S.N., Sinha, M., Peressadko, A., Daltorio, K.A. & Quinn, R.D. 2007 Insects did it first: a micropatterned adhesive tape for robotic applications. *Bioinspiration & biomimetics* **2**, S117.

[2] Daltorio, K.A., Wei, T.E., Horchler, A.D., Southard, L., Wile, G.D., Quinn, R.D., Gorb, S.N. & Ritzmann, R.E. 2009 Mini-Whegs TM Climbs Steep Surfaces Using Insect-inspired Attachment Mechanisms. *The International Journal of Robotics Research* **28**, 285-302. (doi:doi:10.1177/0278364908095334).

[3] Dirks, J.-H. & Federle, W. 2011 Fluid-based adhesion in insects - principles and challenges. *Soft Matter* **7**, 11047-11053. (doi:10.1039/c1sm06269g).

[4] Walker, G. 1993 Adhesion to smooth surfaces by insects—a review. *International Journal of Adhesion and Adhesives* **13**, 6-10.

[5] Busshardt, P., Wolf, H. & Gorb, S.N. 2012 Adhesive and frictional properties of tarsal attachment pads in two species of stick insects (Phasmatodea) with smooth and nubby euplantulae. *Zoology* **115**, 135-141. (doi:10.1016/j.zool.2011.11.002).

[6] England, M.W., Sato, T., Yagihashi, M., Hozumi, A., Gorb, S.N. & Gorb, E.V. 2016 Surface roughness rather than surface chemistry essentially affects insect adhesion. *Beilstein Journal of Nanotechnology* **7**, 1471-1479.

[7] Gorb, E. & Gorb, S. 2002 Attachment ability of the beetle Chrysolina fastuosa on various plant surfaces. *Entomologia Experimentalis et Applicata* **105**, 13-28.

[8] Gorb, E. & Gorb, S. 2009 Effects of surface topography and chemistry of Rumex obtusifolius leaves on the attachment of the beetle Gastrophysa viridula. *Entomologia experimentalis et applicata* **130**, 222-228.

[9] Gorb, E., Voigt, D., Eigenbrode, S.D. & Gorb, S. 2008 Attachment force of the beetle Cryptolaemus montrouzieri (Coleoptera, Coccinellidae) on leaflet surfaces of mutants of the pea Pisum sativum (Fabaceae) with regular and reduced wax coverage. *Arthropod-Plant Interactions* **2**, 247-259.

[10] Gorb, E.V., Hosoda, N., Miksch, C. & Gorb, S.N. 2010 Slippery pores: anti-adhesive effect of nanoporous substrates on the beetle attachment system. *Journal of the Royal Society, Interface / the Royal Society* **7**, 1571-1579. (doi:10.1098/rsif.2010.0081).

[11] Gorb, S.N. 2001 *Attachment Devices of Insect Cuticle*. Dordrecht, The Netherlands, Kluwer Academic Publishers.

[12] Hosoda, N. & Gorb, S.N. 2012 Underwater locomotion in a terrestrial beetle: combination of surface de-wetting and capillary forces. *Proceedings of the Royal Society of London B: Biological Sciences* **279**, 4236-4242.

[13] Langer, M.G., Ruppersberg, J.P. & Gorb, S. 2004 Adhesion forces measured at the level of a terminal plate of the fly's seta. *Proceedings of the Royal Society of London B: Biological Sciences* **271**, 2209-2215.

[14] Geiselhardt, S.F., Federle, W., Prüm, B., Geiselhardt, S., Lamm, S. & Peschke, K. 2010 Impact of chemical manipulation of tarsal liquids on attachment in the Colorado potato beetle, Leptinotarsa decemlineata. *Journal of insect physiology* **56**, 398-404.

[15] Geiselhardt, S.F., Geiselhardt, S. & Peschke, K. 2009 Comparison of tarsal and cuticular chemistry in the leaf beetle Gastrophysa viridula (Coleoptera: Chrysomelidae) and an evaluation of solid-phase microextraction and solvent extraction techniques. *Chemoecology* **19**, 185.

[16] Geiselhardt, S.F., Geiselhardt, S. & Peschke, K. 2011 Congruence of epicuticular hydrocarbons and tarsal secretions as a principle in beetles. *Chemoecology* **21**, 181.

[17] Peisker, H. & Gorb, S.N. 2012 Evaporation dynamics of tarsal liquid footprints in flies (Calliphora vicina)and beetles (Coccinella septempunctata). *The Journal of experimental biology* **215**, 1266-1271. (doi:10.1242/jeb.065722).

[18] Heepe, L., Wolff, J.O. & Gorb, S.N. 2016 Influence of ambient humidity on the attachment ability of ladybird beetles (Coccinella septempunctata). *Beilstein Journal of Nanotechnology* **7**, 1322-1329.

[19] Vötsch, W., Nicholson, G., Müller, R., Stierhof, Y.D., Gorb, S. & Schwarz, U. 2002 Chemical composition of the attachment pad secretion of the locust Locusta migratoria. *Insect biochemistry and molecular biology* **32**, 1605-1613.

[20] Peisker, H., Heepe, L., Kovalev, A.E. & Gorb, S.N. 2014 Comparative study of the fluid viscosity in tarsal hairy attachment systems of flies and beetles. *Journal of the Royal Society Interface* **11**. (doi:10.1098/rsif.2014.0752).

[21] Federle, W., Riehle, M., Curtis, A.S.G. & Full, R.J. 2002 An integrative study of insect adhesion: mechanics and wet adhesion of pretarsal pads in ants. *Integrative and comparative biology* **42**, 1100-1106. (doi:10.1093/icb/42.6.1100).

[22] Baio, J.E., Spinner, M., Jaye, C., Fischer, D.A., Gorb, S.N. & Weidner, T. 2015 Evidence of a molecular boundary lubricant at snakeskin surfaces. *Journal of The Royal Society Interface* **12**. (doi:10.1098/rsif.2015.0817).

[23] Baio, J.E., Weidner, T., Baugh, L., Gamble, L.J., Stayton, P.S. & Castner, D.G. 2012 Probing the orientation of electrostatically immobilized Protein G B1 by time-of-flight secondary ion spectrometry, sum frequency generation, and near-edge X-ray adsorption fine structure spectroscopy. *Langmuir : the ACS journal of surfaces and colloids* **28**, 2107-2112. (doi:10.1021/la203907t).

[24] Weidner, T., Apte, J.S., Gamble, L.J. & Castner, D.G. 2010 Probing the Orientation and Conformation of alpha-Helix and beta-Strand Model Peptides on Self-Assembled Monolayers Using Sum Frequency Generation and NEXAFS Spectroscopy. *Langmuir* **26**, 3433-3440. (doi:10.1021/la903267x).

[25] Weidner, T. & Castner, D.G. 2013 SFG analysis of surface bound proteins: a route towards structure determination. *Physical chemistry chemical physics : PCCP* **15**, 12516-12524. (doi:10.1039/c3cp50880c).

[26] Aragon, S. & Pecora, R. 1976 Theory of dynamic light scattering from polydisperse systems. *The Journal of Chemical Physics* **64**, 2395-2404.

[27] Korosi, G. & Kovats, E.S. 1981 Density and surface tension of 83 organic liquids. *Journal of Chemical and Engineering Data* **26**, 323-332.

[28] Cho, H.-J.J., Sresht, V. & Wang, E.N. 2018 Predicting Surface Tensions of Surfactant Solutions from Statistical Mechanics. *Langmuir*.

[29] Federle, W., Baumgartner, W. & Hölldobler, B. 2004 Biomechanics of ant adhesive pads: frictional forces are rate- and temperature-dependent. *Journal of Experimental Biology* **207**, 67-74. (doi:10.1242/jeb.00716).

[30] Gupta, S., Cochran, H. & Cummings, P. 1998 Nanorheology of liquid alkanes. *Fluid phase equilibria* **150**, 125-131.

[31] Adams, E.M., Champagne, A.M., Williams, J.B. & Allen, H.C. 2017 Interfacial properties of avian stratum corneum monolayers investigated by Brewster angle microscopy and vibrational sum frequency generation. *Chem Phys Lipids* **208**, 1-9. (doi:10.1016/j.chemphyslip.2017.08.002).

[32] Himmelhaus, M., Eisert, F., Buck, M. & Grunze, M. 2000 Self-assembly of n-alkanethiol monolayers. A study by IR-visible sum frequency spectroscopy (SFG). *The Journal of Physical Chemistry B* **104**, 576-584.

[33] Chen, C., Loch, C.L., Wang, J. & Chen, Z. 2003 Different molecular structures at polymer/silane interfaces detected by SFG. *The Journal of Physical …*, 10440-10445.
[34] Ma, G. & Allen, H.C. 2006 DPPC Langmuir monolayer at the air-water interface: Probing the tail and head groups by vibrational sum frequency generation spectroscopy. *Langmuir*, 5341-5349.

[35] Casford, M.T.L., Ge, A., Kett, P.J.N., Ye, S. & Davies, P.B. 2014 The Structure of Lipid Bilayers Adsorbed on Activated Carboxy-Terminated Monolayers Investigated by Sum Frequency Generation Spectroscopy. *The journal of physical chemistry. B*. (doi:10.1021/jp410401z).

[36] Tsige, M. & Patnaik, S.S. 2008 An all-atom simulation study of the ordering of liquid squalane near a solid surface. *Chemical Physics Letters* **457**, 357-361. (doi:https://doi.org/10.1016/j.cplett.2008.04.026).

[37] Mo, H., Evmenenko, G. & Dutta, P. 2005 Ordering of liquid squalane near a solid surface. *Chemical physics letters* **415**, 106-109.

[38] Hirose, C., Yamamoto, H., Akamatsu, N. & Domen, K. 1993 Orientation analysis by simulation of vibrational sum frequency generation spectrum: CH stretching bands of the methyl group. *The Journal of Physical Chemistry* **97**, 10064-10069.

[39] Bellany, L. 1975 The infrared spectra of complex molecules. *Chapman Hall, London* **1**.

[40] Jian, F., Jayas, D.S. & White, N.D. 2006 Vertical movement of adult rusty grain beetles, Cryptolestes ferrugineus, in stored corn and wheat at uniform moisture content. *Journal of Insect Science* **6**, 11.

[41] Benton, A.H. & Crump, A.J. 1981 Observations and the Spring and Summer Behavior of the 12-Spotted Ladybird Beetle, Coleomegilla maculata (Degeer)(Coleoptera: Coccinellidae). *Journal of the New York Entomological Society*, 102-108.

[42] Dirks, J.-H., Clemente, C.J. & Federle, W. 2010 Insect tricks: two-phasic foot pad secretion prevents slipping. *Journal of the Royal Society Interface* **7**, 587-593. (doi:10.1098/rsif.2009.0308).

[43] Bullock, J.M., Drechsler, P. & Federle, W. 2008 Comparison of smooth and hairy attachment pads in insects: friction, adhesion and mechanisms for direction-dependence. *Journal of Experimental Biology* **211**, 3333-3343.

[44] D.G., T., A., B., K.A., E., M., W. & K.F.A., W. 2008 Locomotory behaviour of the seven-spotted ladybird, Coccinella septempunctata, in response to five commonly used insecticides. *Annals of Applied Biology* **152**, 349-359. (doi:doi:10.1111/j.1744-7348.2008.00224.x).

[45] Moore, J., Cui, S., Cochran, H. & Cummings, P. 2000 Rheology of lubricant basestocks: a molecular dynamics study of C 30 isomers. *The Journal of chemical physics* **113**, 8833-8840.

[46] Ludviksson, V. & Lightfoot, E. 1971 The dynamics of thin liquid films in the presence of surface-tension gradients. *AIChE Journal* **17**, 1166-1173.

[47] Labonte, D. & Federle, W. 2015 Scaling and biomechanics of surface attachment in climbing animals. *Philosophical Transactions of the Royal Society B-Biological Sciences* **370**. (doi:10.1098/rstb.2014.0027).

[48] Amador, G.J., Endlein, T. & Sitti, M. 2017 Soiled adhesive pads shear clean by slipping: a robust self-cleaning mechanism in climbing beetles. *Journal of The Royal Society Interface* **14**. (doi:10.1098/rsif.2017.0134).

Chapter 6. Conclusions and Future Work

6.1 Summary of Results

The primary aim of this work was to show that complimentary analytical techniques could be used to systematically probe natural fluid adhesive mechanisms. For both the frog sticky-tongue and insect tarsal fluid adhesive systems, it was shown how organization and structure of molecules at adhesive interfaces contributed greatly to the success of the mechanism. Furthermore, a simple biomimetic insect tarsal adhesive was formulated to gain deeper insights into the effect of bulk composition and structure on both the overall adhesive properties and organization of surface-active adhesive molecules.

Frog tongue mucus was collected from tongue strikes and analyzed with a set of complementary surface analytical techniques - NEXAFS spectroscopy and SFG spectroscopy. NEXAFS images showed a uniform distribution of bond orbitals for various carbon and nitrogen bond orbitals associated with glycoproteins. NEXAFS angle-dependent spectra revealed that glycoprotein backbone amide bonds were arranged in helical structures consistent with fibrillation of proteins. SFG spectra indicated that side chains from the glycoprotein backbone were pointed away from the mucus surface. It was concluded that glycoprotein mucus molecules fibrillate under the strain of tongue retraction, creating a pressure-sensitive adhesive mechanism.

Next, interactions of natural insect tarsal adhesive fluid with substrates of varying wettability were examined with SFG spectroscopy. A layer of hydrocarbons was observed to organize at the fluid-substrate interface regardless of substrate wettability, which contradicted our hypothesis. This hydrocarbon layer was shown to consist of a mixture of branched and unbranched hydrocarbons and exhibited distinctly different chain organization depending upon the substrate of contact, with more uniform organization on hydrophobic surfaces. This difference in organization was correlated directly with previously measured variance in traction for generated for beetles on similar substrates, with less organization tied to more traction force and vice versa. We concluded that fluid chemistry was not dynamic at the insect tarsal fluid-substrate interface, but fluid organization was dynamic, and this had important consequences for adhesion.

Finally, a simple, three component biomimetic insect tarsal emulsion was formulated to resolve the precise mechanisms governing all aspects of insect foot adhesion. SFG spectra of the biomimetic emulsion showed hydrocarbons were the only substrate-active molecule, just as in the natural fluid study. Likewise, organization of this hydrocarbon layer was comparable to that of natural fluid when substrate hydrophobicity was varied. Comparison of the biomimetic emulsion to a fluid of pure squalane using surface tension, rheology and SFG measurements showed that the emulsion had nearly identical surface tension, but a very different rheological profile and organizational response to substrate wettability than pure squalane. Therefore, we concluded that only an emulsion fluid structure provided the optimal balance of traction force promotion, low surface tension for filling asperities and consistent pull-off force for fast escape.

6.2 Future Directions

6.2.1 Real-Time Analysis of Frog Tongue Mucus Structure Change in Response to Strain

In Chapter 3, we determined that glycoprotein molecules at the mucus-tongue surface fibrillate under the strain of tongue pulling during prey retraction. However, the experimental design only allowed for a static time analysis of the mechanism. Observing the structure of glycoprotein molecules at the interface as the strain applied was varied from zero to maximum would allow for a more thorough characterization of the adhesive mechanism. Additionally, it would allow for the comparison of the frog sticky-tongue mechanism to other animal mucus systems which are not capable of generating the same adhesive force. For instance, Bovine Submaxillary Mucin (cow mucus), a readily available glycoprotein mucus, could be used as a comparison system to frog tongue mucus. SFG spectroscopy could be utilized to monitor the secondary and tertiary structure of frog or tongue mucus pinned between two surfaces which are slowly separated. Differences in the structural response to strain may explain why frog tongue mucus is uniquely adapted for adhesion.

6.2.2 Mechanistic Study of the Adhesive Fluid of Flat-Pad Insects

In Chapters 4 and 5, the mechanisms governing the tarsal adhesion of insects were determined. While these mechanisms were generalized for all fluid secreting

insects, there are many that have a distinctly different tarsal anatomy – no setae. Setae have been shown to enhance the magnitude of adhesive force that insect generated with their feet.

Thus, removal of this feature would imply that the adhesive demands of these insects, such as climbing, sticking and hanging, could be met with the pad and fluid only. This may require the adhesive fluid to utilize different mechanisms. Using complimentary surface analytical techniques, the surface composition of flat-pad and hairy-pad insects could be compared with Time-of-Flight Secondary Ion Mass Spectrometry and the organization of these molecules could be probed with SFG spectroscopy. Determination of the adaptations nature makes to similar mechanisms with different demands would inform the design of new adhesives which could withstand deformations or wearing of the backing material over time.

6.3.3 Development and Testing of Stable Biomimetic Adhesive

In Chapter 5, we developed a simple, three component biomimetic emulsion with chemistry specifically chosen to isolate vibrational bonds for analysis with SFG spectroscopy. This fluid was a successful mimic for natural insect tarsal adhesive and was stable over the course of the experiment but was not stable for long periods of time (days). One potential reason for this was that choice of chemicals was limited to molecules which could reasonably exist in natural insect tarsal adhesive.

Now that the mechanism governing this adhesion has been determined, fluid composition could be modified to improve stability in terms of both aggregation of particles and temperature stability. To do this, the composition could be systematically varied and the stability and fluid properties could be tested using freeze/thaw cycles, rheological temperature sweeps and dynamic light scattering. The best emulsions could then be studied with SFG spectroscopy by collecting spectra of fluid in contact over a range of fluid ages (fresh, 1 day old, 3 days old, etc).

Bibliography

Adam, N. 1957 Use of the term ‘Young's Equation’ for contact angles. Nature 180, 809.

Adams, E.M., Champagne, A.M., Williams, J.B. & Allen, H.C. 2017 Interfacial properties of avian stratum corneum monolayers investigated by Brewster angle microscopy and vibrational sum frequency generation. Chem Phys Lipids 208, 1-9. (doi:10.1016/j.chemphyslip.2017.08.002).

Amador, G.J., Endlein, T. & Sitti, M. 2017 Soiled adhesive pads shear clean by slipping: a robust self-cleaning mechanism in climbing beetles. Journal of The Royal Society Interface 14. (doi:10.1098/rsif.2017.0134).

Amenabar, I., Poly, S., Nuansing, W., Hubrich, E.H., Govyadinov, A.A., Huth, F., Krutokhvostov, R., Zhang, L., Knez, M. & Heberle, J. 2013 Structural analysis and mapping of individual protein complexes by infrared nanospectroscopy. Nature communications 4.

Aragon, S. & Pecora, R. 1976 Theory of dynamic light scattering from polydisperse systems. The Journal of Chemical Physics 64, 2395-2404.

Autumn, K. & Gravish, N. 2008 Gecko adhesion: evolutionary nanotechnology. Philosophical Transactions of the Royal Society of London A: Mathematical, Physical and Engineering Sciences 366, 1575-1590.

Autumn, K., Dittmore, A., Santos, D., Spenko, M. & Cutkosky, M. 2006 Frictional adhesion: a new angle on gecko attachment. Journal of Experimental Biology 209, 3569-3579.

Baio, J.E., Jaye, C., Fischer, D.A. & Weidner, T. 2013 Multiplexed Orientation and Structure Analysis by Imaging Near-Edge X-ray Absorption Fine Structure (MOSAIX) for Combinatorial Surface Science. Analytical chemistry 85, 4307-4310.

Baio, J.E., Jaye, C., Fischer, D.A. & Weidner, T. 2014 High-throughput analysis of molecular orientation on surfaces by NEXAFS imaging of curved sample arrays. ACS combinatorial science 16, 449-453.

Baio, J.E., Spinner, M., Jaye, C., Fischer, D.A., Gorb, S.N. & Weidner, T. 2015 Evidence of a molecular boundary lubricant at snakeskin surfaces. Journal of The Royal Society Interface 12. (doi:10.1098/rsif.2015.0817).

Baio, J.E., Weidner, T., Baugh, L., Gamble, L.J., Stayton, P.S. & Castner, D.G. 2012 Probing the orientation of electrostatically immobilized Protein G B1 by time-of-flight secondary ion spectrometry, sum frequency generation, and near-edge X-ray adsorption fine structure spectroscopy. Langmuir : the ACS journal of surfaces and colloids 28, 2107-2112. (doi:10.1021/la203907t).

Baio, J.E., Weidner, T., Samuel, N.T., McCrea, K., Baugh, L., Stayton, P.S. & Castner, D.G. 2010 Multitechnique characterization of adsorbed peptide and protein orientation: LK3(10) and Protein G B1. Journal of Vacuum Science & Technology B 28, C5D1-C5D8. (doi:10.1116/1.3456176).

Bansil, R. & Turner, B.S. 2006 Mucin structure, aggregation, physiological functions and biomedical applications. Current Opinion in Colloid & Interface Science 11, 164-170.

Baugh, L., Weidner, T., Baio, J.E., Nguyen, P.C.T., Gamble, L.J., Slayton, P.S. & Castner, D.G. 2010 Probing the Orientation of Surface-Immobilized Protein G B1 Using ToF-SIMS, Sum Frequency Generation, and NEXAFS Spectroscopy. Langmuir 26, 16434-16441. (doi:10.1021/la1007389).

Bellany, L. 1975 The infrared spectra of complex molecules. Chapman Hall, London 1.

Benton, A.H. & Crump, A.J. 1981 Observations and the Spring and Summer Behavior of the 12-Spotted Ladybird Beetle, Coleomegilla maculata (Degeer)(Coleoptera: Coccinellidae). Journal of the New York Entomological Society, 102-108.

Bullock, J.M., Drechsler, P. & Federle, W. 2008 Comparison of smooth and hairy attachment pads in insects: friction, adhesion and mechanisms for direction-dependence. Journal of Experimental Biology 211, 3333-3343.

Busshardt, P., Wolf, H. & Gorb, S.N. 2012 Adhesive and frictional properties of tarsal attachment pads in two species of stick insects (Phasmatodea) with smooth and nubby euplantulae. Zoology 115, 135-141. (doi:10.1016/j.zool.2011.11.002).

Casford, M.T.L., Ge, A., Kett, P.J.N., Ye, S. & Davies, P.B. 2014 The Structure of Lipid Bilayers Adsorbed on Activated Carboxy-Terminated Monolayers Investigated by Sum Frequency Generation Spectroscopy. The journal of physical chemistry. B. (doi:10.1021/jp410401z).

Celli, J., Gregor, B., Turner, B., Afdhal, N.H., Bansil, R. & Erramilli, S. 2005 Viscoelastic properties and dynamics of porcine gastric mucin. Biomacromolecules 6, 1329-1333.

Chaudhury, M.K. & Whitesides, G.M. 1992 Correlation between surface free energy and surface constitution. Science 255, 1230-1232.

Chen, C., Loch, C.L., Wang, J. & Chen, Z. 2003 Different molecular structures at polymer/silane interfaces detected by SFG. The Journal of Physical …, 10440-10445.

Chen, X., Wang, J., Kristalyn, C.B. & Chen, Z. 2007 Real-Time Structural Investigation of a Lipid Bilayer during Its Interaction with Melittin Using Sum Frequency Generation Vibrational Spectroscopy. Biophysical Journal 93, 866-875. (doi:10.1529/biophysj.106.099739).

Cheng, F., Gamble, L.J. & Castner, D.G. 2008 XPS, TOF-SIMS, NEXAFS, and SPR characterization of nitrilotriacetic acid-terminated self-assembled monolayers for controllable immobilization of proteins. Analytical chemistry 80, 2564-2573.

Cho, H.-J.J., Sresht, V. & Wang, E.N. 2018 Predicting Surface Tensions of Surfactant Solutions from Statistical Mechanics. Langmuir.

Daltorio, K.A., Wei, T.E., Horchler, A.D., Southard, L., Wile, G.D., Quinn, R.D., Gorb, S.N. & Ritzmann, R.E. 2009 Mini-Whegs TM Climbs Steep Surfaces Using Insect-inspired Attachment Mechanisms. The International Journal of Robotics Research 28, 285-302. (doi:doi:10.1177/0278364908095334).

Davies, H.S., Singh, P., Deckert-Gaudig, T., Deckert, V., Rousseau, K., Ridley, C.E., Dowd, S.E., Doig, A.J., Pudney, P.D. & Thornton, D.J. 2016 Secondary Structure and Glycosylation of Mucus Glycoproteins by Raman Spectroscopies. Analytical chemistry 88, 11609-11615.

Dietrich, P.M., Horlacher, T., Girard-Lauriault, P.-L., Gross, T., Lippitz, A., Min, H., Wirth, T., Castelli, R., Seeberger, P. & Unger, W.E. 2011 Multimethod chemical characterization of carbohydrate-functionalized surfaces. Journal of Carbohydrate Chemistry 30, 361-372.

Dirks, J.-H. & Federle, W. 2011 Fluid-based adhesion in insects - principles and challenges. Soft Matter 7, 11047-11053. (doi:10.1039/c1sm06269g).

Dirks, J.-H., Clemente, C.J. & Federle, W. 2010 Insect tricks: two-phasic foot pad secretion prevents slipping. Journal of the Royal Society Interface 7, 587-593. (doi:10.1098/rsif.2009.0308).

Drechsler, P. & Federle, W. 2006 Biomechanics of smooth adhesive pads in insects: influence of tarsal secretion on attachment performance. Journal of Comparative Physiology A 192, 1213-1222.

Endlein, T., Ji, A., Samuel, D., Yao, N., Wang, Z., Barnes, W.J.P., Federle, W., Kappl, M. & Dai, Z. 2013 Sticking like sticky tape: tree frogs use friction forces to enhance attachment on overhanging surfaces. Journal of the Royal Society Interface 10, 1-11.

Engel, M.F.M., vandenAkker, C.C., Schleeger, M., Velikov, K.P., Koenderink, G.H. & Bonn, M. 2012 The polyphenol EGCG inhibits amyloid formation less efficiently at phospholipid interfaces than in bulk solution. Journal of the American Chemical Society 134, 14781-14788. (doi:10.1021/ja3031664)

England, M.W., Sato, T., Yagihashi, M., Hozumi, A., Gorb, S.N. & Gorb, E.V. 2016 Surface roughness rather than surface chemistry essentially affects insect adhesion. Beilstein Journal of Nanotechnology 7, 1471-1479.

Federle, W., Baumgartner, W. & Hölldobler, B. 2004 Biomechanics of ant adhesive pads: frictional forces are rate- and temperature-dependent. Journal of Experimental Biology 207, 67-74. (doi:10.1242/jeb.00716).

Federle, W., Riehle, M., Curtis, A.S.G. & Full, R.J. 2002 An integrative study of insect adhesion: mechanics and wet adhesion of pretarsal pads in ants. Integrative and comparative biology 42, 1100-1106. (doi:10.1093/icb/42.6.1100).

Gainar, A., Stevens, J.S., Jaye, C., Fischer, D.A. & Schroeder, S.L. 2015 NEXAFS Sensitivity to Bond Lengths in Complex Molecular Materials: A Study of Crystalline Saccharides. The Journal of Physical Chemistry B 119, 14373-14381.

Gao, H., Wang, X., Yao, H., Gorb, S. & Arzt, E. 2005 Mechanics of hierarchical adhesion structures of geckos. Mechanics of Materials 37, 275-285.

Geiselhardt, S.F., Federle, W., Prüm, B., Geiselhardt, S., Lamm, S. & Peschke, K. 2010 Impact of chemical manipulation of tarsal liquids on attachment in the Colorado potato beetle, Leptinotarsa decemlineata. Journal of insect physiology 56, 398-404.

Geiselhardt, S.F., Geiselhardt, S. & Peschke, K. 2009 Comparison of tarsal and cuticular chemistry in the leaf beetle Gastrophysa viridula (Coleoptera: Chrysomelidae) and an evaluation of solid-phase microextraction and solvent extraction techniques. Chemoecology 19, 185.

Geiselhardt, S.F., Geiselhardt, S. & Peschke, K. 2011 Congruence of epicuticular hydrocarbons and tarsal secretions as a principle in beetles. Chemoecology 21, 181.

Golbek, T.W., Franz, J., Elliott Fowler, J., Schilke, K.F., Weidner, T. & Baio, J.E. 2017 Identifying the selectivity of antimicrobial peptides to cell membranes by sum frequency generation spectroscopy. Biointerphases 12, 02D406.

Gorb, E. & Gorb, S. 2002 Attachment ability of the beetle Chrysolina fastuosa on various plant surfaces. Entomologia Experimentalis et Applicata 105, 13-28.

Gorb, E. & Gorb, S. 2009 Effects of surface topography and chemistry of Rumex obtusifolius leaves on the attachment of the beetle Gastrophysa viridula. Entomologia experimentalis et applicata 130, 222-228.

Gorb, E., Voigt, D., Eigenbrode, S.D. & Gorb, S. 2008 Attachment force of the beetle Cryptolaemus montrouzieri (Coleoptera, Coccinellidae) on leaflet surfaces of mutants of the pea Pisum sativum (Fabaceae) with regular and reduced wax coverage. Arthropod-Plant Interactions 2, 247-259.

Gorb, E.V., Hosoda, N., Miksch, C. & Gorb, S.N. 2010 Slippery pores: anti-adhesive effect of nanoporous substrates on the beetle attachment system. Journal of the Royal Society, Interface / the Royal Society 7, 1571-1579. (doi:10.1098/rsif.2010.0081)

Gorb, S.N. 2001 Attachment Devices of Insect Cuticle. Dordrecht, The Netherlands, Kluwer Academic Publishers

Gorb, S.N., Sinha, M., Peressadko, A., Daltorio, K.A. & Quinn, R.D. 2007 Insects did it first: a micropatterned adhesive tape for robotic applications. Bioinspiration & biomimetics 2, S117.

Gracias, D., Chen, Z., Shen, Y. & Somorjai, G. 1999 Molecular characterization of polymer and polymer blend surfaces. Combined sum frequency generation surface vibrational spectroscopy and scanning force microscopy studies. Accounts of chemical research 32, 930-940.

Gu, Z., Li, S., Zhang, F. & Wang, S. 2016 Understanding surface adhesion in nature: a peeling model. Advanced Science 3.

Gupta, S., Cochran, H. & Cummings, P. 1998 Nanorheology of liquid alkanes. Fluid phase equilibria 150, 125-131.

Gupta, S.A. & Gupta, R.K. 1998 A parametric study of spin coating over topography. Industrial & engineering chemistry research 37, 2223-2227.

Harding, S., Rowe, A. & Creeth, J. 1983 Further evidence for a flexible and highly expanded spheroidal model for mucus glycoproteins in solution. Biochemical Journal 209, 893-896.

Heepe, L., Wolff, J.O. & Gorb, S.N. 2016 Influence of ambient humidity on the attachment ability of ladybird beetles (Coccinella septempunctata). Beilstein Journal of Nanotechnology 7, 1322-1329.

Himmelhaus, M., Eisert, F., Buck, M. & Grunze, M. 2000 Self-assembly of n-alkanethiol monolayers. A study by IR-visible sum frequency spectroscopy (SFG). The Journal of Physical Chemistry B 104, 576-584.

Hirose, C., Yamamoto, H., Akamatsu, N. & Domen, K. 1993 Orientation analysis by simulation of vibrational sum frequency generation spectrum: CH stretching bands of the methyl group. The Journal of Physical Chemistry 97, 10064-10069.

Hosoda, N. & Gorb, S.N. 2012 Underwater locomotion in a terrestrial beetle: combination of surface de-wetting and capillary forces. Proceedings of the Royal Society of London B: Biological Sciences 279, 4236-4242.

Irschick, D.J., Crosby, A.J. & Federle, W. 2013 The evolution of Gecko adhesion: An integrative perspective. Integrative and Comparative Biology 53, E100-E100.

Jian, F., Jayas, D.S. & White, N.D. 2006 Vertical movement of adult rusty grain beetles, Cryptolestes ferrugineus, in stored corn and wheat at uniform moisture content. Journal of Insect Science 6, 11.

Kleinteich, T. & Gorb, S.N. 2014 Tongue adhesion in the horned frog Ceratophrys sp. Scientific reports 4, 5225-5225. (doi:10.1038/srep05225).

Kleinteich, T. & Gorb, S.N. 2015 Frog tongue acts as muscle-powered adhesive tape. Open Science 2, 150333.

Korosi, G. & Kovats, E.S. 1981 Density and surface tension of 83 organic liquids. Journal of Chemical and Engineering Data 26, 323-332.

Kurouski, D., Deckert-Gaudig, T., Deckert, V. & Lednev, I.K. 2014 Surface characterization of insulin protofilaments and fibril polymorphs using tip-enhanced Raman spectroscopy (TERS). Biophysical journal 106, 263-271.

Labonte, D. & Federle, W. 2015 Scaling and biomechanics of surface attachment in climbing animals. Philosophical Transactions of the Royal Society B-Biological Sciences 370. (doi:10.1098/rstb.2014.0027).

Langer, M.G., Ruppersberg, J.P. & Gorb, S. 2004 Adhesion forces measured at the level of a terminal plate of the fly's seta. Proceedings of the Royal Society of London B: Biological Sciences 271, 2209-2215.

Lewis, S.P., Lewis, A.T. & Lewis, P.D. 2013 Prediction of glycoprotein secondary structure using ATR-FTIR. Vibrational Spectroscopy 69, 21-29. (doi:http://dx.doi.org/10.1016/j.vibspec.2013.09.001).

Li, Y., Pham, J.Q., Johnston, K.P. & Green, P.F. 2007 Contact angle of water on polystyrene thin films: Effects of CO2 environment and film thickness. Langmuir 23, 9785-9793.

Ludviksson, V. & Lightfoot, E. 1971 The dynamics of thin liquid films in the presence of surface-tension gradients. AIChE Journal 17, 1166-1173.

Ma, G. & Allen, H.C. 2006 DPPC Langmuir monolayer at the air-water interface: Probing the tail and head groups by vibrational sum frequency generation spectroscopy. Langmuir, 5341-5349.

Mo, H., Evmenenko, G. & Dutta, P. 2005 Ordering of liquid squalane near a solid surface. Chemical physics letters 415, 106-109.

Moore, J., Cui, S., Cochran, H. & Cummings, P. 2000 Rheology of lubricant basestocks: a molecular dynamics study of C 30 isomers. The Journal of chemical physics 113, 8833-8840.

Morra, M., Occhiello, E. & Garbassi, F. 1990 Knowledge about polymer surfaces from contact angle measurements. Advances in Colloid and Interface Science 32, 79-116.

Noel, A.C., Guo, H.-Y., Mandica, M. & Hu, D.L. 2017 Frogs use a viscoelastic tongue and non-Newtonian saliva to catch prey. Journal of The Royal Society Interface 14, 20160764.

Peisker, H. & Gorb, S.N. 2012 Evaporation dynamics of tarsal liquid footprints in flies (Calliphora vicina)and beetles (Coccinella septempunctata). The Journal of experimental biology 215, 1266-1271. (doi:10.1242/jeb.065722).

Peisker, H., Heepe, L., Kovalev, A.E. & Gorb, S.N. 2014 Comparative study of the fluid viscosity in tarsal hairy attachment systems of flies and beetles. Journal of the Royal Society Interface 11. (doi:10.1098/rsif.2014.0752).

Perez-Vilar, J. & Hill, R.L. 1999 The structure and assembly of secreted mucins. Journal of Biological Chemistry 274, 31751-31754.

Pujari, S.P., Scheres, L., Weidner, T., Baio, J.E., Stuart, M.a.C., van Rijn, C.J.M. & Zuilhof, H. 2013 Covalently attached organic monolayers onto silicon carbide from 1-alkynes: molecular structure and tribological properties. Langmuir : the ACS journal of surfaces and colloids 29, 4019-4031. (doi:10.1021/la400040e).

Scherge, M., Gorb, S. & Gorb, S.N. 2001 Biological micro-and nanotribology, Springer Science & Business Media.

Shen, Y.-R. 1984 The principles of nonlinear optics. New York, Wiley-Interscience, 1984, 575 p.

Smith, A.M. & Morin, M.C. 2002 Biochemical differences between trail mucus and adhesive mucus from marsh periwinkle snails. The Biological Bulletin 203, 338-346

Smith, A.M. 2002 The structure and function of adhesive gels from invertebrates. Integrative and Comparative Biology 42, 1164-1171.

Smith, A.M. 2016 The biochemistry and mechanics of gastropod adhesive gels. In Biological adhesives (pp. 177-192, Springer.

Solomon, D., Lehmann, J., Kinyangi, J., Liang, B., Heymann, K., Dathe, L., Hanley, K., Wirick, S. & Jacobsen, C. 2009 Carbon (1s) NEXAFS Spectroscopy of Biogeochemically Relevant Reference Organic Compounds. Soil Science Society of America Journal 73, 1817-1817. (doi:10.2136/sssaj2008.0228).

Stewart-Ornstein, J., Hitchcock, A.P., Cruz, D.H., Henklein, P., Overhage, J., Hilpert, K., Hale, J.D. & Hancock, R.E.W. 2007 Using intrinsic X-ray absorption spectral differences to identify and map peptides and proteins. Journal of Physical Chemistry B 111, 7691-7699. (doi:10.1021/jp0720993).

Stöhr, J. 2013 NEXAFS spectroscopy, Springer Science & Business Media.

Tsige, M. & Patnaik, S.S. 2008 An all-atom simulation study of the ordering of liquid squalane near a solid surface. Chemical Physics Letters 457, 357-361. (doi:https://doi.org/10.1016/j.cplett.2008.04.026).

Van Oss, C., Arnold, K., Good, R., Gawrisch, K. & Ohki, S. 1990 Interfacial tension and the osmotic pressure of solutions of polar polymers. Journal of Macromolecular Science-Chemistry 27, 563-580.

Vötsch, W., Nicholson, G., Müller, R., Stierhof, Y.D., Gorb, S. & Schwarz, U. 2002 Chemical composition of the attachment pad secretion of the locust Locusta migratoria. Insect biochemistry and molecular biology 32, 1605-1613.

Vötsch, W., Nicholson, G., Müller, R., Stierhof, Y.D., Gorb, S. & Schwarz, U. 2002 Chemical composition of the attachment pad secretion of the locust Locusta migratoria. Insect biochemistry and molecular biology 32, 1605-1613.

Walker, G. 1993 Adhesion to smooth surfaces by insects—a review. International Journal of Adhesion and Adhesives 13, 6-10.

Watry, M.R., Tarbuck, T.L. & Richmond, G.L. 2003 Vibrational sum-frequency studies of a series of phospholipid monolayers and the associated water structure at the vapor/water interface. The Journal of Physical Chemistry B 107, 512-518.

Weidner, T. & Castner, D.G. 2013 SFG analysis of surface bound proteins: a route towards structure determination. Physical chemistry chemical physics : PCCP 15, 12516-12524. (doi:10.1039/c3cp50880c).

Weidner, T., Apte, J.S., Gamble, L.J. & Castner, D.G. 2010 Probing the Orientation and Conformation of alpha-Helix and beta-Strand Model Peptides on Self-Assembled Monolayers Using Sum Frequency Generation and NEXAFS Spectroscopy. Langmuir 26, 3433-3440. (doi:10.1021/la903267x).

Yang, C.S.C., Wilson, P.T. & Richter, L.J. 2004 Structure of Polystyrene at the Interface with Various Liquids. Macromolecules 37, 7742-7746. (doi:10.1021/ma049692s).

Yatawara, A.K., Tiruchinapally, G., Bordenyuk, A.N., Andreana, P.R. & Benderskii, A.V. 2009 Carbohydrate surface attachment characterized by sum frequency generation spectroscopy. Langmuir 25, 1901-1904.

Zappone, B., Patil, N.J., Madsen, J.B., Pakkanen, K.I. & Lee, S. 2015 Molecular structure and equilibrium forces of bovine submaxillary mucin adsorbed at a solid–liquid interface. Langmuir 31, 4524-4533

Zubavichus, Y., Shaporenko, A., Grunze, M. & Zharnikov, M. 2007 NEXAFS spectroscopy of homopolypeptides at all relevant absorption edges: Polyisoleucine, polytyrosine, and polyhistidine. The Journal of Physical Chemistry B 111, 9803-9807

Zubavichus, Y., Shaporenko, A., Grunze, M. & Zharnikov, M. 2009 NEXAFS spectroscopy of biological molecules: From amino acids to functional proteins. Nuclear Instruments and Methods in Physics Research, Section A: Accelerators, Spectrometer, Detectors and Associated Equipment 603, 111-114. (doi:10.1016/j.nima.2008.12.171).